이학박사학위논문

Development of Intracellular Delivery Methods using α-Helical Cell Penetrating Peptides and Affibody Proteins

세포투과성 펩타이드와 기능성단백질을 이용한
세포전달물질 개발

2021년 8월

서울대학교 대학원
화학부 생화학 전공
정 승 은

Development of Intracellular Delivery Methods using α-Helical Cell Penetrating Peptides and Affibody Proteins

지도교수 이 연

이 논문을 이학박사학위논문으로 제출함
2021년 8월

서울대학교 대학원
화학부 생화학전공
정 승 은

정승은의 이학박사학위논문을 인준함
2021년 8월

위 원 장	유 재 훈
부위원장	이 연
위 원	김 석 희
위 원	이 형 호
위 원	김 동 은

Abstract

The cell membrane is an important barrier which protects the cells from the surroundings. The cell membrane is composed of lipid bilayer containing various membrane proteins and carbohydrates. This important structure works as a semi-permeable filter that manages the exchange of materials inside and outside the cells which means cells uptake materials very precisely and selectively. For examples, ions or small hydrophilic nutrients usually use specific channels or transporter proteins to enter the cells whereas hydrophilic macromolecules are unable to go in to the cells efficiently. This selective material transportation of cell membrane works as safeguard of the cells but at the same time, the cell membrane is the most challenging hurdles in developing therapeutic drugs using large-size molecules such as peptide, proteins, antibodies, or nucleic acids. To overcome the poor permeability of drugs, various drug delivery vehicles have been developed such as viruses, polymers, and nanoparticles.

Cell penetrating peptides (CPPs), or protein transduction domains (PTDs), are short peptides that facilitate cellular uptake of various molecular cargoes. Since the transactivator of transcription (TAT) was firstly found as it has remarkable ability to across cell membrane, various artificial cell penetrating sequences have been developed and they have been widely used in various biological and therapeutic applications. In our lab, a new series of Leucine and Lysine rich α-helical cell penetrating peptides, LK peptides

(LKKLLKLLKKLLKLAG), was developed. Those peptides show the cell penetrating ability in the nanomolar range which is extremely efficient compared to conventional CPPs. Furthermore, in the previous research, I found that the cell penetrating ability dramatically increases as it became multimers and the ability is saturated when the sequence is repeated four times (LK-4). However, they do not have any special functions besides high cell penetrating ability across the cell membrane. In order to give special functions to LK peptides, I proposed to introduce affibody proteins to the LK sequences.

Affibody molecules, a member of antibody mimetic families, are small proteins engineered to bind to a large number of target proteins or peptides with very high affinity. The first affibody protein was found on the surface protein – the protein A - of *Staphylococcus aureus* and it was found that the protein A contains five different triple helix domains (E, D, A, B, C), each showing great affinity to antibody. From the domain B of protein A, scientist artificially engineered protein domain Z which can specifically bind to Fc region of immunoglobulin G without affecting Fab region. After developing the first engineered affibody domain Z, a large number of affibody has been developed from domain Z through the phage display technique. In this thesis, two types of affibody proteins – domain Z (Z_{wt}) and $Z_{HER2:342}$ – were introduced LK sequences through simple DNA recombinant technology.

As already mentioned above, domain Z of protein A is known to

bind to Fc region of Immunoglobulin G (IgG) with high affinity (Kd= ~50nM). The first part of the thesis started from the hypothesis that domain Z can give the Fc-binding ability to LK sequences and the recombinant protein LK-domain Z can work as an extremely efficient IgG delivery vehicle at the nanomolar concentration range. Based on various experiments, I figured out that LK-domain Z proteins bind to Fc region of IgG at specific ratio and the proteins successfully deliver IgG across the live cell membrane at nanomolar concentrations without showing any toxicity. I also revealed the penetration mechanisms and kinetics of IgG/LK-domain Z complexes. Furthermore, as a proof-of-concept, I delivered anti- NF-κB IgG to regulate specific signaling pathway of cancer cells and saw the possibility of LK-domain Z protein as an efficient IgG delivery vehicle for the future therapeutics.

In the second part of the thesis, I overcame the critical limitations of various drug delivery vehicles – the lack of selectivity. Here, HER2-overexpressed breast cancer targeted cell penetrating peptide and therapeutics were developed using the affibody named $Z_{HER2:342}$. $Z_{HER2:342}$ is one of the affibody molecules which are derived from Domain Z from the phage display. With the changes of only 13 amino acids on the surface of domain Z, a new affibody – showing totally different characteristics to domain Z – was discovered. $Z_{HER2:342}$ is known to bind to HER2 receptors (Kd= ~22pM) which are usually overexpressed on the membrane of many breast cancer cells and manage the proliferation of various cancer cells. In

this study, $Z_{HER2:342}$ was brought into LK-2 peptides (LKKLLKLLKKLLKL GGLKKLLKLLKKLLKLAG) through DNA recombinant technology to give them the selectivity against HER2-positive breast cancers and I named this protein as LK-2-Z_{HER2}. As I predicted, LK-2-Z_{HER2} showed great targeting effect against HER2-overexpressed cells both *in vitro* and *in vivo.* Furthermore, with anti-cancer therapeutic, doxorubicin, LK-2-Z_{HER2} selectively killed HER2-overexpressed cells *in vitro.*

Based on those two researches in this Ph.D thesis, it is very clear that simple introduction of affibody through DNA recombinant technology is a very simple and easy way to give special function to cell penetrating peptides. Since large number of affibody proteins were developed and are being developed, I can infinitely expand the function of cell penetrating peptides in the future.

Keyword : Cell penetrating peptide, Protein transduction domain, Affibody proteins, anti-cancer therapy, Recombinant protein

Student Number : 2015-22627

PART I. Development of Immunoglobulin G Delivery Vehicle at Nanomolar Concentrations with Domain Z-fused Multimeric α-Helical Cell Penetrating Peptides

PART II. Development of Targeted Drug Delivery Vehicle with Dimeric α-Helical Cell Penetrating Peptide and HER2-Selective Affibody

List of Figures

PART I. Development of Immunoglobulin G Delivery Vehicle at Nanomolar Concentrations with Domain Z-fused Multimeric α-Helical Cell Penetrating Peptides

PART II. Development of Targeted Drug Delivery Vehicle with Dimeric α-Helical Cell Penetrating Peptide and HER2-Selective Affibody

List of Tables

PART I. Development of Immunoglobulin G Delivery Vehicle at Nanomolar Concentrations with Domain Z-fused Multimeric α-Helical Cell Penetrating Peptides

PART II. Development of Targeted Drug Delivery Vehicle with Dimeric α-Helical Cell Penetrating Peptide and HER2-Selective Affibody

PART I. Development of Immunoglobulin G Delivery Vehicle at Nanomolar Concentrations with Domain Z-fused Multimeric α-Helical Cell Penetrating Peptides

1. Abstract

A new vehicle is designed for the intracellular delivery of antibodies at nanomolar concentrations by combination of domain Z, a small affibody with strong binding affinity to Fc regions of immunoglobulin G (IgG), and the multimers of LK sequences, α-helical cell penetrating peptides (CPP) with powerful cell penetrating activities. Domain Z and multimeric LK are fused together to form LK-domain Z proteins. The LK-domain Z can bind with IgG at a specific ratio at nanomolar concentrations by simple mixing. The IgG/LK-domain Z complexes can successfully penetrate live cells at nanomolar concentration and the delivery efficiency is strongly dependent upon the concentrations of IgG/LK-domain Z complex as well as the species and subclasses of IgGs. The IgG/LK-domain Z complexes penetrate cells via ATP-dependent endocytosis pathway and the majority of delivered IgG seems to escape endosome to cytosol. Remarkably, the delivered IgGs are able to control the targeted intracellular signaling pathway as shown in the down-regulation of pro-survival genes by the delivery of anti-NF-κB using an LK-domain Z vehicle with a cathepsin B-cleavable linker between the LK sequence and domain Z. The simple but very efficient intracellular delivery method of antibodies at nanomolar concentrations is expected to

facilitate profound understanding of cell mechanisms and development of new future therapeutics on the basis of intracellular antibodies.

2. Introduction

Antibody is supreme recognizing machinery in nature. Antibody is now an essential therapeutic and diagnostic tool in medical applications as well as a powerful analyzing and imaging tool in biological sciences. Western blotting, enzyme-linked immunosorbent assay (ELISA) and immunohistochemistry (IHC) are all representative methods for analyzing biological samples with high selectivity and sensitivity. The selectivity and sensitivity of antibody are originated from the structural diversity up to 10^9-10^{10} [1] and the target affinity with K_d values in the range from 10^{-9} M to 10^{-12} M, [2] respectively. Notwithstanding, most antibody applications to live biological samples are limited to the cell exterior due to the impermeability of antibody into intact cell membranes. The huge size up to 150 kDa and high surface charges of antibodies severely prohibit the internalization of antibodies into cells.[3] Although detergent permeabilization on fixed or dead cells is enough to deliver antibodies into cells for visualization or analysis,[4] it is difficult to be applied to live cells. If antibodies can be delivered into live cells with minimal damages on cell membranes, they become powerful tools for understanding underlying mechanisms as well as correcting dysfunctional pathways in cells by selective recognition on the corresponding target molecules with outstanding affinity.

In order to deliver antibodies into live cells, physical methods (*i.e.* microinjection [5] and electroporation [6]) and chemical methods (*i.e.* liposomes [7], polymers [8] and nanoparticles [9]) have been developed with limited success. However, such methods often provoke severe damages on cells [10] or inactivation of antibodies during encapsulation or chemical treatment, [11] and are sometimes difficult to be applied to *in vivo* systems due to poor pharmacokinetics or toxicity. [12]

Cell penetrating peptides (CPPs), or protein transduction domains (PTDs), are short amino acid sequences for facilitating cellular uptake of cargo molecules via endocytosis or direct penetration.[13] CPPs are often preferred over other intracellular delivery vehicles due to more biological tolerability from the natural origin.[14] Especially in the delivery of proteins, the CPPs have a clear advantage because they can be fused with protein cargo molecules via genetic engineering.[15] The conjugation or fusion of CPPs may escape the protein inactivation problems during the encapsulation or complexation in chemical delivery vehicles.

Actually, several CPPs have been applied for the intracellular delivery of antibodies. [16] However, most CPPs show their cell penetrating abilities above several micromolar concentrations, which is a severe limitation for the delivery of antibodies with molecular weights of over 150 kDa.[17] The micromolar delivery requires huge amount of antibodies and loses the strength of nanomolar or picomolar affinity of antibodies. Furthermore, since it is difficult to produce and purify individual CPP-fused

antibodies in eukaryotic cells, CPPs are generally connected to the inter-chain cysteine residues or the lysine residues on antibody through chemical conjugation.[15, 18] The chemical conjugation mostly requires unnatural chemical linkers such as maleimides or strong coupling reagents and those processes usually yield heterogeneous products. Non-covalent complexations based on hydrophobic or electrostatic interaction [19] have been suggested for the CPP-based antibody delivery but it is also not free from the issues of heterogeneity and antibody inactivation.

I suggest a new CPP-based non-covalent delivery method for requiring only nanomolar concentrations of antibodies and being free from the heterogeneity issue (**Figure 2.**). Z domain of *Staphylococcal* protein A (SpA), a representative affibody which was engineered from B domain of the protein A to improve specific binding to only the Fc region of immunoglobulin G (IgG), [20] was fused to the C-terminus of a CPP. The domain Z has a relatively small size (6 kDa) for easy expression in the prokaryotic system and furthermore, it has a great binding affinity with K_d of 10-50 nM against a specific epitope in the Fc region. Therefore, the domain Z can be an ideal non-covalent binder for the antibody delivery even at nanomolar concentrations without the heterogeneity issue. As for the powerful CPP at nanomolar concentrations, I selected multimeric forms of the leucine (L)- and lysine (K)-rich amphipathic α-helical peptide sequence (LK-1; LKKLLKLLKKLLKLAG). In our previous reports, multimeric LK sequences showed powerful cell penetrating activity by efficient induction

of endocytosis even at low nanomolar concentrations, which are more than 100-fold lower concentrations than conventional CPPs such as Tat sequence or polyarginines. [21]

In this study, I show dimeric LK (LK-2)- or tetrameric LK (LK-4)-fused domain Z can deliver full-size IgG into living cells at nanomolar concentration range, the lowest concentration that has ever been reported, by simple incubation without any chemical conjugation. Furthermore, I introduce a cleavable peptide linker between LK and domain Z in order to remove any possible interruption of the specific activities of IgGs which can be caused by the non-specific interactions between positively charged LK sequence and other proteins after the intracellular delivery. Using this vehicle, I examine whether the delivered antibody can control intracellular signaling by blocking the function of NF-κB as a proof-of-concept for the future therapeutics using the intracellular antibody.

3. Experimental Methods

3.1. Cell Lines and Cell Culture

HeLa (human cervix epithelial carcinoma) cells were purchased from the American Type Culture Collection (ATCC). *MDA-MB-231* (human breast cancer), *NIH3T3* (mouse embryonic fibroblast) and *Caco-2* (human colorectal adenocarcinoma) cells were purchased from Korean Cell Line Bank. These cells were maintained in high glucose Dulbecco's Modified Eagle's Medium (DMEM) with 10% fetal bovine serum (FBS). *A549* (adenocarcinomic human alveolar basal epithelial cell) cells were purchased from Korean Cell Line Bank and were maintained in Roswell Park Memorial Institute Medium (RPMI) 1640 with 10% fetal bovine serum (FBS). Both cells were maintained at 37 ℃ under 5 % CO_2 condition.

3.2. Antibodies

Human IgG isotype control (Invitrogen, cat#31154), mouse anti-cyclin D1 (DSC-6) antibody (FITC, IgG_{2a} , Santa Cruz, sc-20044), rabbit anti-TOMM20 (F-10) antibody (Alexa-594, Santa Cruz, sc-17764), mouse anti-nuclear pore complex (Mab 414) antibody (Alexa-488, IgG_1, Sigma-Aldrich), mouse IgG_{2a} Isotype control (Sigma-Aldrich, M5409), mouse anti-tubulin (Alexa 488, IgG2a, Abcam, ab195883) and mouse anti-NF-κB p65 (IgG_{2a}, Santa cruz, sc-515045) were purchased from the corresponding distributors and used without further purification.

3.3. Synthesis of LK-2 Peptide

Synthesis of LK-2 peptide (Sequence: LKKLLKLLKKLLKLGG LKKLLKLLKKLLKLAG) was performed by Fmoc-based microwave-assisted solid-phase peptide synthesis (CEM Corporation) with Rink amide MBHA resins (Novabiochem). Firstly, 100 mg of the resins were swelled in *N*,*N*-dimethylformamide (DMF) (Samchun Chemicals, Korea) and deprotected with 20% piperidine in DMF under microwave irradiation (5 W) for 3 min. For the conjugation of each amino acid, Fmoc-protected amino acid (0.354 mmol), benzotriazole-1-yloxy-tris-pyrrolidino-phosphonium hexafluorophosphate (PYBOP) (0.354 mmol) and *N*,*N*-diisopropylethylamine (DIPEA) (0.354 mmol) were added to the resin mixture. Then, the mixture was irradiated by microwave (5 W) for 5 min for the conjugation. The deprotection-conjugation steps were proceeded until the final *N*-terminal amino acid: Fmoc-leucine. The *N*-terminal Fmoc group of the peptide was acetylated by addition of a solution of acetic anhydride (0.3 mmol) and *N*-hydroxybenzotriazole (Sigma-Aldrich) in a mixed solvent (DMF:dichloromethane = 90:10; v/v). The peptide was cleaved from the resin in the cleavage solvent (trifluoroacetic acid (TFA) : triisopropysilane : water = 95:2.5:2.5, v/v) for 2 h at room temperature. The cleaved peptides and resins were separated by filtration and the resins were washed with TFA. TFA was removed by a nitrogen gas and the peptides were precipitated with a mixed solvent (*n*-hexane:diethyl ether = 50:50, v/v). The suspension was centrifuged at 4,500 rpm for 15 min for three times. After the supernatant

was decanted, the precipitate was dissolved in dimethylsulfoxide and the peptide was purified using HPLC with a C18 column. Water and acetonitrile with 0.1% of TFA were used as the eluents.

3.4. Construction of the Expression Vector

The recombinant proteins having hexahistidine tag were designed in the pET28b vector system. For the construction of *pET28b-LK-4-Domain Z*, a synthetic gene encoding the *domain Z* of *Staphylococcal protein A* was purchased (Macrogen, Korea) and amplified by PCR using primers having *SacI* and *XhoI* restriction enzyme sites. The *LK-4* gene was obtained from the vector (*pET28b-LK-4-eGFP*) which was used in the previous study. [21] The insert gene and the vector were both digested by *SacI* and *XhoI* restriction enzymes (New England Biolabs) and they were ligated to make *pET28b-LK-4-Domain Z* using Quick Ligation Kit (New England Biolabs) following the manufacturer's protocol. For the construction of *pET28b-LK-2-Domain Z* and *pET28b-Domain Z*, unnecessary parts were removed from the *pET28b-LK-4-Domain Z* vector using blunt-end-ligation. Whole sequence of LK-4 was eliminated to produce *pET28b-Domain Z* and half of the sequence was removed to produce *pET28b- LK-2-Domain Z*. The desired parts of genes were amplified by PCR using Q5 Hot Start Master Mix (New England Biolabs) and the blunt ends were ligated using KLD Enzyme Mix (New England Biolabs). Lastly, to prepare *pET28b-LK-4-GFLG-Domain Z*, the cathepsin B-cleavable linker, GFLG, was simply

inserted between LK-4 and Domain Z using Q5 Site-Directed Mutagenesis Kit (New England Biolabs). All primer sequences for the recombinant DNA constructs are summarized in **Table 3**..

3.5. Purification of Recombinant Proteins

The recombinant proteins were expressed in *E.coli* systems. *E.Coli Rosetta (DE3) pLysS* (Novagen) was transformed with the plasmids encoding the recombinant proteins. The *E.coli* was cultured in 10 mL of luria-bertani (LB) broth with kanamycin (50 μg/mL) and chloramphenicol (35 μg/mL) for 16 h at 37℃. The culture was expanded by adding the starter culture to a 1 L of LB medium with the same concentrations of two antibiotics. The culture was incubated at 37℃ with shaking at 200 rpm for about 3 h until the OD_{600} of the culture reached 0.4 - 0.6. Isopropyl-β-thiogalactopyranoside (1 mM) was added to the media and the culture was incubated overnight at 16 ℃ with shaking at 200 rpm. The *E.coli* cells were harvested by centrifuge at 6000 rpm for 20 min at 4℃. The pellets were suspended in the lysis buffer (20 mM Tris, 500 mM NaCl, 35 mM imidazole, 0.05% Triton X-100, pH 7.0). The suspension was sonicated by the ultrasonic processor (Sonic & Materials, Inc.) and centrifuged at 15000 rpm for 40 min at 4℃. The supernatant was collected and filtered through a 0.22 μm-syringe filter. The proteins in the supernatant were purified via nickel-nitrilotriacetic acid (Ni-NTA) affinity chromatography (GE Healthcare) and

the salts were exchanged with a storage solution of 20 mM Tris, 200 mM KCl, 1 mM dithiothreitol (DTT) and 10% glycerol by Amicon centrifuge filters (Milipore; MWCO = 10kDa). The concentrations of purified proteins were measured using the Quick Bradford assay (Bio-Rad) and the proteins were stored at -20℃ in the storage solution.

3.6. Isothermal Titration Calorimetry (ITC)

ITC experiments were performed using the Affinity ITC instruments (TA Instruments, New Castle, DE, USA) at 298 K. Human IgG isotype control (Invitrogen) was prepared in Dulbecco's Phosphate-Buffered Saline (DPBS, welgene) that was degassed at 22℃ prior to measurements. For the measurement of binding between IgG and domain Z, 2.5 μL of domain Z (43 μM) was added at intervals of 200 s to the IgG solution in the cell with gentle stirring by using a micro-syringe. For the measurement of binding between IgG and LK-domain Z proteins, 2.5 μL of LK-2-domain Z (43 μM) or LK-4-domain Z (33.4 μM) was added at intervals of 200 s to the IgG solution (2.86 μM and 2.23 μM, respectively).

3.7. Fluorescent Labeling of Proteins

TAMRA Labeling of IgG - The dye 5(6)-carboxytetramethylrhodamine (5,6-TAMRA) (Sigma-Aldrich) was activated to have a succinimide group which

can react with lysines on IgG. 180 μg of 5(6)-TAMRA, 160 μg of 1-ethyl-3-(3-dimethylaminopropyl)carbodiimide (EDC) and 96 μg of *N*-hydroxysuccinimide (NHS) were added to 400 μL of DMSO and the mixture was stirred for 2 h at room temperature. 40 μL of the activated TAMRA solution was added to a solution containing 2 mg of antibodies in a 0.1 M $NaHCO_3$ buffer (pH 8.5) and stirred for another 6 h at room temperature. The excess reagents were removed using a Amicon centrifuge filter (Milipore; MWCO = 50 kDa). At the final step, the buffer was exchanged to the storage solution containing 20 mM Tris, 200 mM KCl, 1 mM DTT and 10% glycerol.

FITC labeling of CPP Proteins – The recombinant CPP proteins were labeled with fluorescein-5-isothiocyanate (FITC, Invitrogen F1906) following the manufacturer's protocol. The excess reagents were removed using an Amicon centrifuge filter (Millipore, MWCO = 10kDa). The labeled proteins were stored in a storage solution containing 20 mM Tris, 200 mM KCl, 1 mM DTT and 10% glycerol before use.

3.8. Fluorescence Anisotropy Measurement

The fluorescence anisotropy was measured with the infinite® 200 Pro instrument (Tecan, Switzerland). The binding between FITC-labeled LK-4-domain Z and human IgG isotype control (Invitrogen) was analyzed in various conditions. The concentration of the FITC-labeled LK-4-domain Z

solution was fixed at 1 μM and the concentrations of the IgG solutions were varied. The fluorescence polarization was measured at the wavelengths of 485/535nm (ex/em).

3.9. Flow Cytometry Analysis (FACS)

Cells (8×10^4 cells per well) were seeded on a 24-well plate and were incubated for 24 h. Each of LK-2 peptide or LK recombinant proteins (final concentrations 0 - 1 mM) was mixed with TAMRA-labeled antibody (final concentration 1 - 100 nM) in 100 μL of Dulbecco's Phosphate-Buffered Saline (DPBS) for 1 h in order to form the IgG/LK-Domain Z complexes. The media in the wells were removed and the cells were treated with the IgG/LK-Domain Z complexes in DMEM with 10% FBS for 24 h. Then, the cells were thoroughly washed twice with DPBS and were incubated with trypsin–ethylenediaminetetraacetic acid (EDTA) (0.25%) for 10 min at 37 ℃ to digest the proteins bound on the cell surface and to detach the cells from the plate. The detached cells were harvested with DPBS and were centrifuged at 4000 rpm for 10 min. The supernatant was removed and the pellet was re-suspended in 200 μL of DPBS containing 2% FBS. The FACS analysis was performed using the BD Accuri C6 (BD Bioscience, USA). A total of 1×10^4 cells were analyzed for each sample and dead cells were excluded by the gating strategy.

3.10. CLSM Imaging

The intracellular distribution of IgG was examined by CLSM. *HeLa* cells were seeded on confocal dish (SPL) with the density of 7.5×10^4 cells/mL and were incubated at 37 ℃, 5% CO_2 for 24 h. The cells were treated with IgG/LK-domain Z complexes for 24 h. The cells were washed twice with DPBS and treated with the Lysotracker Green DND-26 (Invitrogen). The Lysotracker was removed after 2 h and a Hoechst 33342 dye solution (Thermo Fisher Scientific) was added to the cells for another 15 min. The cells were washed thoroughly with DPBS and the images were acquired in DMEM with 10% FBS using the LSM 510 laser scanning confocal microscope (Leica TCS SP8 LIGHTNING confocal microscopy, Wetzlar, Germany). For the imaging with chloroquine, 50 μM chloroquine was treated together with IgG-LK protein complex. For the colocalization images, TAMRA-labeled IgG was mixed with FITC-labeled LK-4-domain Z. The FITC labeling was performed similar to the TAMRA labeling. For the quantitative analysis of free IgG signal, 15 images were obtained for each group and those images were analyzed with IMARIS (Bitplane, UK), the microscopy image analysis software. The total number of cells in 15 images were about 200 - 250 cells.

In addition, the specific binding affinity of anti-tubulin-Alexa 488 antibodies was also checked by CLSM. For the analysis, *HeLa* cells were fixed with a 4% paraformaldehyde solution for 20 min and then

permeabilized with 0.1% Triton X-100 for 20 min. To block the non-specific binding of the antibody, the cells were incubated in 3% bovine serum albumin (BSA) in DPBS for another 20 min. The anti-tubulin-Alexa 488 antibody were mixed with with LK-4-domain Z or with LK-4-GFLG-domain Z for the complex formation. The fixed and permeabilized cells were treated with the complexes in the 3% BSA solution for 4 h. After washing twice with DPBS, the cells were examined using the confocal microscope.

3.11. Cell Viability Assay

The toxicity of the peptide and proteins was measured using the cell counting kit-8 (CCK-8) (Dojindo, Japan). Cells (5×10^3 - 1×10^4 cells per well) in a complete cell culture media were seeded on a 96-well plate and incubated for 24 h. The cells were treated with peptide or protein samples in DMEM containing 10% FBS for 24 h. Following the incubation, the cells were washed with DPBS twice and treated with 100 μL of DMEM containing both 10% FBS and 10% CCK-8 solution. The cells were incubated in the cell culture incubator for 1 h and the absorbance at 450 nm was measured using the microplate reader (Molecular Device Co., Menlo Park, CA).

3.12. Endocytosis Inhibition Studies

HeLa cells (8×10^4 cells per well) were seeded on a 24-well plate and incubated in DMEM containing 10% FBS for 24 h. Cells were pre-treated with various endocytosis inhibitors for 2 h before IgG/LK-4-domain Z complexes were delivered: treatment of 3 mM methyl-β-cyclodextrin, 20 mM sodium azide (NaN_3), 0.45 M sucrose hypertonic media, hypo-K+ buffer condition (140 mM NaCl, 50 mM HEPES, 1 mM $CaCl_2$, 0.5 mM $MgCl_2$), 100 μM amiloride, or 50 nM wortmannin. For the inhibition study at low temperature, cells were pre-incubated at 4℃ for 2 h. IgG (20 nM)/LK4-domain Z (200 nM) complexes were treated on the cells for 3 h. After the treatment, the number of fluorescent cells was counted by FACS.

3.13. Activation of Pro-survival Genes with hTNFα Stimulation

A549 cells (10×10^4 cells per well) were seeded on a 24-well pate and were incubated at 37 °C for 24 h. The media was exchanged to 400 μL media containing human TNFα (Cell Signaling Technology (CST), 8902SC) at 20 ng/mL or 40 ng/mL. After incubation for 5 h, RNA was extracted using the EZ Total RNA Miniprep Kit (Enzynomics, Korea). 200 ng of the extracted RNA was reverse transcribed using the SuPrimeScript RT-PCR kit (GeNet Bio, Korea). SYBR green reactions were performed using TOPreal qPCR

2X premix (Enzynomics, Korea) with the BioRad CFX instrument connected with a real-time PCR equipment. The RT-PCR was performed for three genes: TRAF1, c-IAP and Bcl-xL. The primer sequences are shown in **Table 4**. The final gene expression levels were all normalized to the house-keeping gene GAPDH.

3.14. Inhibition of NF-κB-related Gene Expression

A549 cells (10×10^4 cells per well) were seeded on a 24-well plate and were incubated at 37 ℃ for 24 h. The cells were treated either with IgG/LK-4-domain Z or with IgG/LK-4-GFLG-domain Z complexes for 24 h. JSH-23 (20 μM) was used as the positive control (Sigma-Aldrich, J4455). For the complex formation, each of 300 nM mouse IgG_{2a} isotype control or anti-NF-κB IgG_{2a} was mixed with 650 nM of LK-4-domain Z or LK-4-GFLG-domain Z for 1 h. After 24 h-incubation with complexes, the cells were stimulated with hTNFα at 20 ng/mL for 5 h and RT-PCR was performed following the same protocol described above.

3.15. Inhibition of NF-κB Nuclear Translocation

A549 cells (50×10^4 cells per well) were seeded on a 6-well plate and incubated at 37 ℃ for 24 h. The cells were treated with each sample: JSH-23 (20 μM), $mIgG_{2a}$ (300nM)/LK-4-GFLG-domain Z (650nM) and anti-NF-

κB (300nM)/LK-4-GFLG-domain Z (650nM) for 24 h. Then, the cells were stimulated with hTNFα (20 ng/mL) for 5 h. The proteins in the nucleus were extracted using the NE-PER^{TM} Nuclear and Cytoplasmic Extraction Reagents (Thermo #78833) following the manufacturer's protocol. The extracted proteins from all experimental groups were quantified by Bradford assay. The same amounts of proteins from each sample were used for the ELISA assay. The amounts of nuclear NF-κB were quantified using the NF-κB p65 ELISA Kit (abcam, ab176648) following the manufacturer's protocol. The relative amount of nuclear NF-κB was calculated by linear comparison of the absorbance at 450 nm.

4. Results and Discussion

4.1 IgG binding affinity of CPP-domain Z

In our previous reports, the LK dimer (LK-2) and tetramer (LK-4) showed much higher penetration activity than the monomeric LK sequence and Tat at low nanomolar concentrations.[21] In order to add specific binding affinity on IgG into the CPP, I fused the LK-2 and LK-4 with domain Z affibody as shown in **Figure. 1A**. The amino acid sequences of domain Z, LK-2 and LK-4 are shown in **Table 1**. Owing to relatively small sizes (< 20 kDa) of all the fused proteins without glycosylation, they could be produced in the *Escherichia coli* system. The recombinant LK-domain Z proteins with the *N*-terminal His-tag were easily purified by the Ni-nitrilotriacetic acid (NTA) affinity chromatography. The protein purification was confirmed by the sodium dodecyl sulfate-polyacrylamide gel electrophoresis (SDS-PAGE) analysis.

I checked whether those recombinant proteins maintained the IgG-binding function. The binding affinity between each protein and human IgG isotype control was measured through the Isothermal Titration Calorimetry (ITC) (**Figure. 1B**). Domain Z showed the K_d value of 24.7 nM, which well corresponds to the K_d value of domain Z to the human IgG (10-50 nM) in the previous report.[22] The dissociation constants of LK-2-domain Z and

LK-4-domain Z to human IgG were measured as 51.5 nM and 124.0 nM, respectively. The LK multimers may interrupt the interaction between domain Z and IgG to slightly lower the binding affinity, however, they still possessed the strong binding affinity to human IgG at nanomolar concentrations. All the recombinant proteins showed both negative ΔH and ΔS indicating that the binding is strongly driven by the enthalpic factor from the attractive interaction between two proteins against the unfavorable entropic factor (**Table 2**).

The stoichiometry of the binding between the CPP-domain Z and IgG could be calculated from the ITC assay. The molar ratios of LK-2-domain Z/IgG and LK-4-domain Z/IgG complexes were calculated as 1.617 and 1.763, respectively. The values indicate that almost two CPP-domain Z molecules bind to one IgG molecule. The ratios are not significantly different from the molar ratio of IgG/free domain Z of 1.816. Considering that IgG has two symmetric Fc regions, each of which can be a target of domain Z, I suppose that the values are quite reasonable. [23] It is expected that both LK-2-domain Z and LK-4-domain Z can form rather homogeneous 2:1 complexes with IgG through similar binding modes of domain Z.

I examined whether binding between CPP-domain Z and IgG could be maintained in endosomal pH conditions or cytosolic reducing conditions by fluorescence anisotropy (**Figure. 3**). The data showed no significant difference among binding profiles in all treated conditions. I envisioned that the non-covalent complexes between CPP-domain Z and IgG could be

maintained in endosomes or cytosol after the endocytosis.

Meanwhile, the binding of positive-charged CPPs on IgG may interfere with the selective binding affinity of IgG on the target molecule. I checked whether anti-tubulin antibodies retain their selectivity on tubulin even after the complexation with CPP-domain Z (**Figure. 4**). The IgG/CPP-domain Z complexes showed similar binding selectivity on tubulin compared to free IgG even in presence of CPP-domain Z at 650 nM. The results support that the CPP-domain Z complexation may not interrupt the selective function of antibodies.

Our strategy for the intracellular IgG delivery is illustrated in **Figure. 2.**. I could obtain strong non-covalent complexes by simple mixing of the LK multimer-domain Z affibody and IgG even in the range of nanomolar concentrations. The powerful cell penetrating activity of the LK multimer can induce endocytosis and deliver the IgG cargos into cells at the nanomolar concentrations without dissociation.

4.2. Intracellular delivery IgG by CPP-domain Z

Before applying the CPP-domain Z as the IgG delivery carrier, I analyzed the cytotoxicity of the proteins by Cell Counting kit-8 (**Figure 5**). LK-2, LK-2-domain Z, LK-4-domain Z and domain Z were separately treated to *HeLa* (human cervical carcinoma) cells for 24 h. The short LK-2 peptide had been synthesized through the classical solid phase peptide synthesis

protocol and purified by HPLC (**Figure 6.**). None of the CPP, domain Z and the CPP-fused proteins showed notable cytotoxicity up to 1 μM.

In order to track the intracellular delivery of IgG, I labeled human IgG isotype control with (5, 6)-carboxytetramethylrhodamine (5,6-TAMRA) dye. The TAMRA-labeled IgG (20 nM) was mixed with CPP or CPP-domain Z at various concentrations. After 1 h-pre-incubation, the mixture was treated to *HeLa* cells. After 24 h-treatment, the internalization was analyzed by fluorescence-activated cell sorting (FACS) and confocal laser scanning microscopy (CLSM).

From the FACS results, I found that the free CPP, LK-2, cannot deliver IgG to cells even at 1 μM (**Figure 7**). Although LK-2 represents a hydrophobic face on a side of the α-helical bundle [24, 25] and can deliver small chemicals into cells by non-covalent complex formation, [26] it fails to deliver the extremely large and hydrophilic IgG into cells successfully. On the other hand, the delivery efficiency was dramatically enhanced by the introduction of domain Z to the LK-2 sequence. The IgG at 20 nM can penetrate into cells by complexation with LK-2-domain Z even at 20 nM.

The delivery efficiency is highly dependent upon the concentration of CPP-domain Z. I clearly observed that the penetrated amount of IgG increased in the concentration range below a certain point (~ 200 nM). However, the delivery efficiency was decreased when too much excess of CPP-domain Z was used. Since LK multimers can induce endocytosis via the interaction of heparan sulfate proteoglycan (HSPG) receptors,[21] the

excess free LK-domain Z may compete with the IgG/LK-domain Z complexes in the interaction with the HSPG receptors and this competition may result in the reduced delivery efficiency. In order to support the hypothesis, I performed the competition assay with excess amount of LK-2 peptide (**Figure 8**). The intracellular uptake of IgG was clearly interrupted in presence of the excess LK-2. LK-4-domain Z showed higher IgG delivery efficiency than LK-2-domain Z at every concentration point. Although LK-4-domain Z showed 2.4-fold lower binding affinity to IgG than LK-2-domain Z (**Figure 1B**), the greater activity of LK-4 over LK-2 on the induction of endocytosis [21] probably caused the higher efficiency of the IgG delivery.

The outstanding activity of LK-domain Z for the intracellular IgG delivery was further confirmed by CLSM imaging. Treatment of free IgG and IgG/LK-2 peptide without domain Z showed negligible TAMRA fluorescence inside the cells (**Figure 9**). On the other hand, LK-2-domain Z or LK-4-domain Z showed strong red fluorescence inside the cells by successful delivery of IgG (**Figure 9**). The red fluorescence signals of IgG were shown as puncta inside the cells. They were mainly distributed in cytoplasm, however, some of them were observed even in the nucleus labeled with Hoechst 33342 in both 2-dimensional and 3-dimensional Z-stack images (**Figure 10**). Both FACS and CLSM results confirmed the powerful activity of LK-domain Z for the intracellular delivery of IgG even when both IgG and LK-domain Z were used in low nanomolar

concentrations.

The potential of LK-4-domain Z as the IgG delivery carrier was also examined in other cell lines (**Figure 11**). LK-4-domain Z can successfully deliver IgG into *A549* (human alveolar basal epithelial cancer), *MDA-MB-231* (human breast cancer), *Caco-2* (human colorectal adenocarcinoma) and *NIH3T3* (mouse fibroblast) cells at the IgG concentration of 20 nM although the delivery activities were varied according to the cells. The delivery activity was somewhat increased in the serum-free condition. The LK-4-domain Z showed no cytotoxicity on those cells up to 1 μM. On the basis of these results, I selected *HeLa* as the representative cell line for further studies.

4.3. The domain Z-binding effect on the IgG/LK-4-domain Z complex

I have already confirmed that the delivery efficiency is clearly dependent upon the concentration of LK-domain Z (**Figure 7**). Now I also examined the dependence on the IgG concentration (**Figure. 12A**). As the IgG concentration increased, the higher cellular uptake was observed. Similar to the result in **Figure 7**, the saturation and rather decrease of cellular uptake was also observed when too much amount of LK-domain Z was added to the mixture.

I further checked whether the ratio between the IgG and LK-4-domain Z is the important factor for the delivery efficiency. I compared the delivery efficiency by varying the IgG concentrations at a fixed

concentration of LK-4-domain Z (200 nM) as well as at fixed ratios of IgG/LK-4-domain Z of 2 and 10 (**Figure. 12B**). In the graph, I could observe the general increase according the IgG concentration up to 100 nM. I re-plotted the graphs in **Figure. 12A** and **12B** in terms of the concentration of IgG/LK-domain Z complex using the dissociation constant and stoichiometry obtained from ITC (K_d=124.0 nM and LK-4-domain Z/IgG ratio = 1.763) (**Figure 13**). Remarkably, the delivery efficiency at the same concentration of IgG/LK-domain Z complex showed almost the same cellular uptakes despite the complexes were prepared at the six different mixing conditions. The result clearly demonstrates that the determining factor for the delivery efficiency is the amount of the IgG/LK-domain Z complex and that the specific interaction between domain Z and IgG at nanomolar concentrations is essential in this system.

Since the complex formation determines the delivery efficiency, I checked the effect of the complex formation time by varying time of the pre-incubation between IgG and LK-domain Z prior to the treatment on *HeLa* cells. However, there was no significant effect of the pre-incubation time on the delivery efficiency (**Figure 14**). The same efficient cellular uptake was observed even without the pre-incubation (0 min). It was predicted that IgG and LK-domain Z could form the complex within very short time in the mixture or in the extracellular matrix of cells before the endocytosis.

It was previously reported that the binding affinity of protein A of

Staphylococcus aureus is dependent upon the origins and subclasses of IgG. [27] For example, protein A is known to have strong binding affinity to human IgG_1, IgG_2 and IgG_4, medium binding affinity to mouse IgG_2 and IgG_3 and weak/none binding affinity to human IgG_3 or mouse IgG_1. [28] Since domain Z is derived from the protein A, the binding behavior of domain Z is expected to follow that of the protein A. In order to investigate the relationship between the affinity and the IgG delivery efficiency, I compared the amounts of fluorescence positive *HeLa* cells after treatment of the complexes from LK-4-domain Z (200 nM) and various types of IgG (20 nM) (**Figure 15**). The delivery efficiency followed the order: mouse IgG_{2a} ~ human IgG > rabbit IgG > mouse IgG_1. This result supports that IgGs having a weak affinity to protein A or domain Z are hard to be delivered into cells using the LK-4-domain Z protein. The species and the subclass of IgG must be considered in the intracellular delivery using the LK-domain Z protein vehicle.

Next, I examined whether the binding between domain Z and IgG is maintained after the delivery. After separate labeling of IgG and LK-4-domain Z with TAMRA and fluorescein-5-isothiocyanate (FITC), respectively, I treated *HeLa* cells with the complexes of TAMRA-IgG (20 nM) and FITC-LK-4-domain Z at various concentrations. After 24 h-incubation, I tracked the intracellular distribution of IgG and LK-4-domain Z simultaneously (**Figure 16A**). In all groups, majority of red fluorescence signals were observed as yellow co-localized signals with green

fluorescence. The results indicated that IgG was almost co-localized with LK-4-domain Z. The percentage of free or released IgG was calculated from red fluorescence intensity without the co-localization using the image analysis tool (IMARIS) (**Figure 16B**). The more LK-4-domain Z was used, the less free IgG was found inside the cells, which is quite reasonable on the basis of the domain Z-IgG binding-dissociation equilibria. The strong binding between LK-4-domain Z and IgG is maintained even after the delivery into cells. This result well corresponds with those from the fluorescence anisotropy (**Figure 3**).

4.4. The cell penetrating kinetics and mechanism of IgG/LK-4-domain Z complex

The cell penetrating kinetics of IgG/LK-4-domain Z complex was observed in this part. In the previous study with LK-4-fused enhanced green fluorescence protein (eGFP), LK-4 could induce endocytosis much more rapidly than the monomeric LK or Tat sequence.[21] The IgG/LK-4-domain Z complex also started to penetrate cells at 1 h-incubation point and the uptaken amount was gradually increased with time (**Figure 17**). In terms of fluorescence-positive cells, almost all cells could uptake IgG within 12 h. The cellular uptake profile of the IgG/LK-4-domain Z complex is quite similar to that of LK-4-eGFP at low nanomolar concentrations in the previous report.[21]

Various mechanisms including endocytosis, direct penetration and translocation through the formation of a transitory structure have been suggested even in the same CPP penetration.[13, 14, 21] In order to investigate the penetrating mechanism of the IgG/LK-4-domain Z complex, the cellular uptake of the complexes was compared under different conditions that inhibit cellular internalization: 4 ℃-incubation (energy depletion and decrease of membrane fluidity), methyl-β-cyclodextrin (methyl-β-CD, inhibition of caveolae-mediated endocytosis by extracting cholesterol), sodium azide (NaN_3, inhibition of ATP synthesis), hypertonic sucrose media (0.45 M sucrose, inhibition of clathrin-mediated endocytosis), potassium depletion (inhibition of clathrin-mediated endocytosis), amiloride (inhibition of macropinocytosis) and wortmannin (inhibition of receptor-mediated endocytosis and macropinocytosis) (**Figure 18**). [29] The inhibition profile was dependent on the concentration of LK-4-domain Z. At 40 nM of LK-4-domain Z, the cellular uptake of IgG was almost completely blocked by the 4℃ treatment and inhibited over 60 % by methyl-β-CD. The other inhibitory conditions showed no remarkable effect on the uptake at this concentration. At 200 nM of LK-4-domain Z, all the treating conditions showed certain inhibitory effects on the IgG internalization: almost complete inhibition at 4℃, 50% inhibition by methyl-β-CD, 20-30% inhibition by NaN_3, hypertonic sucrose media, amiloride and wortmannin, 10% inhibition under the potassium depletion condition.

Considering that the low-temperature treatment and methyl-β-CD

showed the highest inhibition effect on the IgG internalization but NaN_3 showed only marginal effect, I inferred that membrane fluidity might be critical to the IgG entry by LK-4-domain Z. However, at 200 nM of LK-4-domain Z, the 10-30% inhibition by other inhibitory conditions indicated the internalization might proceed through various mechanisms: macropinocytosis, clathrin/caveolae-mediated endocytosis, or energy-independent penetration mechanisms.

For the delivery strategy through the endocytosis mechanism, the endosomal escape is always a big hurdle to enter cytosol. I compared the CLSM images of *HeLa* cells treated with TAMRA-labeled IgG/LK-domain Z complexes with and without chloroquine, a well-known endosomal disruption reagent (**Figure 19**). Since the cells were stained with LysoTracker Green, the escape of IgG from endosome or lysosome could be estimated by the co-localization between red and green fluorescence. It was clear that chloroquine treatment could help the endosomal escape of IgG as shown in the reduction of yellow signals but significant amount of endosome-free IgG was observed even without the endosomal disruption reagent. As shown in the mechanism study (**Figure 18**), the energy-independent pathway in the LK-domain Z-based delivery can be one possible reason for the endosome-free IgG. From the results, I concluded that significant part of IgG delivered by the LK-domain Z vehicle could overcome the barrier of endosomal membrane.

4.5. The regulation of NF-κB signaling by intracellular delivery of antibodies

Now I tried to examine whether the delivered antibodies can specifically control an intracellular signaling pathway. I selected the regulation of nuclear factor-kappa B (NF-κB)-related signaling pathway as the proof-of-concept of this strategy. NF-κB is one of the main transcription factors that regulate inflammatory signaling pathways. [30] NF-κB exists as a complex with its inhibitor, IκBα, in cytoplasm while it is in an inactivated state. When various inflammatory signals stimulate receptors to degrade the IκBα, free NF-κB can be translocated to nucleus and induces transcription of the downstream genes.

In this study, I intended to inhibit the NF-κB pathway by using IgG targeting NF-κB (anti-NF-κB). I envisioned that the IgG-bound NF-κB is hard to penetrate across nuclear membrane and the transcription of downstream genes can be inhibited by the treatment of anti-NF-κB (**Figure 20**). When *A549* cells (adenocarcinomic human alveolar basal epithelial cells) were stimulated with human tumor necrosis factor-α (hTNFα) at concentrations over 20 ng/mL, the transcription of TNF receptor-associated factor 1 (TRAF1), cellular inhibitor of apoptosis (c-IAP) and B-cell lymphoma-extra large (Bcl-xL), three representative pro-survival genes responding to the NF-κB signaling, was greatly enhanced by 2-100 folds in

the quantification by RT-PCR (**Figure 21**).

Initially, I checked change of the transcription levels of TRAF1, c-IAP and Bcl-xL in the hTNFα-activated state by treatment of anti-NF-κB/LK-4-domain Z complexes. Here, JSH-23, a chemical compound that inhibits the translocation of NF-κB without affecting IκBα [31], was used as the positive control. However, I could not observe any significant down-regulation of transcription of TRAF1, c-IAP and Bcl-xL when I treated 300 nM of anti-NF-κB as a complex with LK-domain Z (**Figure 22**). Considering the results that the binding between domain Z and antibodies still remains (**Figure 16**) and the selectivity of antibodies are not significantly disrupted by the domain Z binding (**Figure 4**), I suspected that the positively charged LK-4 sequences bound to anti-NF-κB may interact with other cytosolic proteins to interfere with the efficient access to the target protein, NF-κB.

In order to free the delivered IgGs from the LK sequence after the internalization, I designed a new vehicle having an enzymatic cleavable linker between the LK-4 and the domain Z (LK-4-GFLG-domain Z). The glycine-phenylalanine-leucine-glycine (GFLG) sequence is known to be cleaved by cathepsin B, a cancer cell-rich lysosomal protease, and this sequence is widely used for the intracellular release of anti-cancer therapeutics. [32, 33, 34] I expected that the GFLG cleavage in *A549* cells will result an IgG/domain Z complex by the elimination of the highly-charged LK-4 sequence from the IgG/LK-4-GFLG-domain Z complex and

will help the access to NF-κB (**Figure 20**).

The activity of LK-4-GFLG-domain Z was checked before the vehicle was applied to the gene regulation study (**Figure 23**). Similar to the non-GFLG version, LK-4-GFLG-domain Z could successfully deliver human IgG to the various cell lines (*HeLa, A549, MDA-MB-231, Caco-2* and *NIH3T3*) with or without FBS. In addition, LK-4-GFLG-domain Z showed no significant toxicity up to 1 μM. LK-4-GFLG-domain Z showed no interruption to the selective binding of anti-tubulin antibodies.

When 100 nM TAMRA-labeled human IgG was delivered inside *HeLa* cells with LK-4-GFLG-domain Z and LK-4-domain Z vehicles, both of vehicles showed similar delivery efficiency (**Figure 24**). However, the intracellular distributions of TAMRA-IgG were somewhat different from each other. The IgGs delivered by LK-4-domain Z were mainly observed as puncta in restricted areas whereas those delivered by LK-4-GFLG-domain Z were distributed in much broader areas in the cytoplasm (**Figure 24A,** white arrows). I compared the fluorescence distribution more quantitatively using the image analysis program (Image J). After the fluorescence intensity at a pixel was obtained throughout a single cell and the intensity/pixel value was averaged. The averaged intensity/pixel value of each cell was plotted for the comparison of fluorescence localization in the cells treated with LK-domain Z and LK-GFLG-domain Z complexes, respectively (**Figure 24B**). In the comparison of 40 cells per group, much higher (4-fold) intensity/pixel values were obtained when IgGs were delivered with LK-4-domain Z. The

result indicated that IgGs delivered by LK-GFLG-domain Z were distributed in a 4-fold larger area compared to those delivered by LK-domain Z. I inferred that the IgGs may diffuse inside the cytoplasm more freely through the GFLG cleavage and are able to find the corresponding target molecules.

With LK-4-GFLG-domain Z in hand, I examined whether the nuclear translocation of NF-κB could be inhibited by the delivery of anti-NF-κB antibodies by the ELISA assay (**Figure 25**). With the hTNFα stimulation, the amounts of nuclear NF-κB increased about 3.3-fold, which indicated the activation of nuclear translocation of NF-κB. When treated with JSH-23, the nuclear translocation NF-κB was inhibited by 26%. When treated with anti-NF-κB/LK-4-GFLG-domain Z complexes, the translocation was inhibited more efficiently, by 69%. Interestingly, a certain level of inhibition (35%) of the NF-κB translocation was observed when the control mouse IgG_{2a} ($mIgG_{2a}$) was treated as the complex with LK-4-GFLG-domain Z (**Figure 26**)

Next, I measured the activity of anti-NF-κB delivered by LK-4-GFLG-domain Z on the NF-κB-related gene expression in *A549* cells. With the treatment of anti-NF-κB at the concentration of 300 nM as complexes with LK-4-GFLG-domain Z, the reduction by 30-50% was observed in the transcription levels of all three marker genes, TRAF1, c-IAP and Bcl-xL, compared to the vehicle only (**Figure 27**). Neither free anti-NF-κB nor non-specific $mIgG_{2a}$/LK-4-GFLG-domain Z complexes showed reduction of the

transcription level. This result clearly demonstrated the activity of intracellular anti-NF-κB for the inhibition of the NF-κB pathway.

Based on these results, it is clear that our vehicle based on LK-sequence and domain Z can actually deliver active antibodies into live cells without functional loss by simple mixing. The intracellular anti-NF-κB can be developed as future anti-inflammatory or anti-cancer drugs considering that the NF-κB pathway is closely related to the pro-survival genes controlling cancer cell proliferation. As a proof of such concept, I checked the cell viability after the treatment of anti-NF-κB on *A549* cells. Only the anti-NF-κB/LK-4-GFLG-domain Z complexes decreased the cell viability by 30% whereas none of anti-NF-κB, the vehicle or non-specific $mIgG_{2a}$/LK-4-GFLG-domain Z complexes affected the cell viability (**Figure 28**).

5. Conclusions

In this study, I proposed a new strategy for the intracellular delivery of IgG at nanomolar concentrations. Domain Z affibody with specific nanomolar binding affinity to the Fc regions and multimeric LK sequence with strong cell penetrating activity were fused together to make multimeric LK-domain Z carriers for the IgG delivery. By simple but homogeneous complexation between IgG and LK-domain Z without covalent bonding, I could successfully deliver the IgG into cells at concentrations less than 10 nM and investigate various factors influencing the delivery efficiency. The delivered IgG could actually regulate the targeted signaling pathway inside live cells as shown in the inhibition of NF-κB-related gene expression. I believe that this simple but powerful method for the intracellular IgG delivery could facilitate profound understanding of cellular mechanisms and developing future therapeutics by using the antibodies as the controlling molecules inside cells.

6. References

[1] B. Alberts, A. Johnson, J. Lewis, M. Raff, K. Roberts, P. Walter. Molecular Biology of the Cell, 4thedition, Garland Science, NewYork, USA **2002**.

[2] J. P. Landry, Y. Ke, G. Yu, X. D. Zhu, *J. Immunol Methods*. **2015**, 417, 86.

[3] T. A. Slastnikova, A. V. Ulasov, A. A. Rosenkranz, A. S. Sobolev, *Front. Pharmacol*. **2018** 9, 1208.

[4] A. C. Cuello, J. V. Priestley, C. Milstein. *Proc. Natl. Acad. Sci.* **1982** 79, 665.

[5] a) K. T. Riabowol, R. J. Vosatka, E. B. Ziff, N. J. Lamb, J. R. Feramisco, *Mol. Cell. Biol.* **1988** 8; b) V. Gire, D. Wynford-thomas. *Mol. Cell. Biol.* **1998** 18, 1611; c) Y. Ma, S. A. Prigent, T. L. Born, C. R. Monell, J. R. Feramisco, B. L. Bertolaet, *Cancer Res.* ***1999*** 59, 5341.

[6] a) R. Chakrabarti, D. E. Wylie, S. M. Schuster, *J. Biol. Chem.* **1989** 264, 15494; b) A. L. Marschall, C. Zhang, A. Frenzel, T. Schirrmann, M. Hust, F. Perez, S. Dubel, *mAbs*. **2014** 6:4, 943 ; c) S. Conic, D. Desplancq, A. Ferrand, V. Fischer, V. Heyer, B. R. San Martin, J. Pontabry, M. Oulad-Abdelghani, B. N. Kishore, G. D. Wright, N. Molina, E. Weiss, L. Tora, *J. Cell Biol.* **2017** 217:4, 1537 .

[7] B. Chatin, M. Mevel, J. Devalliere, L. Dallet, T. Haudebourg, P. Peuziat, T. Colombani, M. Berchel, O. Lambert, A. Edelman, B. Oitard. *Mol. Ther.-Nucl. Acids*, **2015** 4, e244.

[8] a) Y. Lee, T. Ishii, H. J. Kim, N. Nishiyama, Y. Hayakawa, K. Itaka, K. Kataoka. *Angew. Chem. Int. Ed.* **2010** 49, 2552; b) G. Liu, S. Ma, S. Li, R. Cheng, F. Meng, H. Liu, Z. Zhong, *Biomaterials*. **2010** 31, 7575 ; c) X. Tian. S. Nyberg. P. S. Sharp. J. Madsen. N. Daneshpour. S. P. Armes, J. Berwick, M. Azzouz, P. Shaw, N. J. Abbott, G. Battaglia. *Sci. Rep.* **2015** 5, 11990.

[9] a) H. Chiu, W. Deng, H. Engelke, J. Helma, H. Leonhardt, T. Bein. *Sci. Rep.* **2016** 6, 25019; b) Z. Song, L. Liu, X. Wang, Y. Deng, Q. Nian, G. Wang, S. Zhu, X. Li, H. Zhou, T. Jiang, X. Xu, R. Tang, C. Qin. *Chem. Commun.* **2016** 52, 1879.

[10] A. S. Narang, R. Chang, M. A. Hussain. *J. Pharm. Sci.* ***2013*** 102, 3867.

[11] F. Sousa, P. Castro, P. Fonte, P. J. Kennedy, M. T. Neves-Petersen, B. Sarmento. *Expert. Opin. Drug. Del.* **2016** 29, 1.

[12] G. Freund, A. Sibler, D. Desplancq, M. Oulad-Abdelghani, M. Vigneron, J. Gannon, M. H. Van Regenmortel, E. Weiss. *mAbs* **2013** 5:4, 518 .

[13] a) F. Madani, S. Lindberg, U. Langel, S. Futaki, A. Graslund. *J. Biophys.* **2011**; b) N. Ben-Dov, R. Korenstein. *Biochim. Biophys. Acta.* ***2015*** 1848, 869 .

[14] a) H. Derakhshankhah, S. Jafari. *Biomed. Pharmacother.* **2018** 108, 1090 ; b) T. Singh, A. S. N. Murthy, H. Yang, J. Im. *Drug Delivery.* **2018** 25, 2005 .

[15] a) S. G. Petel, E. J. Sayers, L. He, R. Narayan, T. L. Williams, E. M. Mills, R. K. Allemann, L. Y. P. Luk, A. T. Jones, Y.H. Tsai. *Sci. Rep.* **2019** 9, 6298; b) X. Chang, Y. Hou. Int. J. *Biochem. Mol. Biol*. **2018** 9, 1.

[16] a) M. Hu, P. Chen, J. Wang, D. A. Scollard, K. A. Vallis, R. M. Reilly. *Eur. J. Nucl. Med. Mol. Imaging.* **2007** 34, 368; b) S. A. Ali, S. Teow, T. C. Omar, A. S. Khoo, T. S. Choon, N. M. Yusoff. *PloS One.* **2016** 11, 1; c) J. Zhang, H. Xiong, J. Cao, S. Wang, X. Guo, B. Lin, Y. Zhang, J. Zhao, Y. Wang, T. Zhang, Q. Yuan, J. Zhang, N. Xia. *Theranostics*. **2018** 8, 549; d) B. Chen, B. F. Erlanger. *Cancer Lett*. **2006** 244, 71; e) M. Akishiba, T. Takeuchi, Y. Kawaguchi, K. Sakamoto, H. –H. Yu, I. Nakase, T. Takatani-Nakase, F. Madani, A. Graslund, S. Futaki. *Nat. Chem*. **2017** 9, 751.

[17] P. J. Hoskin, Radiotherapy in Practice – Radioisotope Therapy, Oxford University Press, UK **2007**.

[18] C. R. Behrens, E. H. Ha, L. L. Chinn, S. Bowers, G. Probst, M. Fitch-Bruhns, J. Monteon, A. Valdiosera, A. Bermudez, S. Lio-Chan, T. Wong, J. Melnick, J. Theunissen, M. R. Flory, D. Houser, K. Venstrom, Z. Levashova, P. Sauer, T. Migone, E. H. van der Horst, R. L. Halcomb, D. Y. Jackson. *Mol. Pharmaceutics.* **2015** 12, 3986 .

[19] M. C. Morris, J. Depollier, J. Mery, F. Heitz, G. Divita. *Nat. Biotechnol*. **2001**

19, 1173.

[20] B. Jansson, M. Uhlen, P. Nygren. *FEMS Immunol. Med. Microbiol*. **1998** 20, 69 .

[21] J. H. Oh, S.-E. Chong, S. Nam, S. Hyun, S. Choi, H. Gye, S. Jang, J. Jang, S. W. Hwang, J. Yu, Y. Lee. *Adv. Sci.* **2018** 5, 1800240.

[22] A. C. Braisted, J. A. Wells. *Proc. Natl. Acad. Sci*. **1996** 93, 5688.

[23] F. Yu, P. Jarver, P. Nygren. *PloS One.* **2013** 8:2, e56597.

[24] S. Jang, S. Hyun, S. Kim, S. Lee, I. Lee, M. Baba, Y. Lee, J. Yu. *Angew. Chem. Int. Ed.* **2014** 53, 10086.

[25] S. Hyun, Y. Lee, S. M. Jin, J. Cho, J. Park, C. , K. –S. Kim, Y. Lee, J. Yu. *ACS Cent. Sci*. **2018** 4:7, 885.

[26] Y. Kim, S. Hwang, R. Khalmuratova, S. Kang, M. Lee, Y. Song, J. W. Park, J. Yu, H. W. Shin, Y. Lee. *J. Control. Release*. **2020** 317, 181.

[27] S. Nohlden, Master thesis, Linkoping University, February, **2008**.

[28] GE Healthcare, Affinity Chromatography, Vol.1:Antibodies, GE Healthcare, Uppsala, Sweden.

[29] A. I. Ivanov, *Methods. Mol. Biol*. **2008** 440, 15-33.

[30] J. Napetschnig, H. Wu. *Annu. Rev. Biophys*. **2013** 42, 443.

[31] H. -M. Shin, M. -H. Kim, B. H. Kim, S. –H. Jung, Y. S. Kim, H. J. Park, J. T. Hong, K. R. Min, Y. Kim. *FEBS Lett*. **004** 574, 50.

[32] S. J. Lee, Y. Jeong, H. Park, D. H. Kang, J. Oh, S. Lee, H. C. Lee. *Int. J. Nanomed*. **2015** 10, 5489.

[33] Y. Zhong, L. Shao, Y. Li. *Int. J. Oncol*. **2013** 42, 373.

[34] D. Dheer, J. Nichlas, R. Shankar. *Adv. Drug Deliv. Rev*. **2019** 151, 130.

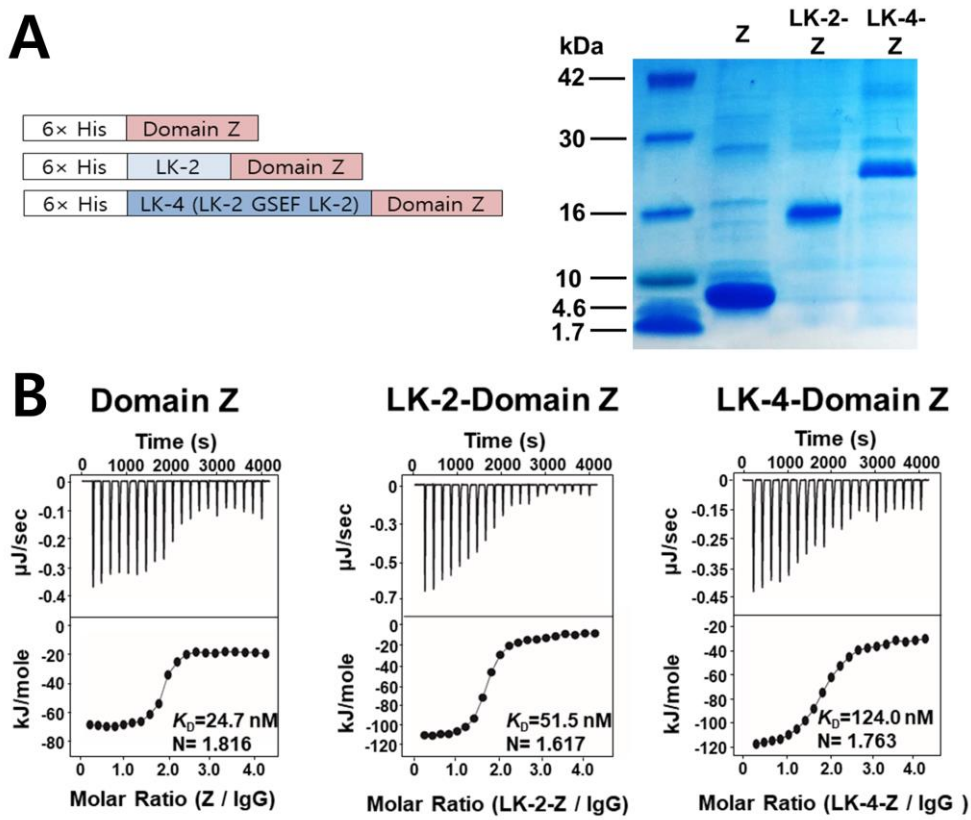

Figure 1. LK-2- and LK-4-fused domain Z for complexation and intracellular delivery of IgG. (A) The constructions of domain Z, LK-2-domain Z and LK-4-domain Z. SDS-PAGE analysis of the purified proteins: domain Z (9.4 kDa), LK-2-domain Z (13.7 kDa) and LK-4-domain Z (17.9 kDa). (B) The ITC analysis for the binding between IgG and CPP-domain Z.

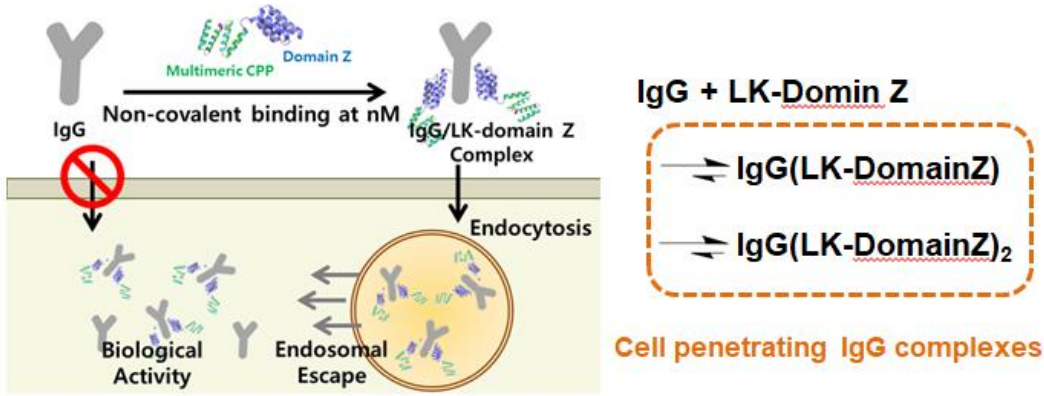

Figure 2. **Schematic diagram of LK-4-domain Z as an IgG deliver carrier.**

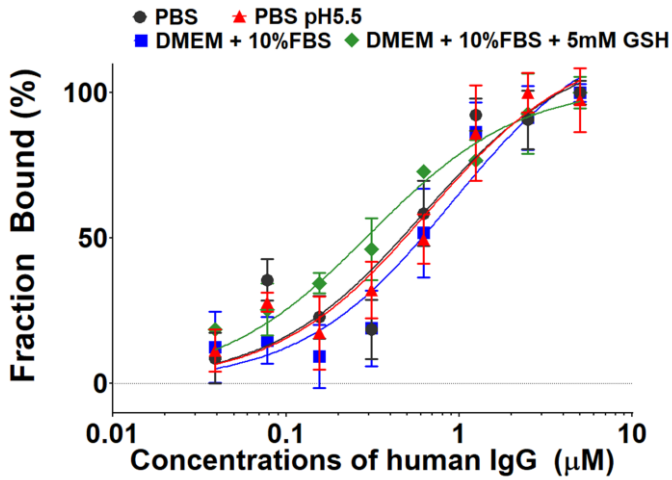

Figure 3. Fluorescence anisotropy in the binding between IgG and LK-4-domain Z. The binding between FITC-labeled LK-4-domain Z (1 μM) and human IgG isotype control at various concentrations was examined by fluorescence anisotropy. Binding properties at PBS, PBS pH5.5, culture media and culture media containing 5mM glutathione were compared. The data points are shown as the average values ± S.E.M (*n*=5).

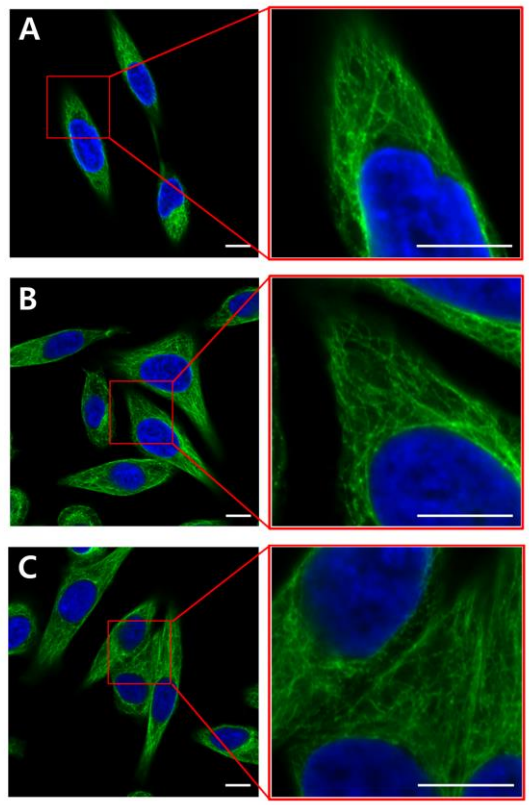

Figure 4. Retention of the selective binding affinity of anti-tubulin-Alexa488 antibodies complexed with LK-4-domain Z. *HeLa* cells were fixed and permeabilized with Triton X-100, and treated with each complex. Representative images of the cells treated with (A) free anti-tubulin-Alexa488 (20 nM), (B) the complex between anti-tubulin-Alexa488 (20 nM) and LK-4-domain Z (200 nM), and (C) the complex between anti-tubulin-Alexa488 (40 nM) and LK-4-domain Z (650 nM). Nuclei were stained as blue with Hoechst 33342. Scale bar = 10 μm.

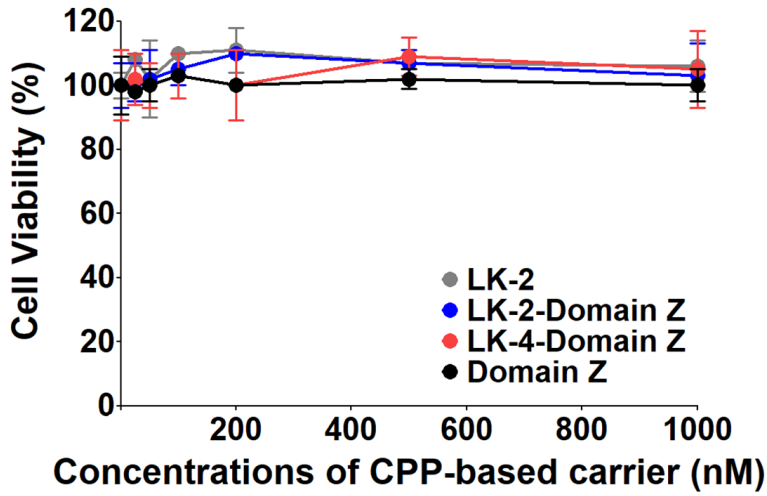

Figure 5. Cytotoxicity of LK-2 peptide, LK-2-domain Z, LK-4-domain Z and domain Z on *HeLa* cells after 24 h-incubation.

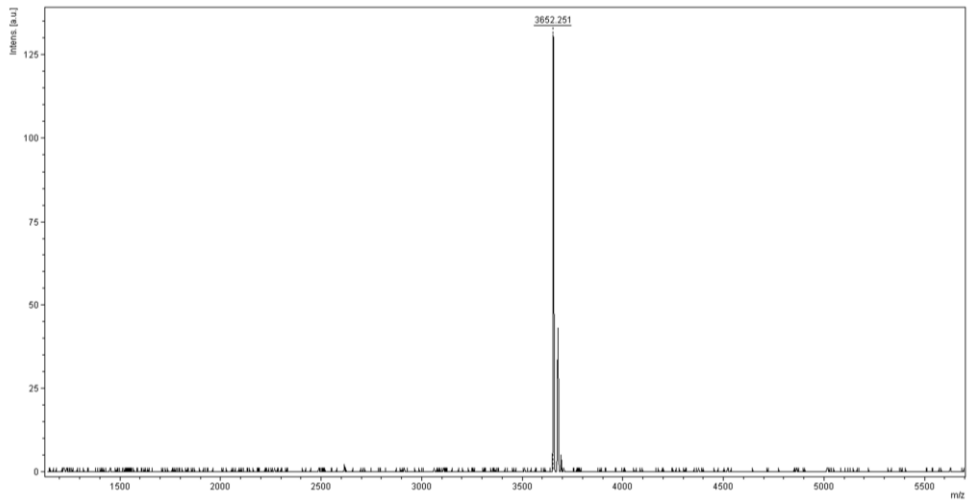

Figure 6. The MALDI-TOF MS spectrum of the LK-2 peptide without domain Z

Ac-LK-2. MS[M+H]+ : 3649.94 (calcd.), 3652.25 (found)

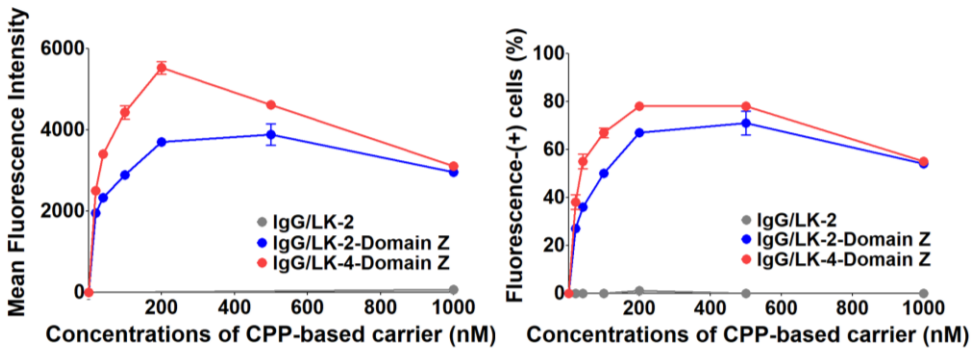

Figure 7. The cellular uptake of TAMRA-labeled IgG delivered by various CPP

FACS results of *HeLa* cells treated with the mixture of TAMRA-labeled human IgG (20 nM) and each CPP-based carrier at various concentrations for 24 h. Mean fluorescence intensity (MFI) (left) and fluorescence-positive cell percentage (right) of 10,000 cells are shown. The data points are shown as the average values ± standard deviation (n = 3).

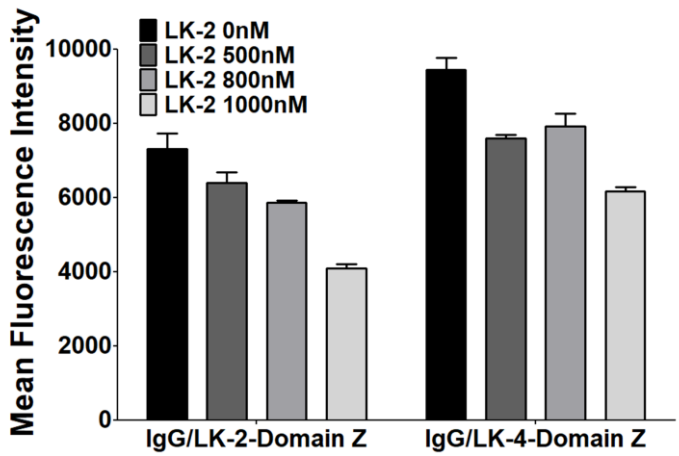

Figure 8. Competition analysis on cellular uptake of TAMRA-IgG in presence of excess amounts of LK-2 peptide. TAMRA-IgG (20 nM) was delivered either by LK-2-domain Z (200 nM) or LK-4-domain Z (200 nM) in the presence of various concentrations of LK-2 peptide. The data points are shown as the average values ± standard deviation (*n* = 3).

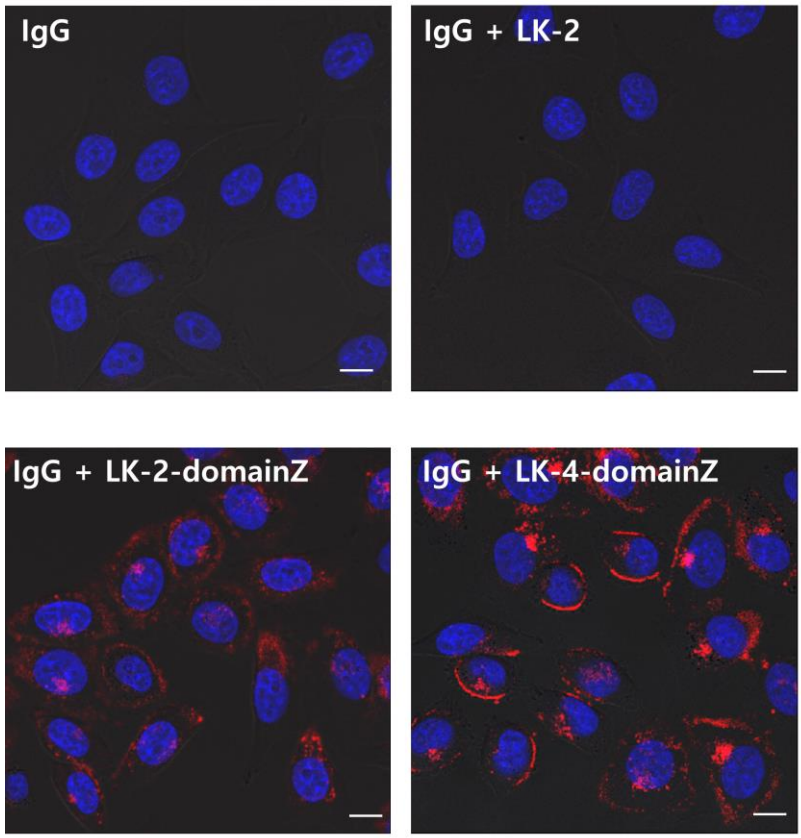

Figure 9. Representative CLSM images of *HeLa* cells treated with TAMRA-IgG only, TAMRA-IgG/LK-2, TAMRA-IgG/LK-2-domain Z and TAMRA-IgG/LK-4-domain Z complexes for 24 h. The concentrations of IgG and LK-4-domain Z were 20 nM and 200 nM, respectively. The blue fluorescence signal corresponds to the Hoechst 33342-stained nuclei. Scale bar = 10 μm. All IgG/CPP-based carrier mixtures were pre-incubated for 1 h before the treatment.

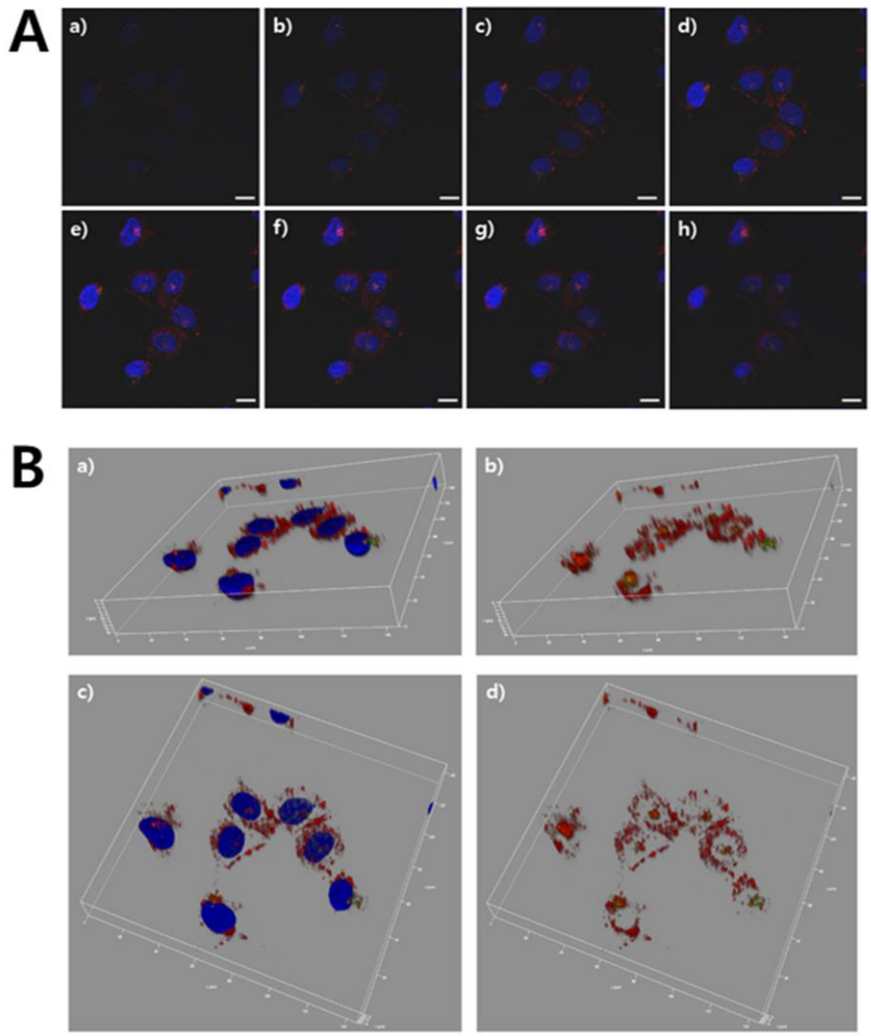

Figure 10. Representative CLSM images of *HeLa* cells treated with TAMRA-IgG/LK-4-domain Z for 24 h. The concentrations of TAMRA-IgG and LK-4-domain Z were 20 nM and 200 nM, respectively. (A) Z stack Images from bottom (a) to top (h) of *HeLa* cells treated with TAMRA-IgG/LK-4-domain Z. Nuclei were stained with Hoechst 33342. Scale bar = 10 μm. (B) 3D-reconstructed images from the Z-stack images with the view from side (a and b) and from top (c and d). Images were constructed with (a and c) and without (b and d) the Hoechst 33342 signals.

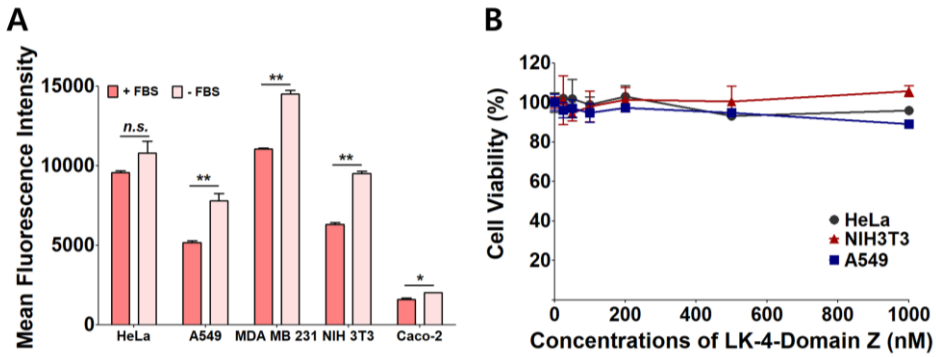

Figure 11. Delivery efficiency and cytotoxicity of LK-4-domain Z on various cell lines. (A) Cellular uptake (mean fluorescence intensity) of TAMRA-IgG (20 nM) delivered by LK-4-domain Z (200 nM) on *HeLa*, *A549*, *MDA-MB-231*, *Caco-2* and *NIH3T3* cells. TAMRA-IgG/LK-4-domain Z complexes were treated on cells for 24 h either in the presence or absence of 10% fetal bovine serum (FBS) in the media. The data points are shown as the average values ± standard deviation (n = 3). The data was analyzed using two-tailed Student's t-tests. (*) and (**) indicate $0.01 < p \leq 0.05$ and $p \leq 0.01$, respectively. *n.s.* indicates there was no significant difference. (B) Cytotoxicity of LK-4-domain Z vehicle on *HeLa*, *A549* and *NIH3T3* cells. Cells were treated with LK-4-domain Z for 24 h. The data points are shown as the average values ± standard deviation (n = 3).

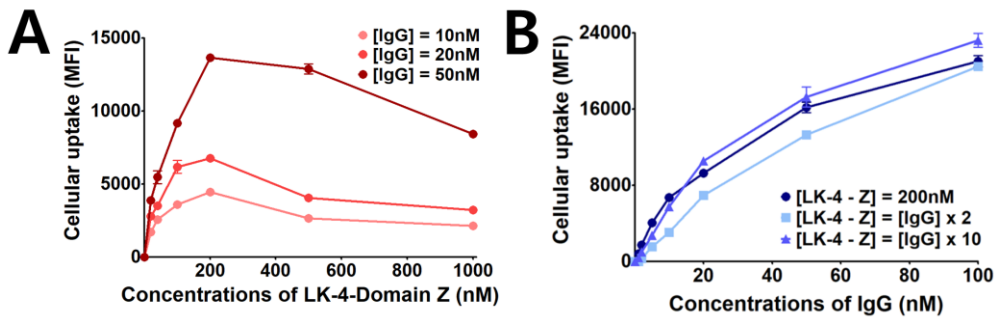

Figure 12. Effect of IgG and vehicle concentrations on delivery efficiency.

(A) Effect of IgG concentrations on the delivery efficiency. Mean fluorescence intensity (MFI) of *HeLa* cells treated with the mixture of TAMRA-labeled human IgG and LK-4-domain Z at various concentrations for 24 h. The data points are shown as the average values ± standard deviation (n =3). (B) MFI of *HeLa* cells treated with the mixture of TAMRA-labeled human IgG and LK-4-domain Z at a fixed concentration (200 nM) of LK-domain Z or at fixed IgG/LK-4-domain Z ratios (2 and 10) for 24 h. The data points are shown as the average values ± standard deviation (n =3).

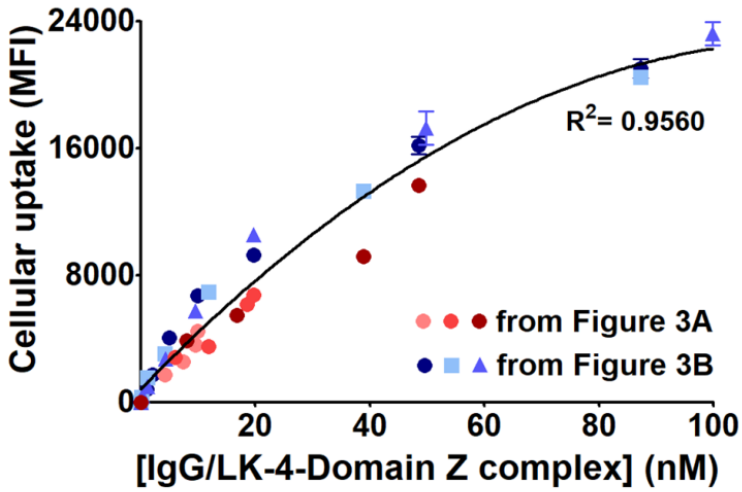

Figure 13. The relationship between the concentration of IgG/LK-domain Z complex ([IgG/LK-domain Z]) and the delivery efficiency.

The data in Figure 12A and 12B were re-plotted in terms of the complex concentration unless [LK-4-domain Z] was over 500 nM. The data points are shown as the average values ± standard deviation (*n* =3).

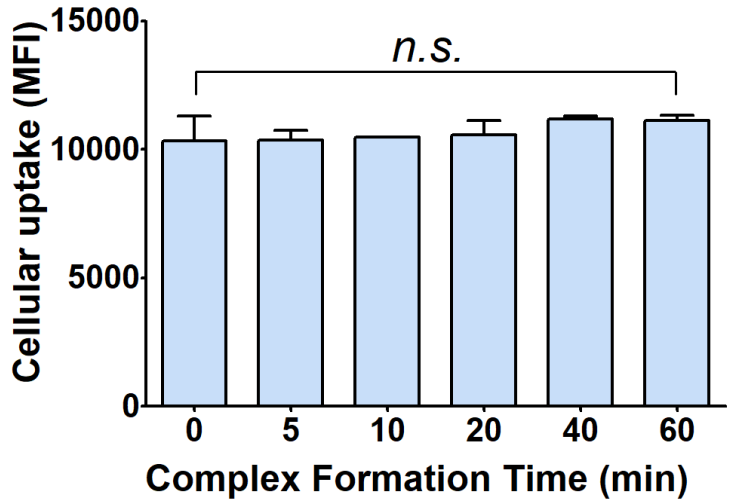

Figure 14. Effect of complex formation time on the delivery efficiency. TAMAR-human IgG (20 nM) and LK-4-domain Z (200 nM) were pre-incubated for various time and the complex was treated on *HeLa* cells for 24 h.

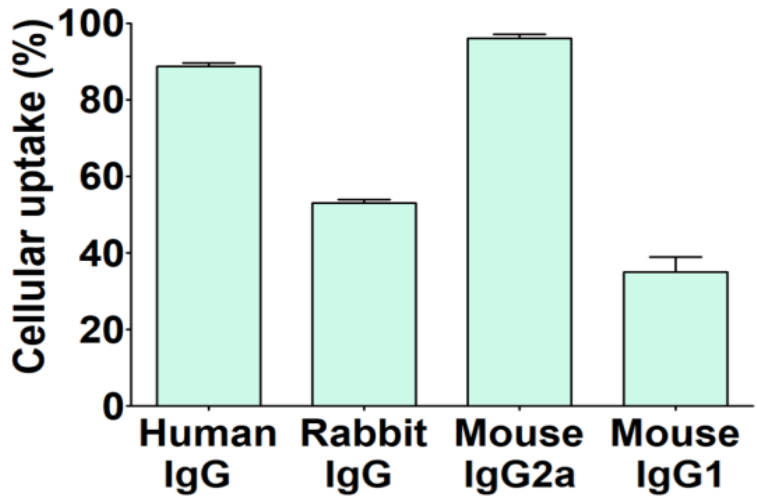

Figure 15. Effect of IgG subtypes on the delivery efficiency. Each type of fluorescent-labeled IgG (20 nM) was treated on *HeLa* cells with LK-4-domain Z (200 nM) for 24 h. The data points are shown as the average values ± standard deviation (*n* =3).

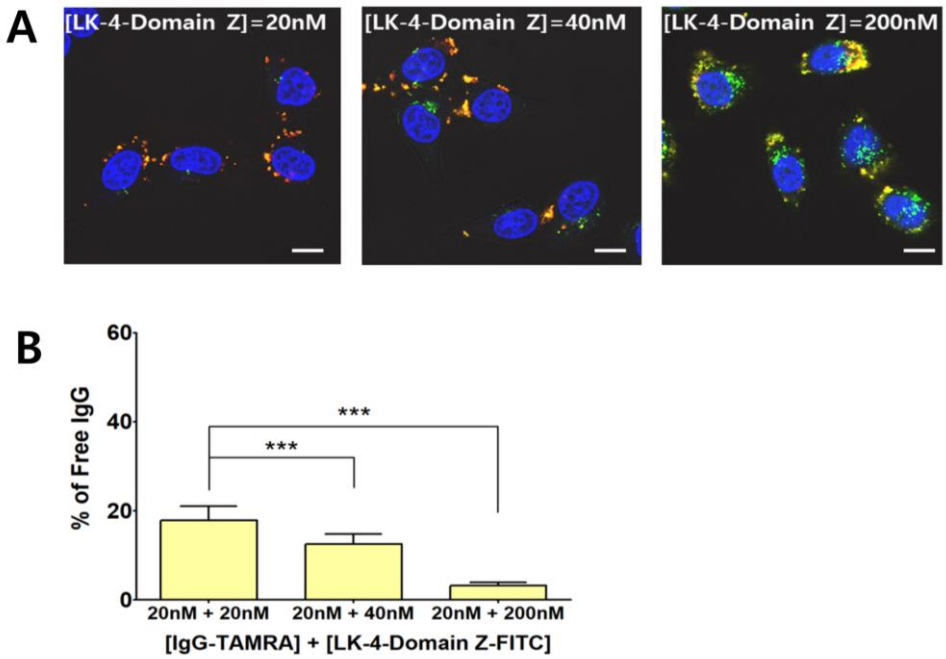

Figure 16. Intracellular distribution of IgG and LK-4-domain Z

(A) Representative CLSM images of *HeLa* cells treated with the complex between TAMRA-human IgG (red)/FITC-LK-4-domain Z complex (green) for 24 h. The concentration of TAMRA-IgG was 20 nM. The blue fluorescence signal corresponds to the Hoechst 33342-stained nuclei. Yellow fluorescence represents the co-localization of red and green fluorescence. Scale bar = 10μm. (B) Quantification of free IgG percentages calculated through the IMARIS software. 15 independent images containing approximately 200 cells were analyzed (n = 15). Without indication, all IgG/CPP-based carrier mixtures were pre-incubated for 1 h before the treatment. The data points are shown as the average values ± standard deviation. The data were analyzed using two-tailed Student's *t*-tests. (***) indicates $p < 0.001$.

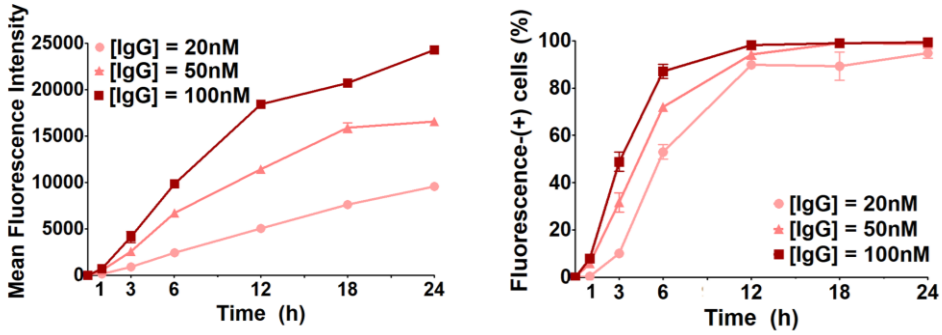

Figure 17. Cell penetrating kinetics of IgG/LK-4-domain Z complex. Cellular uptake kinetics of the TAMRA-IgG/LK-4-domain Z complexes on *HeLa* cells. Mean fluorescence intensity (MFI) (left) and fluorescence-positive cell percentage (right) of 10,000 cells are shown. The data points are shown as the average values ± standard deviation (n = 3).

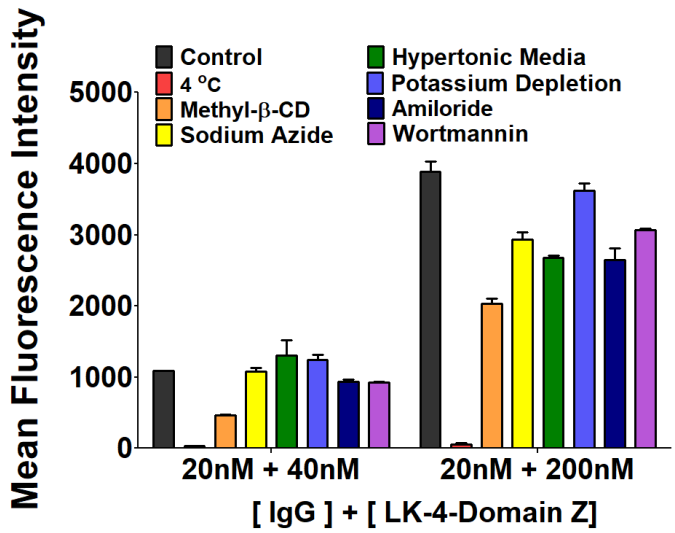

Figure 18. Cell penetration inhibition assay. *HeLa* cells were pre-treated with various inhibitory conditions for 2 h before they were treated with TAMRA-IgG/LK-4-domain Z for 3 h. PBS treated cells were used as a control. The data points are shown as the average values ± standard deviation (n = 3). Without indication, the concentrations of TAMRA-IgG and LK-4-domain Z were 20 nM and 200 nM, respectively.

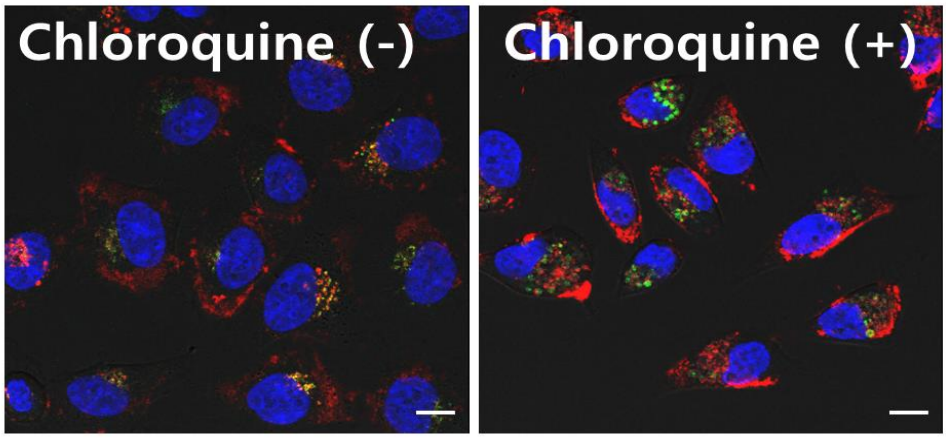

Figure 19. Representative CLSM images of *HeLa* cells treated with TAMRA-IgG/LK-4-domain Z with/without chloroquine (50 μM). Nuclei were stained as blue with Hoechst 33342 and late endosomes and lysosomes are stained as green with LysoTracker green DND-26. Scale bar = 10 μm.

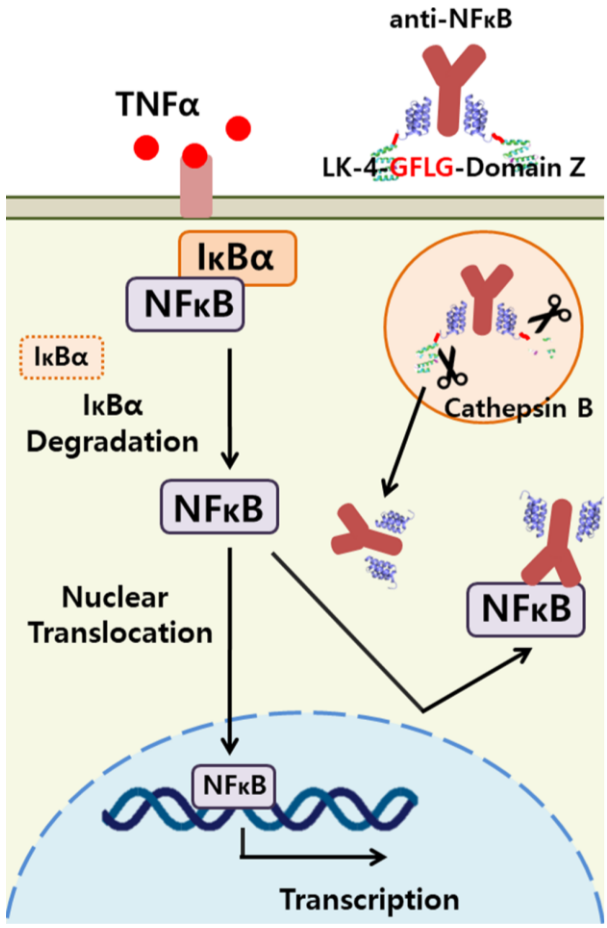

Figure 20. **Schematic diagram of NF-κB-involved signaling pathway and the strategy for the inhibition of the nucleus translocation of NF-κB by intracellular delivery of anti-NF-κB.**

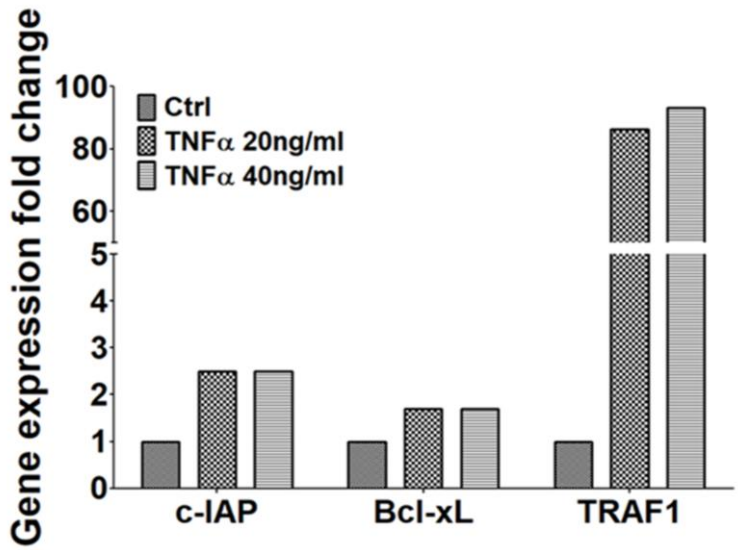

Figure 21. NF-κB driven gene expression fold change in A549 cells through TNFα stimulation. *A549* cells were stimulated with TNFα at 20 ng/mL and 40 ng/mL for 5 h and the gene expression was measured by RT-PCR using the GAPDH standard. Only PBS treatment is used as the control.

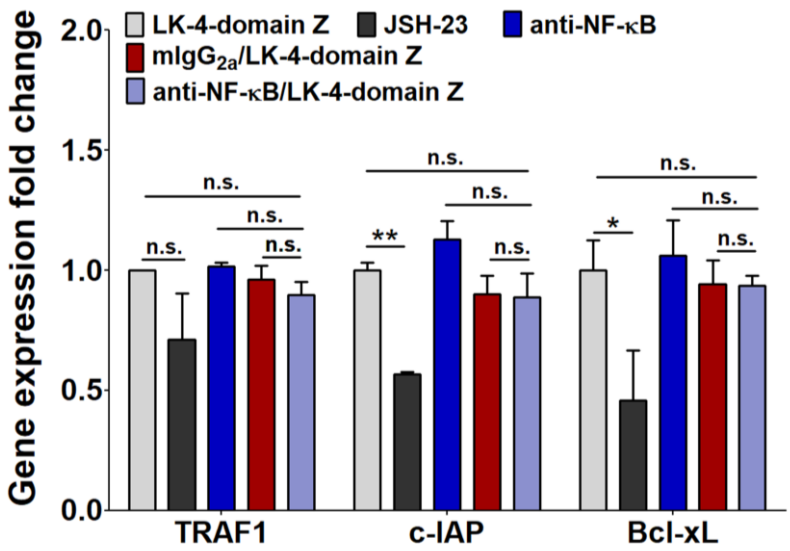

Figure 22. Change of NF-κB-related gene expression by anti-NF-κB antibodies delivered by LK-4-domain Z. *A549* cells were treated with each sample for 20 h and stimulated with hTNFα at 20 ng/mL for 5 h. Antibodies were treated at a concenetration of 300 nM as complexes with LK-4-domain Z (650 nM). The data points are shown as the average values ± standard deviation (n = 4). The data was analyzed using two-tailed Student's *t*-tests. (*) and (**) indicate $0.01 < p \leq 0.05$ and $p \leq 0.01$, respectively. *n.s.* indicates there was no significant difference.

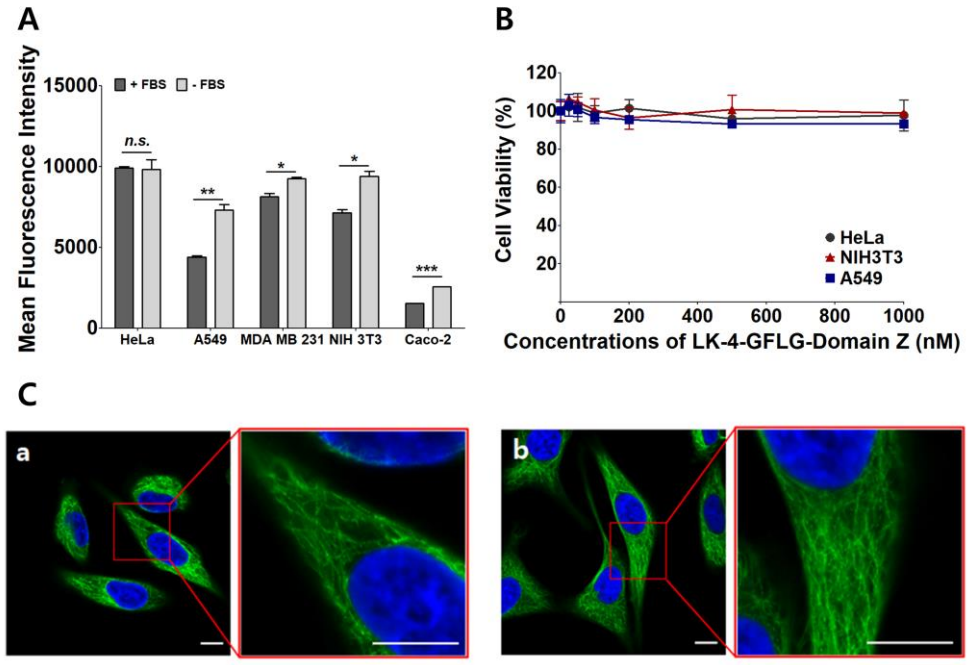

Figure 23. Characterization of LK-4-GFLG-domain Z vehicle. (A) Cellular uptake of TAMRA-IgG (20 nM) delivered by LK-4-GFLG-domain Z (200 nM) on *HeLa*, *A549*, *MDA-MB-231*,*Caco-2* and *NIH3T3* cells. TAMRA-IgG/LK-4-GFLG-domain Z complexes were treated on cells for 24 h either in the presence or absence of 10% fetal bovine serum (FBS) in the media. The data was analyzed using two-tailed Student's *t*-tests. (*), (**) and (***) indicate $0.01 < p \leq 0.05$, $p \leq 0.01$ and $p \leq 0.001$, respectively. n.s. indicates there was no significant difference. The data points are shown as the average values ± standard deviation (n = 3). (B) Cytotoxicity of LK-4-domain Z vehicle on *HeLa*, *A549* and *NIH3T3* cells. Cells were treated with LK-4-GFLG-domain Z for 24 h. The data points are shown as the average values ± standard deviation (n = 3). (C) Retention of the selective binding affinity of anti-tubulin-Alexa488 antibodies complexed with LK-4-GFLG-domain Z. *HeLa* cells were fixed and permeabilized with Triton X-100, and treated with each complex. The complex between anti-tubulin-Alexa488 (20 nM) and LK-4-GFLG-domain Z (200 nM) was used for the left image (a) and the complex between anti-tubulin-Alexa488 (40 nM) and LK-4-GFLG-domain Z (650 nM) was used for the right image (b). Nuclei were stained as blue with Hoechst 33342. Scale bar = 10 μm.

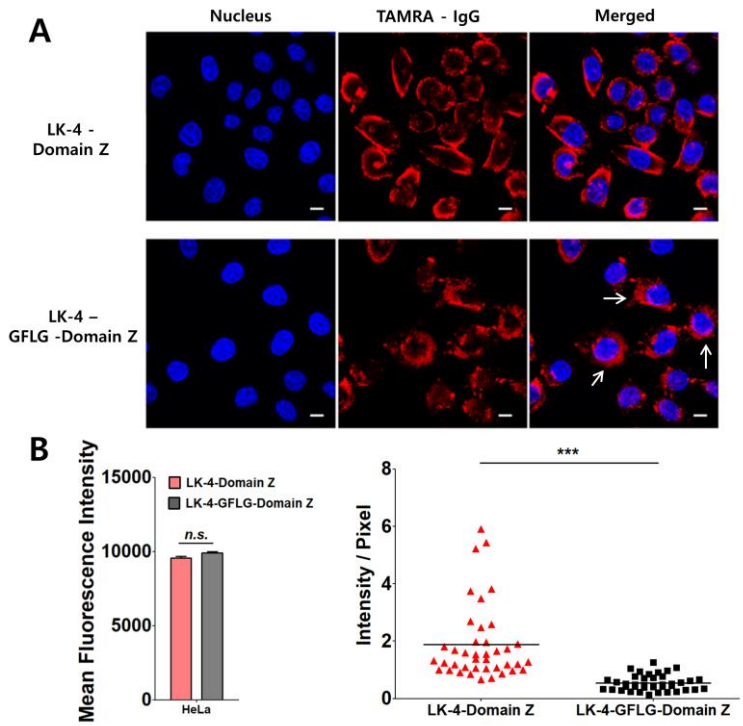

Figure 24. Comparison of IgG intracellular distribution in the delivery by LK-4-domain Z and LK-4-GFLG-domain Z. (A) Representative CLSM images of *HeLa* cells treated with TAMRA-labeled human IgG isotype control (100 nM) as the complexes either with LK-4-domain Z or LK-4-GFLG-domain Z (200 nM) for 24 h. Nuclei were stained as blue with Hoechst 33342. Scale bar = 10 μm. White arrows indicate the broader distribution of IgGs delivered by LK-4-GFLG-domain Z than those by LK-4-domain Z. (B) Comparison of the cellular uptake of TAMRA-IgG (20 nM) delivered by LK-4-domain Z and LK-4-GFLG-domain Z (200 nM) on *HeLa* cells. The cells were treated with the complexes for 24 h. The data points are shown as the average values ± standard deviation (n = 3). The data was analyzed using two-tailed Student's t-tests. *n.s.* indicates there was no significant difference. (C) Comparision of fluorescence intensity distributions in *HeLa* cells treated either with TAMRA-IgG (100 nM)/LK-4-domain Z (200nM) complex or TAMRA-IgG (100nM)/LK-GFLG-domain Z (200nM). 40 cells were randomly selected and the red fluorescence intensity at each pixel was obtained using Image J. The intensity/pixel values in each cell were averaged and indicated as red triangles (LK-4-domain Z) and black squares (LK-GFLG-doamin Z). The averaged (intensity/pixel) ± S.D values were calculated as 1.89±1.29 and 0.54±0.27 for LK-4-domain Z and LK-4-GFLG-domain Z, respectively.The data was analyzed using two-tailed Student's t-test. (***) indicates $p \leq 0.001$.

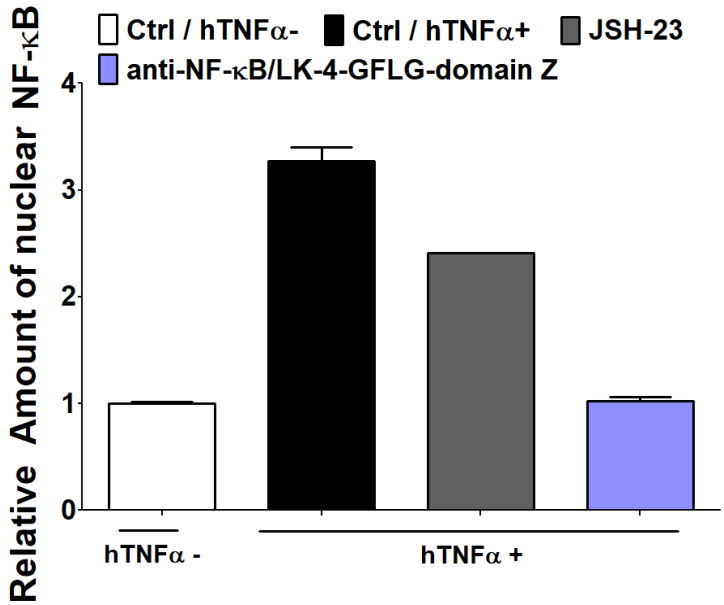

Figure 25. Comparison of NF- κB located in nucleus of *A549* cells. The amount of NF-κB was quantified by anti-NF-κB ELISA and expressed as relative amount compared to the non-activated control (hTNFα-). PBS with or without hTNFα is used as controls. The data points are shown as the average values ± standard deviation (*n* = 2).

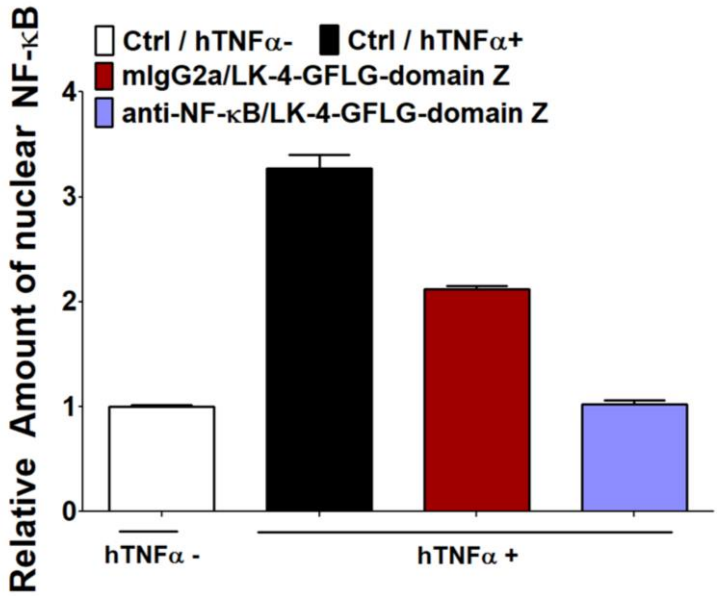

Figure 26. Comparison of NF-κB located in nucleus of *A549* cells treated with $mIgG_{2a}$ and anti-NF-κB complexed with LK-4-GFLG-domain Z. The amounts of NF-κB were quantified by anti-NF-κB ELISA and were expressed as relative amount compared to the non-activated control (hTNFα -). *A549* cells were treated with each sample at the antibody concentration of 300 nM for 20 h and stimulated with hTNFα at 20 ng/mL for 5 h. The concentration of LK-4-GFLG-domain Z was 650 nM. PBS with or without hTNFα is used as controls. The data points are shown as the average values ± standard deviation (n = 2).

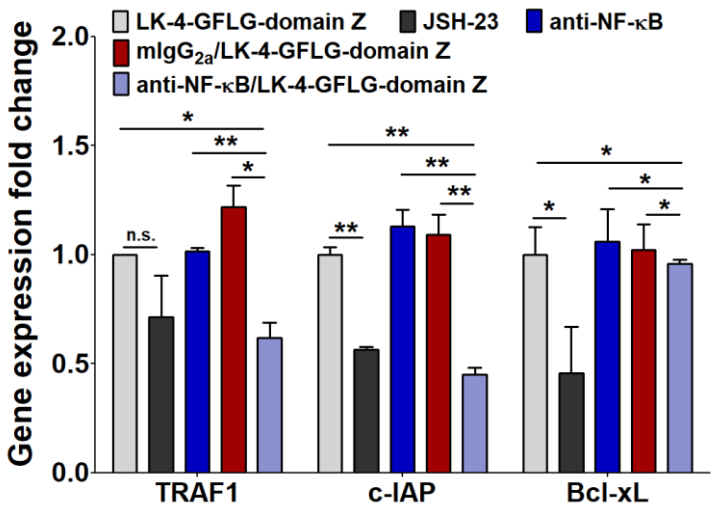

Figure 27. Changes of NF-κB-related gene expression by antibodies delivered by LK-4-GFLG-domain Z. *A549* cells were treated with each sample at the antibody concentration of 300 nM for 20 h and stimulated with hTNFα at 20 ng/mL for 5 h. The concentration of LK-4-GFLG-domain Z was 650 nM. The data points are shown as the average values ± standard deviation (n = 4). The data were analyzed using two-tailed Student's t-tests. (*) and (**) indicate $0.01 < p \leq 0.05$ and $p \leq 0.01$, respectively. *n.s.* indicates that there was no significant difference.

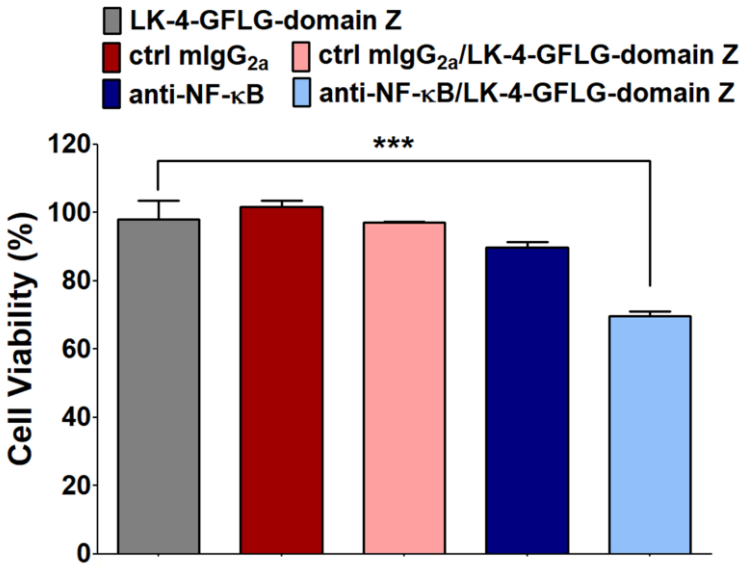

Figure 28. Cytotoxicity of anti-NF-κB on *A549* cells. Cell numbers are compared by the CCK-8 assay after 24 h-treatment of LK-4-GFLG-domain Z, mouse IgG2a isotype control (mIgG2a), anti-NF-κB, mIgG2a/LK-4-GFLG-domain Z, and anti-NF-κB/LK-4-GFLG-domain Z. The concentrations of antibody and LK-4-GFLG-domain Z were 300 nM and 650 nM, respectively. The data points are shown as the average values ± standard deviation (n = 3). The data were analyzed using two-tailed Student's t-tests. (***) indicates $p \leq 0.001$.

	Sequence
Domain Z	VDNKFNKEQQNAFYEILHLPNLNEEQRNAFIQSLKDDPSQSANL LAEAKKLNDAQAPK
LK-2	LKKLLKLLKKLLKLGGLKKLLKLLKKLLKLAG
LK-4	LKKLLKLLKKLLKLGGLKKLLKLLKKLLKLAGGSEFLKKLLKLLKKL LKLGGLKKLLKLLKKLLKLAG

Table 1. Amino acid sequences of domain Z, LK-2 and LK-4

Complex	K_d	*Binding stoichiometry (N)*	*⊿H (kJ/mol)*	△S (J/mol·K)
IgG/domain Z	24.7×10^{-9} M	1.816	-55.07	-39.07
IgG/LK-2-domain Z	51.5×10^{-9} M	1.617	-100	-195.9
IgG/LK-4-domain Z	124.0×10^{-9} M	1.763	-100	-203.2

Table 2. The ITC analysis data for the binding between IgG and CPP-domain Z.

Gene constructs	Primers (5' to 3')	Method
***Domain Z* amplifications**	For: TTCGAGCTCCGTCGAC	Gene synthesis and amplification
	Rev:GTGCTCGAGTTATTTCGGGG	
pET28b - LK-4 - Domain Z	For : TTCGAGCTCCGTCGAC	*SacI / XhoI* restriction enzyme cut and ligation
	Rev: GTGCTCGAGTTATTTCGGGG	
pET28b - LK-2 - Domain Z	For: AGCTCCGTCGACGTTG	Blunt-end ligation
	Rev: CTTGAACTCAGAGCCACCA	
pET28b - Domain Z	For: GTCGACGTTGACAACAAATTCAAC	Blunt-end ligation
	Rev: GAATTCCATATGGCTGCCG	
pET28b – LK-4-GFLG-Domain Z	For: CTTGGGAATTCGAGCTCCGTCGAC	Site Directed Mutagenesis
	Rev: GAATCCCGGATCCGAAGACTTACCA	

Table 3. Primer sequences for the recombinant DNA constructs

Gene	Primers (5’ to 3’)	
c-IAP1	For	AGGAGGTTGCAAGAAGAACG
	Rev	GGCACATTCCTGGCATACTAC
Bcl-xL	For	GGCTGCTTGGGATAAAGATG
	Rev	AGGCTTCTGGAGGACATTTG
TRAF1	For	AAGCACAGAATCCCAGATCC
	Rev	AGCTCTCCGTTTTCAAGTCG
GAPDH	For	CAACGACCACTTTGTCAAGC
	Rev	TTCCTCTTGTGCTCTTGCTG

Table 4. Primer Sequences for RT-PCR

PART II. Development of Targeted Drug Delivery Vehicle with Dimeric α-Helical Cell Penetrating Peptide and HER2-Selective Affibody

1. Abstract

I have developed a cell penetrating peptide (CPP) system with high selectivity and penetrability at nanomolar concentrations with the combination of an HER2-selective affibody, $Z_{HER2:342}$ (Z_{HER2}), and the dimeric α-helical leucine and lysine-rich peptide, LK-2. The Z_{HER2} and LK-2 are linearly fused together and expressed in the prokaryotic system to create LK-2-Z_{HER2} protein, which can successfully distinguish and penetrate HER2-overexpressing cancer cells at nanomolar concentrations. LK-2-Z_{HER2} has the ability to intracellularly deliver doxorubicin as a conjugate form to enhance its anti-cancer effect on HER2-overexpressing breast cancers with a great selectivity. The selective penetrability was confirmed *in vitro*, in 3D spheroids, and *in vivo* models. LK-2-Z_{HER2} has the capabilities to overcome the weak points of current CPPs such as poor penetrability at low concentrations and lack of selectivity, by combining powerful CPP and affibody sequences.

2. Introduction

It is a tough task for biomacromolecules to overcome the plasma membrane due to their intrinsic impermeability. Viruses, lipids, polymers and nanoparticles have been used for the intracellular delivery of difficultly penetrable molecules with successes [1, 2] but efforts to develop more efficient and selective vehicles are ongoing. Among them, cell penetrating peptides (CPPs), mostly constituted of positively charged or amphipathic amino acid sequences, can effectively deliver various cargo molecules inside the cell [3]. Compared to other delivery vehicles with sizes > 30-50 nm, the size of CPPs is only <1-2 nm and this may be beneficial to penetrate dense tissues [4,5] and also elude from the reticuloendothelial system in capturing large particles in circulation [6]. Additionally, CPP structures constructed from natural amino acids are regarded as highly biocompatible [7].

However, most CPPs can penetrate cells only at > μM, which are significantly high concentrations for large-sized cargo molecules [8, 9]. Moreover, they indiscriminately penetrate into plasma membranes irrespective of cell types although they show somewhat enhanced penetrating activity in heparan sulfate proteoglycan receptor (HSPG)-rich cells [10-12]. The high penetrating concentration and low selectivity are the main issues currently limiting clinical applications of CPPs in practice [13].

Previously, our group reported that a dimer of leucine (L) and lysine (K)-rich α-helical amphipathic peptide (LK-2 peptide:

LKKLLKLLKKLLKLGGLKKLLKLLKKLLKLAG) could largely overcome the concentration issue because it can efficiently penetrate cells at low nanomolar concentrations; this is 100-1000 times lower than those required for the penetration of the TAT peptide [14, 15]. The LK-dimer or LK-multimers can deliver small anti-cancer drugs, proteins, and even full-sized antibodies into cells at 10-100 nM [16-18]. However, the selectivity issue still exists in the penetration of the LK peptides because the penetration is highly dependent upon HSPG receptors, which are generally abundant in the plasma membrane of most cell types [15].

Meanwhile, various strategies have been applied to obtain selectivity for CPPs as well as other delivery vehicles [3]. Nanoparticular formulations with CPPs allow a certain degree of accumulation at tumor sites due to the enhanced permeation and retention (EPR) effect [19]. pH- or enzyme-responsive moieties or amino acid sequences were introduced for the selective penetration of CPPs or for the specific release of cargo molecules in the tumor microenvironments [20-22]. More directly, many small ligands recognizing target cells were conjugated to CPPs, allowing for selective penetration [23, 24]. All these methods could enhance selectivity of CPPs but the selectivity window is still narrow due to their limited discriminating abilities. Ideally, the most delicate selectivity can be obtained by using antibodies, which has a nanomolar or picomolar target binding affinity (K_d), as ligands. However, the CPP-antibody conjugation inevitably yields heterogeneous mixtures. The production of homogeneous antibody-

fused CPP requires complicated and expensive expression and purification steps [25, 26].

Here, I introduce a new active targeting-penetration strategy at nanomolar concentrations by using a fusion protein of the LK peptide and a target-selective affibody. Affibodies are small engineered proteins (~ 6 kDa) which can be easily expressed in prokaryote systems but show ability comparable to antibodies [27, 28]. Among varieties of affibodies derived from staphylococcal protein A, the affibody named $Z_{HER2:342}$ which has a very specific affinity to human epidermal growth factor receptor 2 (HER2), was described in a previous report [29, 30]. Possessing an even higher HER2-binding affinity (K_d = 22 pM) than conventional HER2-selective antibodies such as Trastuzumab, $Z_{HER2:342}$ has been chosen as a selective ligand for development of HER2-targeted drugs [31]. In this study, our strategy to obtain HER2-selective penetrating activity was to combine the LK-dimer with $Z_{HER2:342}$ (**Figure 1**). Since the LK-dimer has powerful penetrating activity at nanomolar concentrations and $Z_{HER2:342}$ has picomolar binding affinity to HER2, I expected that their combination can become an ideal example for a specific recognition-and-penetration by CPP-based pharmaceuticals.

3. Experimental Methods

3.1 Cell lines and cell culture

SKBR-3, HCC-1937, BT474 and MCF-7 cells were purchased from Korean Cell Line Bank. *SKBR-3* and *HCC-1937* cells were maintained in Roswell Park Memorial Institute Media (RPMI-1670, Welgene) with 10% fetal bovine serum (FBS) at 37˚C under 5% CO_2 condition. *BT474* and *MCF-7* cells were maintained in high glucose Dulbecco's Modified Eagle's Medium (DMEM, welgene) with 10% FBS at 37˚C under 5% CO_2 condition.

3.2 Construction of the expression vector

The recombinant proteins with a histidine tag were prepared in pET28b vector system.

Construction of pET28b-LK-2-Domain Z (Z_{wt}) and pET28b-Domain Z(Z_{wt}):

For the constuction of pET28b-LK-2-Domain Z (Z_{wt}), the synthetic gene encoding the *Domain Z* (Z_{wt}, Macrogen, Korea) was amplified by PCR using primers having *SacI* and *XhoI* restriction enzyme sites. This fragment was inserted into the vector *(pET28b-LK-2-eGFP)* from the previous study [15] after the eGFP part was removed with *SacI* and *XhoI* restriction enzymes (NEB, New England Biolabs). The ligation was carried out using Quick Ligation Kit (NEB) following the manufacturer's protocol. In order to create pET28b-Domain Z(Z_{wt}) from pET28b-LK-2-Domain Z vector, the unnecessary *LK-2* (LKKLLKLLKKLLKLGGLKKLLKLLKKLLKLAG) part was removed using blunt-end-ligation technique. The desired parts of

genes were amplified by PCR using Q5 Hot Start Master Mix (New England Biolabs) and the blunt ends were ligated using KLD Enzyme Mix (New England Biolabs).

Construction of pET28b-LK-2-$Z_{HER2:342}$, pET28b-$Z_{HER2:342}$ and pET28b-LK-2-$Z_{HER2:342}$-cys:

The plasmid having *LK-2-Z_{HER2}* was prepared through exactly the same protocol how LK-2-Z_{wt} was prepared but the synthetic gene encoding $Z_{HER2:342}$ (Macrogen, Korea) was used instead of Z_{wt}. To prepare *pET28b-$Z_{HER2:342}$*, LK-2 part was removed through blunt-end-ligation technique. The genes were amplified using Q5 Hot Start Master Mix and ligated by KLD Enzyme Mix (New England Biolabs). For *pET8b-LK-2-Z_{wt}-cys*, a cystein was inserted using site directed mutagenesis (New England Biolabs).

3.3 Purification of the recombinant proteins

The proteins were expressed in *E.coli Rosetta* (DE3) *pLysS* (Novagen). The *E.coli* was transformed with the plasmids containing the material information. The *E.coli* was resuspended in 10 mL of liquid luria-bertani (LB) broth culture with kanamycin (50 μg/mL) and chloramphenicol (35 μg/mL) for 16 h at 37℃. This 10 mL culture was transferred to 1L of fresh LB broth medium with the same concentrations of two antibiotics and the mixture was incubated at 37 ℃ with shaking for about 3 h until the culture density of OD_{600} reached 0.4-0.8. The protein expression was induced by the treatment of 1 mM isopropyl-β-thiogalactopyranoside (IPTG) and the

culture was maintained at 16℃ with a gentle shaking at 200 rpm for overnight. The *E.coli* cells were harvested by the centrifugation at 6000 rpm for 20 min at 4℃ and then were resuspended in a lysis buffer (20 mM Tris, 500 mM NaCl, 35 mM imidazole, 0.05% Triton X-100, pH 7.0). To avoid the protein degradation during the lysis step, α-toluenesulfonyl fluoride (PMSF) was added to the suspension. The suspension was sonicated by the ultrasonic processor (Sonic & Materials, Inc.) and then centrifuged at 15000 rpm and 4℃ for 40 min. The supernatant was collected and filtered using a 0.22 μm syringe filter and loaded on a nichel-nitrilotriacetic acid (Ni-NTA) affinity chromatography column (GE Healthcare). The proteins were eluted by an elution buffer. The salts in the final product were exchanged with a storage solution of 20 mM Tris, 200 mM KCl, 1 mM dithiothreitol (DTT) and 10% glycerol by the Amicon centrifuge filteration (Milipore). The concentrations of the purified proteins were calculated using the Quick Bradford assay (Bio-Rad) and the proteins were stored at -20℃ until use.

3.4. FITC-labeling of proteins

The proteins were labeled with fluorescein-5-isothiocyanate (FITC, Invitrogen F1906) following the manufacturer's protocol. Each of LK-2-Z_{wt} (3.3 mg/mL, 300 μL), LK-2-Z_{HER2} (3.3 mg/mL, 300 μL) and Z_{HER2} (3.0 mg/mL, 300 μL) was mixed with 700 μL of a 0.1 M $NaHCO_3$ buffer (pH 8.5) and the mixture was added with 100 μL of a FITC solution (1 mg/mL in DMSO). After incubation at 37 ℃ for 3 h, the excess FITC was removed

and the proteins were concentrated using a 10 KDa Amicon centrifuge filter (Millipore). The final products were stored in the solution containing 20 mM Tris, 200 mM KCl, 1 mM dithiothreitol (DTT) and 10% glycerol. The labeling degree was calculated via the following equation: Moles dye per mole protein = [A_{max} of the labeling protein / ε' × protein concentration (M)] × dilution factor, where A_{max} was the absorbance at 494 nm and ε' was the molar extinction coefficient of FITC (68,000 $M^{-1}cm^{-1}$). I adjusted the labeling degreee to 15% for each sample.

3.5. Flow cytometry analysis (FACS)

SKBR-3, HCC-1937, BT474 or *MCF-7* (1.0×10^5 cells per well) was seeded on a 24-well plate and were incubated for 24 h. In order to study the selective uptake of proteins (Figure 2A, Figure S3 and Figure S4), various concentrations of the FITC labeled recombinant proteins were treated on cells for 1 h. For the kinetic study (Figure 2C), the cellular uptake of the FITC labeled recombinant proteins at 200 nM were measured at various time points. The media were removed and the cells were thoroughly washed twice with DPBS. Cells were detached using trypsin-ethylenediaminetetraacetic acid (EDTA) (0.25%) for 10 min at 37℃ and this step could digest the proteins attached on the cell surface. Then, the detached cells were suspended in DPBS and were centrifuged at 4000 rpm for 10 min. The supernatant was removed after the centrifugation and the pellets were resuspended in 200 μL DPBS containing 2% FBS. The FACS

analysis was performed using the BD Accuri C6 (BD Bioscience, USA). A total of 1×10^4 cells were analyzed for each sample and dead cells were excluded by the gating strategy.

3.6. siRNA knockdown assay

SKBR-3 cells were seeded on a 24-well plate (1.0×10^5 cells/well) and were incubated under 37℃ and 5% CO_2 condition for 24 h.

For HER2 knockdown study, HER2 siRNA (Santa Cruz, sc-156048) was used to knockdown the expression of HER2 receptors. As a control, siRNA-A (Santa Cruz, sc-37007) was used. The siRNA-lipofectamine 2000 complexes were prepared in opti-MEM media following the manufacturer's protocol. Each of the complexes including 40pmol of siRNA in 500 μL of the culture media was treated to the cells in a well. After 48 h-treatment of siRNA, the cells were washed with PBS thoroughly. Then, 100nM, 200 nM and 500 nM of FITC-labeled LK-2-Z_{HER2} proteins were treated on the cells for 1 h. The cellular uptake was measured by the FACS analysis.

For Xylosyltransferase-1 (XylT-1) knockdown study, XylT-1 siRNA (santa cruz, sc-61817) was used to shorten the length of heparan sulfate proteoglycan and siRNA-A (santa cruz, sc-37007) was used as a negative control. The cells were treated with the complexes of 40pmol siRNA with 1μL of lipofectamine 2000 in 500μM culture media for 48 h. Then, 200 nM of FITC-labeled LK-2-Z_{HER2} proteins was treated on the knock down cells for 1 h.

The FACS analysis was performed using the BD Accuri C6 (BD Bioscience, USA). A total of 1×10^4 cells were analyzed for each sample and dead cells were excluded by the gating strategy.

3.7. Competitive blocking assay with anti-HER2 antibody

The competition assay was carried out with anti-HER2 antibody (abcam, ab201332 targeting human HER2 extracellular domain). *SKBR-3* cells were seeded on a 24-well plate (1.0×10^5 cells/well) and were incubated at 37℃ and 5% CO_2 for 24 h. The anti-HER2 antibody was pretreated on the cells at the concentration of 2 μg/mL for 3 h. Cells were thoroughly washed twice with DPBS. Then, 100nM, 200nM and 500nM of FITC-labeled-LK-2-Z_{HER2} was treated for next 1 h. The cellular uptake was measured by FACS (BD Accuri C6, BD Bioscience, USA). A total of 1×10^4 cells were analyzed for each sample and dead cells were excluded by the gating strategy.

3.8. Cellular uptake measurement on *SKBR-3* with endocytosis inhibitors

SKBR-3 cells (1.0×10^5 cells per well) were seeded on a 24-well plate and incubated in RPMI containing 10% FBS for 24 h. Cells were pre-treated with various endocytosis inhibitors for 3h and the cells were washed thoroughly twice with DPBS. Then, 200nM FITC-labeled LK-2-Z_{HER2} were treated on cells under various conditions: 3 mM methyl-β-cyclodextrin, 20 mM sodium azide (NaN_3), 0.45 M sucrose hypertonic media, hypo-K+

buffer condition (140 mM NaCl, 50 mM HEPES, 1 mM CaCl2, 0.5 mM MgCl2), or 50 nM wortmannin. For the inhibition study at low temperature, cells were pre-incubated at 4 ˚C for 3 h. The cellular uptake was analyzed via FAC analysis. A total of 1×10^4 cells were analyzed for each sample and dead cells were excluded by the gating strategy.

3.9. Confocal laser scanning microscopy (CLSM) observation of cells

Cells were seeded on a confocal dish (SPL) with the density of 1.5×10^5 cells/mL and were incubated at 37℃ and 5% CO_2 for 24 h. The cells were then treated with the samples for 1 or 24 h. The cells were thoroughly washed with DPBS for twice and the nuclei were stained with Hoechst 33342 dye (Thermo Fisher Scientific) for 15 min. The images were acquired in RPMI + 10%FBS using the confocal microscope Leica TCS SP8 X (Leica, Germany). The FITC fluorescence was detected at the excitation and emission wavelengths of 495 nm and 519 nm, respectively. The DOX fluorescence was detected at the excitation and emission wavelengths of 470 nm and 595 nm, respectively.

To obtain immunostaining images of HER2 expression levels of *SKBR-3*, *HCC-1937, BT474 and MCF-7* cells and *SKBR-3* cells treated with siRNA, the cells were fixed with 4% paraformaldehyde. The cells were thoroughly washed twice with DPBS and blocked with 3% BSA in PBS solution for 30 min. The fixed cells were labeled with anti-HER2 antibody (abcam, ab241325), followed by Donkey anti-Rabbit IgG H&L (Invitrogen, A21207)

following manufacturer's protocol. Neu siRNA (HER2 siRNA, santa cruz, sc-156048) was used to knockdown HER2 receptors and siRNA-A (Santa Cruz, sc-37007) was used as a negative control in the concentrations of 80pmol in 1mL.

3.10. Preparation of protein-DOX and protein-Cy5.5 conjugates

LK-2-Z_{HER2}-cys and Z_{HER2}-cys proteins, which possess a cysteine at each C-terminus of LK-2-Z_{HER2} and Z_{HER2}, respectively, were prepared in the *E. coli* system. Aldoxorubicin (INNO-206, AdooQ, Cat no. A12326) and sulfo-cyanine 5.5 maleimide (Lumiprobe, Cat no.27380) were used to create protein-DOX and protein-Cy5.5 conjugates, respectively. Solutions of LK-2-Z_{HER2}-cys and Z_{HER2}-cys were prepared at 100 μM in a degassed 20 mM Tris buffer (pH 7-7.5) on ice. To reduce disulfide bond, 100× molar excess of TCEP (tris-carboxyethylphosphine) was added to the protein solutions and the mixture was placed in ice bath for 20 min. Either aldoxorubicin or sulfo-cyanine 5.5 maleimide was dissolved in DMSO and 20× molar excess of the reagent was added to the mixture. The mixture was throughly mixed for overnight at 16℃. The excess aldoxorubicin or sulfo-cyanine 5.5 maleimide was removed using a 10 KDa Amicon centrifuge filter (Milipore). The final products were stored in a solution containing 20 mM Tris, 200 mM KCl, 1 mM dithiothreitol (DTT) and 10% glycerol. The labeling degree was calculated via the following equation:

$$\text{Labeling degree} = \frac{A_{max}\ of\ the\ labeling\ protein}{\varepsilon' \times protein\ concentration\ (M)} \times dilution\ factor$$

where A_{max} and ε' were the absorbance at 481 nm and 10,410 $M^{-1}cm^{-1}$ for the doxorubicin labling and those were the absorbance at 650 nm and 235,000 $M^{-1}cm^{-1}$ for the Cy5.5 labeling. The labeling degrees of doxorubicin and Cy5.5 were calculated as ~65% and 10-30%, respectively.

3.11. Cell viability assay

The cytotoxicity of each sample was measured using the cell counting kit-8 (CCK-8) (Dojindo, Japan). Both of *SKBR-3* and *HCC-1937* cells (8×10^3 per well) in RPMI+10%FBS were seeded on a 96-well plate and incubated for 24 h. The cells were treated with each sample in DMEM + 10%FBS with various concentrations for 24 h. Following the incubation, the cells were washed with PBS twice and were treated with 100 μL of DMEM + 10%FBS + 10% CCK-8. The cells were incubated in the cell culture incubator for 1 h and the absorbance at 450 nm was measured using a microplate reader (Molecular Device Co., Menlo Park, CA).

3.12. *BT474* spheroid formation and the CLSM imaging

BT474 cells were seeded in a round-bottom 96 well plate at density of 2×10^4 cells per a well and cultured for 3 days. After aspiration of culture medium, Cy5.5-labeled Z_{HER2} or LK-2-Z_{HER2} was treated at 200 μM and incubated for 1-24 h. After the incubation, the *BT474* spheroids were

washed several times with DPBS, and then fixed with 4% paraformaldehyde for 30 min. The fixed spheroid was observed by CLSM (LSM 510, Zeiss, Germany) with a Cy5.5 filter set.

3.13. Tumor xenograft model

Female Nu/Nu nude mice were purchased from Koatech Technology Corporation (Pyeongtaek, Republic of Korea). To obtain the *BT474* and *MCF-7* xenograft models, 5×10^6 cells of each cell line were mixed with Matrigel (100 μL) and subcutaneously injected into the left and right thighs of Nu/Nu nude mice, respectively. An estradiol supplement (estradiaol cypionate 1 mg/mL, 100 μL) was injected subcutaneously into the neck area to increase tumor engraftment rate.

All procedures of animal research were provided in accordance with the Laboratory Animals Welfare Act, the Guide for the Care and Use of Laboratory Animals and the Guidelines and Policies for Rodent experiment provided by the IACUC (Institutional Animal Care and Use Committee) in school of medicine, The Catholic University of Korea (Approval number: CUMS-2020-0359-01).

3.14. *In vivo* and *ex vivo* imaging

100 μL of Cy5.5-labeled LK-2-Z_{HER2} (3.75 μM) was administered intravenously into the *BT474* and *MCF-7* tumor-bearing mice. Whole body fluorescence images were taken by IVIS Lumina XRMS (PerkinElmer, Inc,

Waltham, MA, USA) with a Cy5.5 filter under respiratory anesthesia. Blood samples were collected at different time points and the fluorescence of the sample was analyzed by IVIS Lumina XRMS. Euthanasia was performed five hours post-injection and major organs and tumors were excised for *ex vivo* imaging and they were also analyzed by IVIS Lumina XRMS.

3.15. Immunofluorescence imaging of tissues

The tumor tissues excised from *BT474* tumor-bearing xenograft were fixed for 16 h with 4% paraformaldehyde, and immersed in a sucrose solution overnight. They were embedded in optimal cutting temperature (OCT) compound and stored at -80 ^{o}C. The frozen tissue was sectioned with a thickness of 10 μm, which were washed with PBS and then incubated with 20 μg/mL of CD31 antibody labeled with FITC (eBioscience, San Diego, CA, USA) for 2 h in a humidified chamber. They were counterstained with 1 μg/mL of Hoechst 33342. The sectioned tissues were observed by the CLSM (LSM 510, Zeiss, Germany).

3.16. Measuremet of acute toxicity

Blood samples (500 μL) were obtained from abdominal vena cava 24 h post intravenous injection of LK-2-Z_{HER2} (10μM in 100μL per a mouse) or saline. The plasma was isolated from the blood samples and the concentrations of alanine transaminase (ALT), aspartate transaminase (AST), alkaline phosphatase (ALP), blood urea nitrogen (BUN) and creatinine (CREA)

were measured using DRI-CHEM NX 500 (Fujifilm Corporation, Tokyo, Japan).

4. Results and Discussion

4.1. Material Designs and Overall scheme

I prepared a fusion protein (LK-2-Z_{HER2}) of the LK-dimer (LK-2) and $Z_{HER2:342}$ in the *Escherichia coli* system. The amino acid sequence of each part is summarized in **Table 1**. Successful purification of LK-2-Z_{HER2} by the histidine-tag-specific Ni-nitrilotriacetic acid (NTA) affinity chromatography was confirmed by the sodium dodecyl sulfate-polyacrylamide gel electrophoresis (SDS-PAGE) analysis (**Figure 2**). I labeled the purified proteins with fluorescein-5-isothiocyanate (FITC) and adjusted the labeling degree to 15% per protein molecule for quantitative comparison of cellular uptake.

4.2. HER2-targeted penetration ability of LK-2-Z_{HER2}

The selective cellular uptake of LK-2-Z_{HER2} was studied on HER2-overexpressing *SKBR-3* and HER2-negative *HCC-1937* human breast cancer cell lines (**Figure 3**). **Figure 4** shows the fluorescence-activated cell sorting (FACS) results after 1 h-incubation with LK-2-Z_{HER2} at various concentrations. LK-2-Z_{HER2} shows a remarkable difference in penetrating ability in the two cell lines even at 25 nM. LK-2-Z_{HER2} penetrated *SKBR-3* cells over 12-times more efficiently than *HCC-1937* cells at concentrations below 200 nM. The difference in the penetrating ability was somewhat reduced at concentrations higher than 500 nM, where LK-2-Z_{HER2} showed saturated penetration to *SKBR-3*

and started to increase the penetration probably due to the accumulation of the LK-2 sequence at such concentrations. As a control, I measured the selective penetrating activity of LK-2 fused with the wild type domain Z (LK-2-Z_{wt}), the affibody lacking the HER2 binding affinity (**Figure 5**). LK-2-Z_{wt} showed indiscriminating penetrating ability in both cells, and much lower than the uptake of LK-2-Z_{HER2} to *SKBR-3* cells. Additionally, the $Z_{HER2:342}$ affibody without the LK-2 sequence showed minimal penetrating ability to both cells (**Figure 6**).

4.3. Mechanism and kinetic studies of LK-2-Z_{HER2}

When HER2 expression was inhibited by the treatment of HER2-siRNA (**Figure 7**), the penetration of LK-2-Z_{HER2} to *SKBR-3* cells remarkably decreased by 37%-77% (**Figure 8**). Additionally, when the HER2 receptors were sterically blocked by an anti-HER2 antibody, the penetrating ability was similarly inhibited by 58%-70% (**Figure 9**). The results clearly support that the amount of HER2 receptors at the cell surface and the binding of LK-2-Z_{HER2} to the receptor were the key factors determining the selective enhancement of the penetrating ability to *SKBR-3* cells.

The uptake mechanism of LK-2-Z_{HER2} was further investigated in *SKBR-3* cells treated with various endocytosis inhibiting conditions [32]: 4˚C-incubation (energy depletion and reduction of membrane fluidity), NaN_3 (inhibition of ATP synthesis), methyl-β-cyclodextrin

(inhibition of caveolae-mediated endocytosis), hypertonic sucrose media or K^+-depletion (inhibition of clathrin-mediated endocytosis), wortmannin (inhibition of receptor-mediated endocytosis and micropinocytosis) (**Figure 10**). The results indicate that energy and membrane fluidity are critical for the entry of LK-2-Z_{HER2}, and the endocytosis mechanism is quite complicated including caveolae- or clathrin-mediated endocytosis. Since HSPG receptors mediate the endocytosis of many cationic CPPs including LK-2 [10-12 14-18], I also compared the uptake of LK-2-Z_{HER2} into *SKBR-3* cells with or without the treatment of xylosyltransferase-1 siRNA, which inhibits the elongation of heparan sulfate on cell membrane [33, 34] (**Figure 11**). The cellular uptake significantly decreased in HSPG-immature cells, implying the endocytosis mediated by HSPG binding.

The penetrating kinetics of LK-2-Z_{HER2} also provided a clue for the mechanism of selective entry (**Figure 12**). While the penetration of LK-2-Z_{HER2} to *HCC-1937* cells was rather slow and took several hours, the penetration to *SKBR-3* cells was very rapid and almost saturated within 1 h. The picomolar HER2-binding affinity of $Z_{HER2:342}$ might increase the concentration of the LK sequence on the plasma membrane and accelerate the HSPG-mediated induction of endocytosis at low concentrations. The rapid induction of endocytosis at such low concentrations would be beneficial for the selective delivery of drugs *in vivo*, where dilution in physiological fluids is significant and the

residual time on the target tissue is short during rapid circulation [35, 36].

The intracellular distribution of LK-2-Z_{HER2} was visualized using confocal laser scanning microscopy (CLSM). The green fluorescence from FITC-labeled proteins was observed as dots inside the plasma membrane (**Figure 13**). The discrete non-diffused localization of LK-2-Z_{HER2} was similar to the intracellular distribution of LK-4-Z_{wt} in our previous report [18]. Although amphipathic CPPs such as the LK sequence generally show only marginal endosomal escape ability, significant portions of the LK-fused proteins were observed in cytosolic parts after the uptake. The positively charged LK sequence might interact with cytoplasmic proteins and interfere with free diffusion of LK-2-Z_{HER2} inside cells [18].

4.4. LK-2-Z_{HER2} as HER2-overexpressed cell targeted drug delivery vehicle

As a proof-of-concept for the selective drug delivery to HER2-positive breast cancer cells, I prepared a conjugate between LK-2-Z_{HER2} and doxorubicin (DOX), a well-known anti-cancer drug (**Figure 14**). In order to form a non-random homogeneous conjugate, I added a cysteine residue at the *C*-terminus of LK-2-Z_{HER2}. Aldoxorubicin, an FDA-approved prodrug of DOX which possesses a maleimide group for the cysteine conjugation and a cleavable hydrazone linker for the release of

free DOX [37], was successfully conjugated to the *C*-terminus of LK-2-Z_{HER2} via a thioether bond to produce LK-2-Z_{HER2}-DOX. The conjugation efficiency of doxorubicin conjugates was calculated as ~63% per protein and the mixtures of the protein vehicles (LK-2-Z_{HER2}) and the conjugates (LK-2-Z_{HER2}-DOX) were used in subsequent studies.

Figure 15 shows the CLSM images of *SKBR-3* and *HCC-1937* cells treated with LK-2-Z_{HER2}-DOX at the DOX concentration of 200 nM. The DOX fluorescence can be visualized as red fluorescence (λ_{max} = 595 nm) with the excitation at 470 nm. The DOX fluorescence was hardly detected in *HCC-1937* cells whereas significantly higher level of the DOX fluorescence was found in *SKBR-3* cells. This meant that LK-2-Z_{HER2} could deliver the conjugated DOX to HER2-positive cells with selectivity.

The toxicity of LK-2-Z_{HER2}-DOX was compared to that of free DOX, LK-2-Z_{HER2} and Z_{HER2}-DOX by the CCK assay. Free DOX showed only marginal toxicity (> 80% viability) up to 200 nM and ~70% viability at 1 μM on both of *SKBR-3* and *HCC-1937* cells (**Figure 16**). The IC_{50} values of free DOX were calculated as 2.81 μM and 3.47 μM for *SKBR-3* and *HCC-1937*, respectively. DOX-free LK-2-Z_{HER2} showed negligible toxicity up to 20 μM on both cell lines (**Figure 17**). In addition to this, neither part of the vehicle alone (LK-2 nor Z_{HER2}) showed notable toxicity on both cell lines (**Figure 18**). On the other hand, LK-2-Z_{HER2}-DOX showed a remarkable difference in toxicity

between the two cell lines (**Figure 16**). The viability of *SKBR-3* cells treated with LK-2-Z_{HER2}-DOX was below 60% even at 25 nM and dropped to below 20% at 200 nM, whereas that of *HCC-1937* cells was maintained in the range of 60-70% up to 200 nM. The IC_{50} values of LK-2-Z_{HER2}-DOX on *SKBR-3* and *HCC-1937* were calculated as 75 nM and 442 nM, respectively. The comparison of toxicity between LK-2-Z_{HER2} and LK-2-Z_{HER2}-DOX (**Figure 18**) implied that the selective toxicity was caused by the delivery of DOX by the LK-2-Z_{HER2} vehicle. Z_{HER2}-DOX, which lacks the LK-2 sequence, showed slightly higher toxicity than free DOX on both cells (**Figure 19**). However, on *SKBR-3* cells, the cytotoxic effect of Z_{HER2}-DOX was much lower than LK-2-Z_{HER2}-DOX. Additionally, non-covalent mixtures of LK-2-Z_{HER2} and DOX showed similar cytotoxicity to that of free DOX (**Figure 20**). These results clearly indicated that both selective targeting and penetration ability of the DOX conjugates are important to selective toxicity on HER2-overexpressing cells.

4.5 Selective penetration into HER2-overexpressing spheroids

The combination of LK-2 and Z_{HER2} can enable the vehicle to recognize HER2 and to penetrate the cells. Indeed, LK-2-Z_{HER2} showed similar selectivity to other cell types according to the HER2 expression. LK-2-Z_{HER2} showed selective penetration to another HER2-overexpressing cell line, *BT474*, whereas only minimal penetration to

HER2-negative *MCF-7* cell line (**Figure 21**). LK-2-Z_{wt} showed similar low uptake efficiency on both cells. Since it was difficult to generate the mouse xenograft model with *SKBR-3* and *HCC-1937* cells [38], I instead used *BT474* and *MCF-7* cells for the *in vivo* and spheroid experiments as below.

I could show another critical merit of the combination between LK-2 and Z_{HER2} in the spheroid model. Although Z_{HER2} showed the selective binding on the surface of the spheroid of *BT474*, it was difficult to penetrate into the deep center of the spheroid even after 24 h (**Figure 22A**). On the contrary, LK-2-Z_{HER2} could efficiently penetrate into the inner part of the spheroid. When the spheroid was treated with sulfo-cyanine5.5 (Cy5.5)-labeled LK-2-Z_{HER2}, 1.5-3.0 times higher fluorescence was observed in the CLSM image compared to that treated with Cy5.5-labeled Z_{HER2} during the 1-24 h incubation period (**Figure 22B)**. Three-dimensional spheroid with a diameter of over 500 μm is considered as a close mimicry of a cancerous tissue [39, 40]. Therefore, I could expect that the CPP-affibody combination might have a great potential to enhance the therapeutic effect of drugs on thick tumor tissues resulting from selective recognition and penetration into the tissue.

4.6 *in vivo* biodistribution of LK-2-Z_{HER2}

Finally, I confirmed whether LK-2-Z_{HER2} could selectively target HER2(+) cancer *in vivo*. A tumor xenograft model was generated by subcutaneous injection of HER2(+) *BT474* and HER2(-) *MCF-7* human breast cancer cells to each thigh of Nu/Nu mice. Cy5.5-labeled LK-2-Z_{HER2} was intravenously injected to the mice and the fluorescence images were obtained by an *in vivo* imaging system (IVIS) at each time point after the injection (**Figure 23**). Significant accumulation of LK-2-Z_{HER2} was observed in the *BT474* tumor after 1 h. Since negligible accumulation was observed in the *MCF-7* tumor, I confirmed that Z_{HER2}-based active targeting actually worked in this system over the EPR effect-based passive targeting which could not distinguish the two tumor tissues. The higher Cy5.5-fluorescence intensity in *BT474* tumor over *MCF-7* tumor was also clearly observed in a CLSM image of the tissue slices of the harvested tumors (**Figure 24**). Particularly, the fluorescence of the Cy5.5-labeled LK-2-Z_{HER2} was not confined near the CD31-stained blood vessels (green) but widely distributed in the deeper tumor tissue, which confirmed its efficient tissue penetration *in vivo* (**Figure 25**).

The LK-2-Z_{HER2} system is a rare example of selective CPPs which can be simply expressed in the prokaryotic system without requiring any additional chemical reactions. Although the combination of Z_{HER2} and TAT was reported for the delivery of plasmid DNA at micromolar

concentrations in a previous study [41], LK-2-Z_{HER2} has demonstrable advantages in nanomolar working concentrations. However, there still are some weak points of LK-2-Z_{HER2} that should be overcome before practical *in vivo* applications. The half-life of the intravenous injected LK-2-Z_{HER2} in blood was below 2 h (**Figure 26**). And significant accumulation in liver and kidney was also observed in the biodistribution, possibly causing some side effects (**Figure 27**). The highly permanent positive charges from lysine residues might be one of the main reasons to provoke rapid removal from the circulation by the reticuloendothelial system or aggregation with negatively charged serum proteins [20, 42]. Introduction of inducible positive charges nearby tumor tissues could be suggested as a way to address the pharmacokinetics [20]. Meanwhile, although LK-2-Z_{HER2} showed a significant accumulation in some organs, the plasma analysis of mice after 24 h post intravenous injection of LK-2-Z_{HER2} indicated acute systemic toxicity was negligible in this stage (**Table 3**). Chronic toxicity of this vehicle may be investigated in future study.

5. Conclusions

I developed a new targeting strategy based on a selective CPP-based delivery vehicle mounted with an affibody. Importantly, the whole molecule can be easily produced in a prokaryotic expression system. Using the combination of LK-2 and Z_{HER2} affibody, I obtained LK-2-Z_{HER2}, which exhibits selective recognition and penetration on HER2(+) cells at nanomolar concentrations. The CPP-affibody conjugate can have clear advantages over other activatable CPPs due to its targeting accuracy, and also over the CPP-antibody conjugate for the production process. Along with further development of affibodies targeting other biomolecules, various CPP-affibody conjugates which are able to recognize and penetrate specific target cells could be available by substituting the affibody part. Intracellular biomolecules in a specific target cell can be selectively accessed for biomedical uses by this platform system with macromolecular pharmaceuticals.

6. References

[1] Y. H. Chung, H. Cai and N. F. Steinmetz, *Adv. Drug Delivery Rev.* **2020**, 156, 214-235

[2] E. W. Neuse, *Met. –Based Drugs.* **2008**, 469531

[3] G. C. Kim, D. H. Cheon and Y. Lee, *Biochim. Biophys. Acta, Proteins Proteomics*. **2021**, 1869, 140604

[4] S. Hyun, Y. Lee, S. M. Jin, J. Cho, J. Park, C. Hyeon, K. Kim, Y. Lee and J. Yu, *ACS Cent. Sci.* **2018**, 4, 885-893

[5] D. Raucher and J. S. Ryu, *Trend Mol. Med.* **2015**, 21, 9, 560-570.

[6] J. Baas, N. Senninger and H. Elser, *Z. Gastroenterol.* **1994**, 32(2), 117-123.

[7] J. Habault and J. Poyet, *Molecules.* **2019**, 24, 927-943.

[8] S. W. Jones, R. Christison, K. Bundell, C. J. Voyce, S. M.V. Brockbank, P. Newham and M. A. Lindsay, *Br. J. Pharmacol.* **2005**, 145, 1093-1102

[9] S. G. Patel, E. J. Sayers, L. He, R. Narayan, T. L. Williams, E. M. Mills, R. K. Allemann, L. Y. P. Kuk, A. T. Jones and Y. Tsai, *Sci. Rep.* **2019**, 9, 6298.

[10] H. C. Christianson and M. Belting, *Matrix. Biol.* 2014, **35**, 51-55

[11] C. Chen, K. Tsai, P. Kuo, P. Chang, W. Wang, Y. Chuang and M. D. Chang, *Biomed. Res. Int.* **2015**, 237969

[12] A. Wittrup, S. Zhang and M. Belting, *Methods Mol. Biol.* **2011**, 683, 99-115.

[13] S. Reissmann, *J. Pept. Sci.* **2014**, 20, 760-784

[14] S. Jang, S. Hyun, S. Kim, S. Lee, I. Lee, M. Baba, Y. Lee and J. Yu, *Angew. Chem. Int. Ed.* **2014**, 53, 10086-10089

[15] J. H. Oh, S. –E. Chong, S. Nam, S. Hyun, S. Choi, H. Gye, S. Jang, J. Jang, S. W. Hwang, J. Yu and Y. Lee, *Adv. Sci.* **2018**, 5, 100840.

[16] Y. Kim, S. Hwang, R. Khalmuratova, S. Kang, M. Lee, Y. Song, J. Park, J. Yu, H. Shin and Y. Lee, *J. Control. Release.* **2020**, 317, 181-194

[17] S. H. Nam, Y. Lee, J. H. Ahn, C. K. Chung, H. Yang, S. Jang and S. B. Park, *Eur. J. Pharm. Sci.* **2020**, 144, 105210

[18] S. –E. Chong, J. H. Oh, K. Min, S. Park, S. Choi, J. H. Ahn, D. Chun, H. H. Lee, J. Yu and Y. Lee, *J. Control. Release.* **2021**, 330, 161-172.

[19] L. A. Bennie, H. O. McCarthy and J. A. Coulter, *Cancer Nanotechnol.* **2018**, 9, 10.

[20] S. H. Nam, J. Jang, D. H. Cheon, S. –E. Chong, J. H. Ahn, S. Hyun, J. Yu and Y. Lee, *J. Control. Release.* **2021**, 330, 898-906.

[21] Q. He, J. Chen, J. Yan, S. Cai, H. Xiong, Y. Liu, D. Peng, M. Mo and Z. Liu, *Asian J. Pharm. Sci.* **2020**, 15, 416-448

[22] S. Li, H. Cheng, W. Qiu, L. Liu, S. Chen, Y. Hu, B. Xie, B. Li and X. Zhang, *ACS Appl. Mater. Interfaces.* **2015**, 7, 28319-28329.

[23] Y. Liu, L. Mei, C. Xu, Q. Yu, K. Shi, L. Zhang, Y. Wang, Q. Zhang, H. Gao, Z. Zhang and Q. He, *Theranostic.* **2016**, 6(2), 177-191

[24] I. Martin, M. Teixido and E. Giralt, *Pharmaceuticals.* **2010**, 3, 1456-1490.

[25] J. Ye, M. C. Shin, Q. Liang, H. He and V. C. Yang, *J. Control. Release.* **2015**, 205, 58-69

[26] M. Sauter, M. Strieker, C. Kleist, A. Wischnjow, V. Daniel, A. Altmann, U. Haberkorn and W. Miel, *J. Controlled Release.* **2020**, 322, 200-208.

[27] J. Löfblom, J. Feldwisch, V. Tolmachev, J. Carlsson, S. Ståhl and F. Y. Frejd, *FEBS Lett.* **2010**, 584, 2670-2680

[28] F. Y. Frejd and K. Kim, *Exp. Mol. Med.* **2017**, 49, e306.

[29] C. Eigenbrot, M. Ultsch, A. Dubnovitsky, L. Abrahmsén and T. Härd, *Proc. Natil. Acad. Sci.* **2010**, 107(34**)**, 15039-15044

[30] A. Orlova, M. Magnusson, T. L. J. Eriksson, M. Nilsson, B. Larsson, I. Höidén-Guthenberg, C. Widström, J. Carlsson, V. Tolmachev, S. Ståhl and F. Y. Nilsson, *Cancer Res.* **2006**, 66(8), 4339-4348.

[31] V. Tolmachev, *Curr. Pharm. Des.* **2008**, 14, 2999-3019.

[32] A. I. Ivanov, *Methods Mol. Biol.* **2008**, 440, 15-33

[33] A. Xiong, S. Kundu and K. Forsberg-Nilsson, *FEBS J.* **2014**, 281(22), 4993-5008

[34] S. Schön, C. Prante, S. Müller, M. Schöttler, L. Tarnow, J. Kuhn, K. Kleesiek and C. Cötting, *Kidney Int.* **2005**, 68(4**)**, 1483-1490

[35] G. M. Thurber, S. C. Zajic and K. D. Wittrup, *J. Nucl. Med.* **2007**, 48, 995-9

[36] K. D. Orcutt, K. A. Nasr, D. G. Whitehead, J. V. Frangioni and K. D. Wittrup, *Mol. Imag. Biol.* **2011**, 13, 215-221.

[37] F.C. Charmberlain, R.L. Jones and S. P. Chala, *Future Oncol*. **2019**, 15, 13.

[38] Charles River Laboratories, Charles River Immunodeficient Models Xenograft Data Catalog, Massachusetts, U.S.A., **2014**

[39] M. Zanoni, F. Piccinini, C. Arienti, A. Zamagni, S. Santi, R. Polico, A. Bevilacqua and A. Tesei, *Sci. Rep.* **2016**, 6, 19103-19113

[40] A. S. Nunes, A. S. Barros, E. C. Costa, A. F. Moreira and I. J. Correia, *Biotechnol. Bioeng.* **2019**, 116, 206-226.

[41] S. Govindarajan, J. Sivakumar, P. Garimidi, N. Rangaraj, J. M. Kumar, N. M. Rao and V. Gopal, *Biomaterials*. **2012**, 33, 2570-2582

[42] H. H. Gustafson, D. Holt-Casper, D. W. Grainger and H. Ghandehari, *Nano Today***. 2015**, 10(4), 487-510

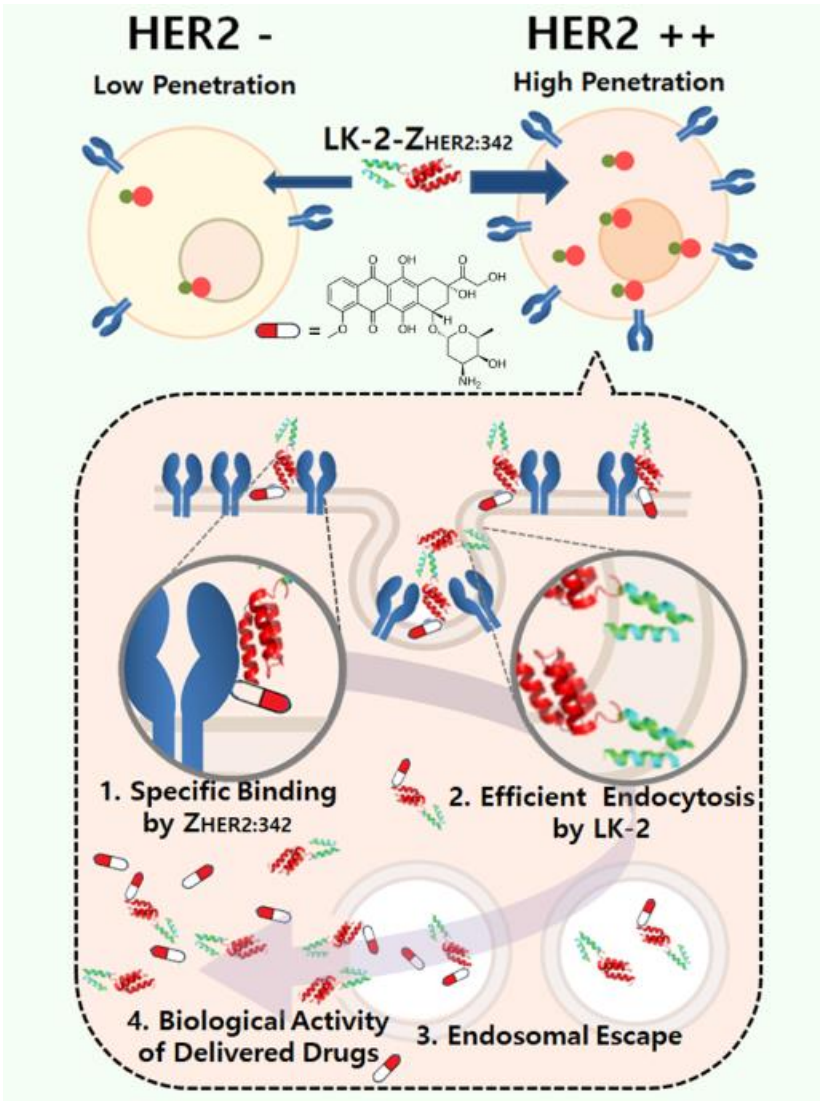

Figure 1. The overall schematic image of LK-2-Z_{HER2} as a selective cell penetrating vehicle on HER2-overexpressing cancer cells at nanomolar concentrations by combination of a dimeric cell penetrating peptide (LK-2) and an HER-2 selective affibody ($Z_{HER2:342}$).

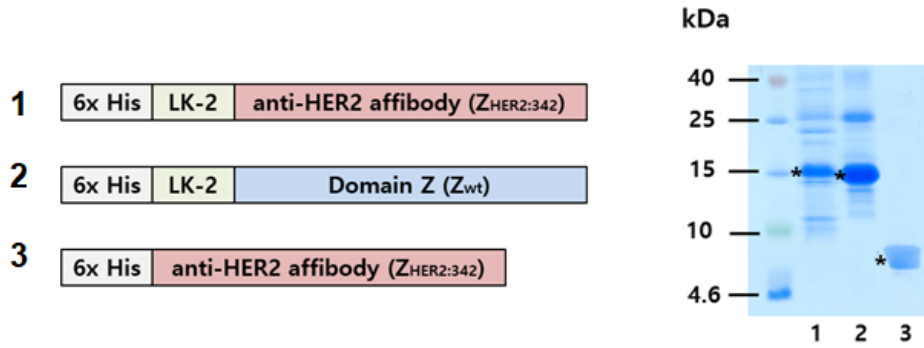

Figure 2. The constructions and purification of the recombinant proteins. The constructions of LK-2-Z_{HER2} (1) , LK-2-Z_{wt} (2) and Z_{HER2} (3). The SDS-PAGE analysis of the purifide proteins: LK-2-Z_{HER2} (13.7kDa), LK-2-Z_{wt} (13.7 kDa) and Z_{HER2} (9.5 kDa).

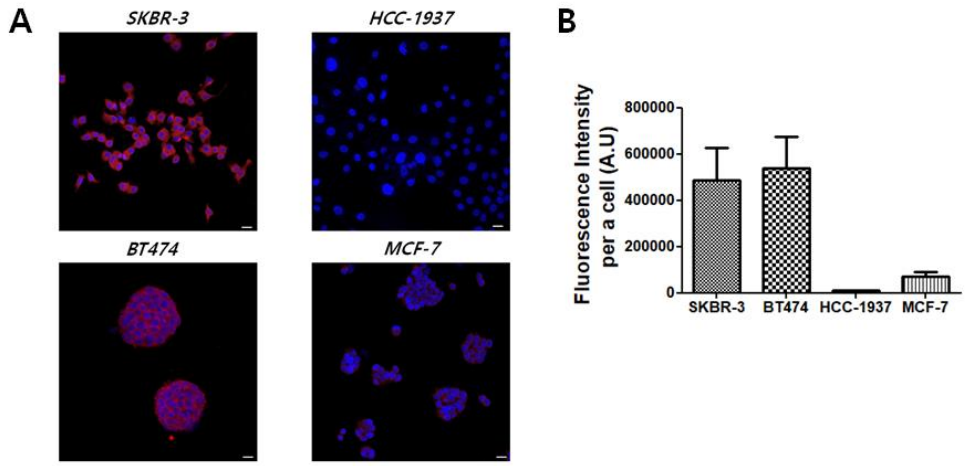

Figure 3. HER2 expression level of *SKBR-3, HCC-1937, BT474* and *MCF-7* (A) Representative confocal laser microscopy (CLSM) images of SKBR-3, HCC-1937, BT474, and MCF-7 cells. The cells were fixed 4% paraformaldehyde. The fixed cells were labeled with anti-HER2 antibody, followed by Donkey anti-rabbit IgG H&L (Alexa 594) antibody. Scale bar = 20μm. (B) Quantification of HER2 receptors labeled with antibodies through Image-J program. The average values of fluorescent intensity per a cell were plotted. The data points are shown as the average values ± standard deviation. 35 cells were analyzed.

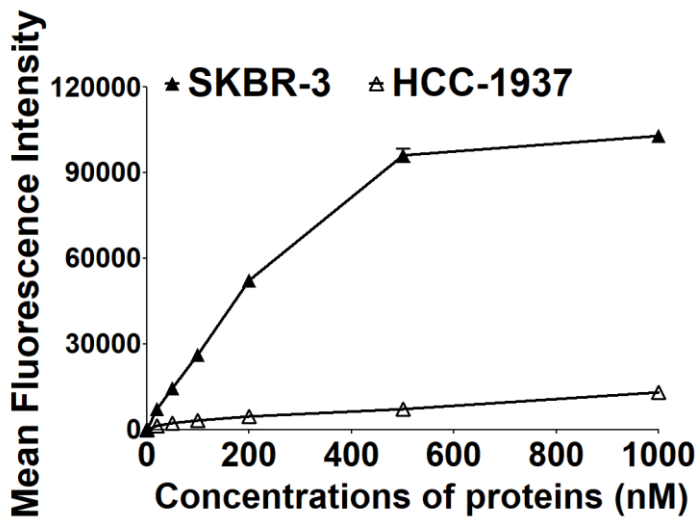

Figure 4. FACS results for selective cellular uptake of FITC-labeled LK-2-Z_{HER2} at various concentrations on *HCC-1937* (HER2-) and *SKBR-3* (HER2++) cells after 1h-incubation.

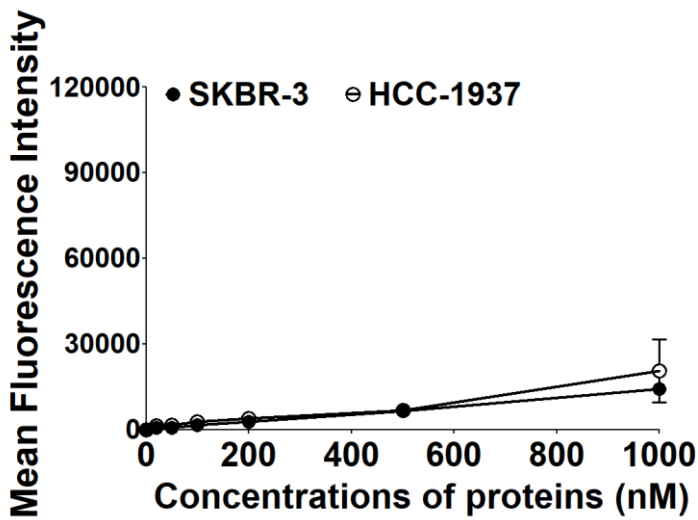

Figure 5. FACS results for the cellular uptake of FITC-labeled LK-2-Z_{wt} at various concentrations on *HCC-1937* (HER2-) and *SKBR-3* (HER2++) cells after 1h-incubation. Mean fluorescence intensity (MFI) of 10,000 cells are shown. The data points are shown as the average values with ± standard deviations (*n*=3).

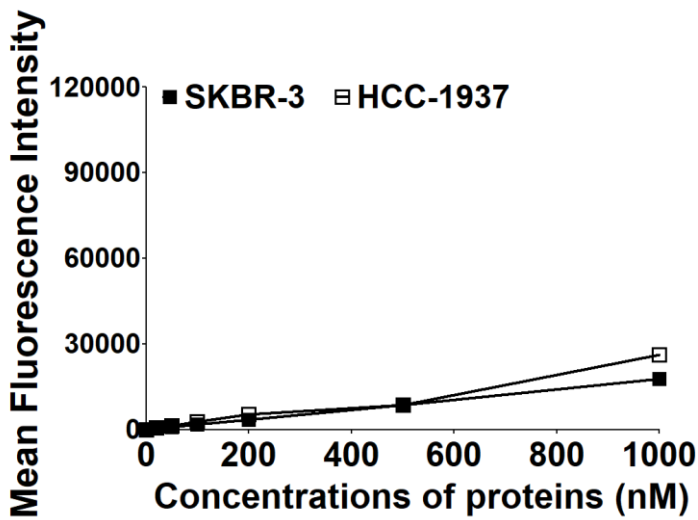

Figure 6. FACS results for the cellular uptake of FITC-labeled $Z_{HER2:342}$ at various concentrations on *HCC-1937* (HER2-) and *SKBR-3* (HER2++) cells after 1h-incubation. Mean fluorescence intensity (MFI) of 10,000 cells are shown. The data points are shown as the average values with ± standard deviations (n = 3).

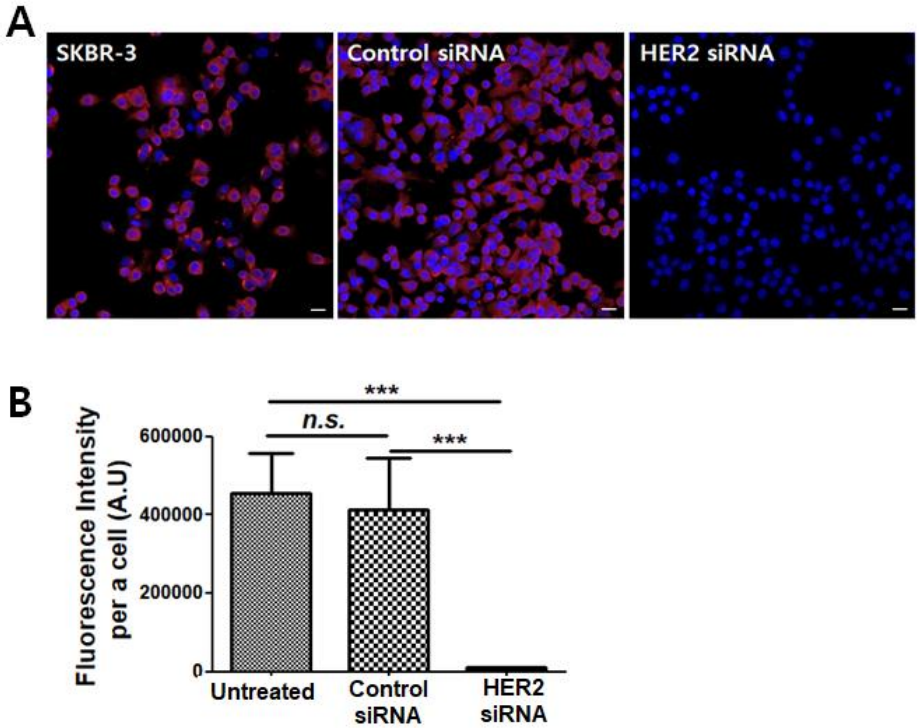

Figure 7. HER2 expression levels of HER2-knockdown *SKBR-3*. (A) The HER2 expression levels of *SKBR-3* cells treated either with control siRNA or HER2 siRNA were analysed. Cells were fixed 4% paraformaldehyde. The fixed cells were labeled with anti-HER2 antibody, followed by Donkey anti-rabbit IgG H&L (Alexa 594) antibody. Scale bar = 20μm. (B) Quantification of HER2 receptors labeled with antibodies through Image-J program. The average values of fluorescent intensity per a cell were plotted. The data points are shown as the average values ± standard deviation. 35 cells were analyzed. The data were analyzed using two-tailed Student's *t*-tests. (***) indicates $p \leq 0.001$.

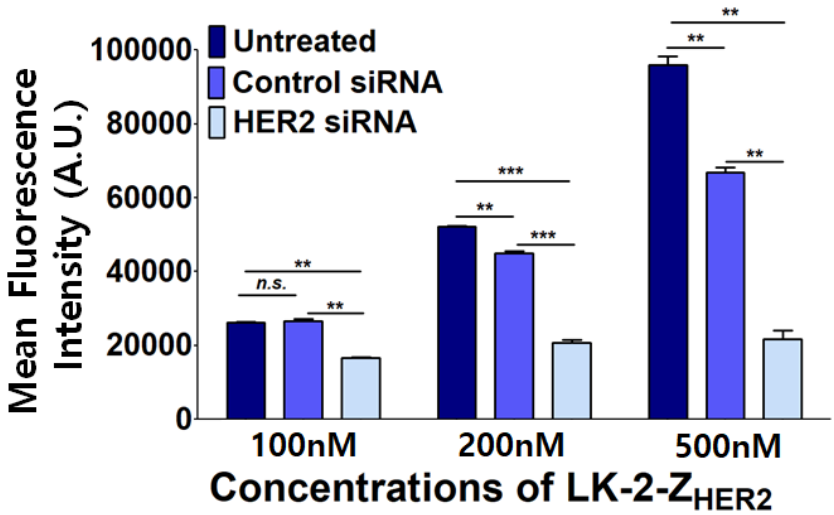

Figure 8. Cellular uptake of FITC-labeled LK-2-Z_{HER2} on *SKBR-3* and HER2-knockdown *SKBR-3*. The cellular uptake levels of FITC-labeled LK-2-Z_{HER2} were compared in untreated cells, control siRNA (siRNA-A, Santa cruz, sc-37007)-treated cells, and HER2-siRNA-treated cells by the FACS analysis. Cells were transfected with siRNA for 48 h and then were treated with FITC-labeled LK-2-Z_{HER2} for 1 h. The data points are shown as the average values ± standard deviation (n = 3). The data were analyzed using two-tailed Student's t-tests. (**) and (***) indicate $p \leq 0.01$ and $p \leq 0.001$, respectively.

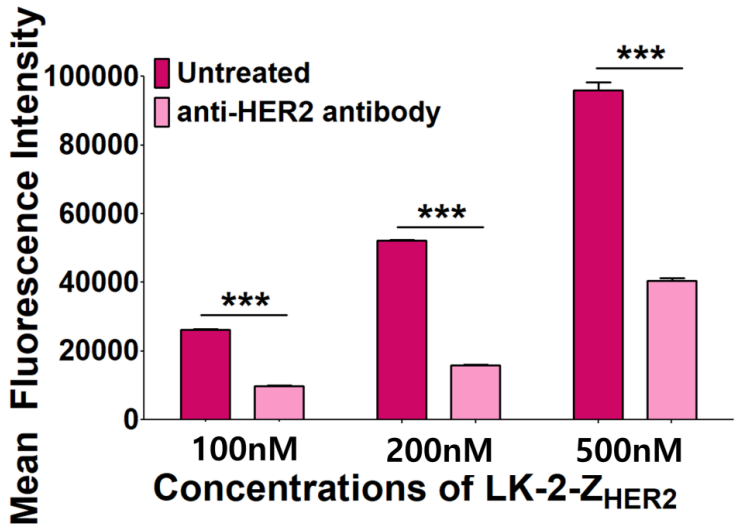

Figure 9. Cellular uptake of FITC-labeled LK-2-Z_{HER2} on *SKBR-3* and on HER2-blocked *SKBR-3*. HER2 receptors were blocked by anti-HER2 antibody targeting extracellular domain of HER2 for 3 h and the cells were treated with various concentrations of FITC-labeled LK-2-Z_{HER2} for 1 h. The cellular uptake of FITC-labeled LK-2-Z_{HER2} was measured by the FACS analysis. The data are shown as the average values with ± standard deviations (n=3). The data were analyzed using two-tailed Student's t-tests. (***) indicates $p \leq 0.001$.

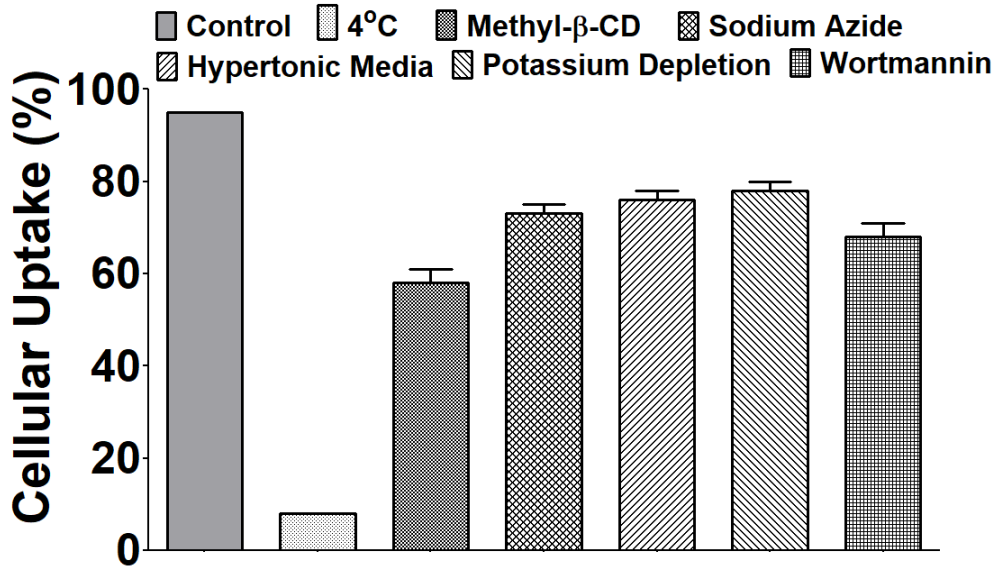

Figure 10. Cellular uptake of FITC-labeled LK-2-Z_{HER2} on *SKBR-3* treated with various endocytosis inhibitors. *SKBR-3* cells were pre-treated with various endocytosis inhibitors for 3 h and they were treated with 200nM of FITC-labeled LK-2-Z_{HER2} for next 1 h. PBS treated cells were used as a control. The data points are shown as the average values ± standard deviation.

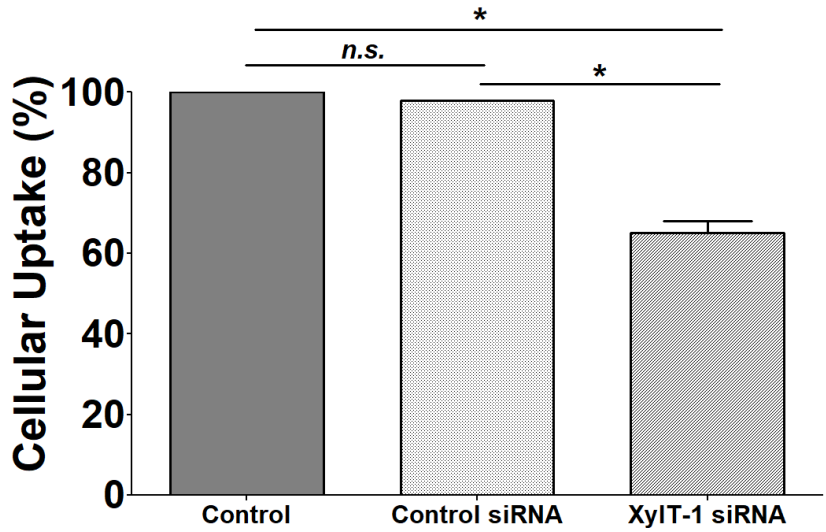

Figure 11. Cellular uptake of FITC-labeled LK-2-Z_{HER2} on *SKBR-3* treated with XylT-1 siRNA. *SKBR-3* cells were treated either with control siRNA and XylT-1 siRNA for 48 h and they were treated with 200nM FITC-labeled LK-2-Z_{HER2} for 1 h. The data points are shown as the average values ± standard deviation (n = 3). The data were analyzed using two-tailed Student's t-tests. (*) indicates $0.01 < p \leq 0.05$.

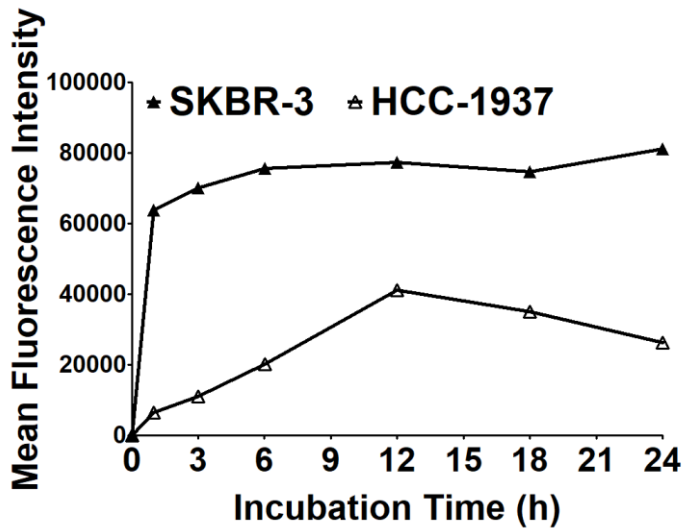

Figure 12. Cellular uptake kinetics of FITC-labeled LK-2-Z_{HER2} at 200 nM on *HCC-1937* and *SKBR-3* cells.

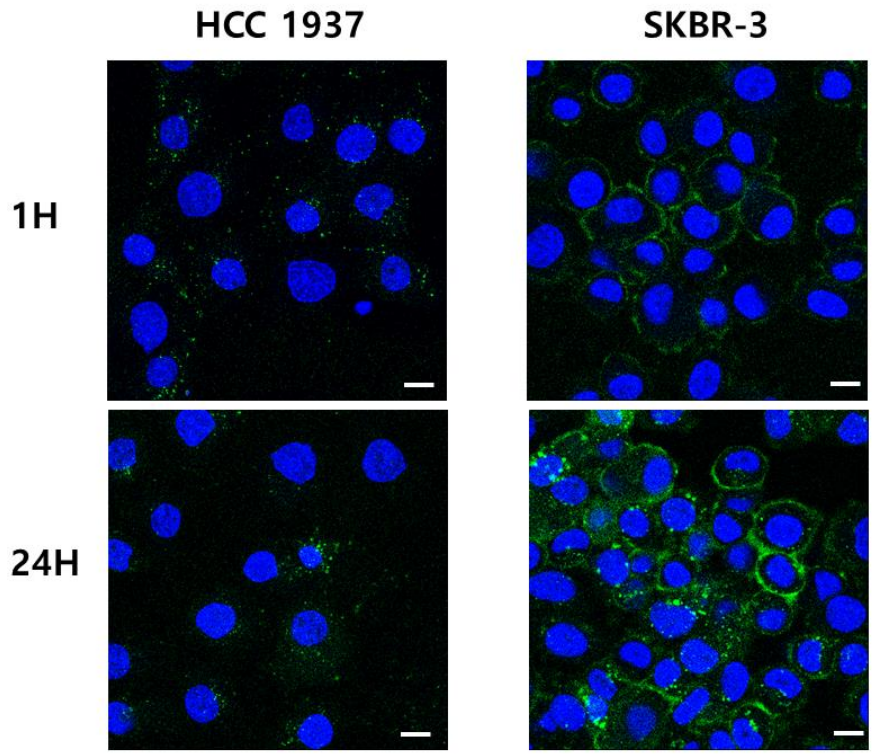

Figure 13. Representative CLSM images of cells treated with FITC-labeled LK-2-Z_{HER2}. *HCC-1937* and *SKBR-3* cells were treated with FITC-labeled LK-2-Z_{HER2} at 200 nM for 1 h and 24 h. Nuclei were stained with Hoechst 33342. Scale bar = 10 μm.

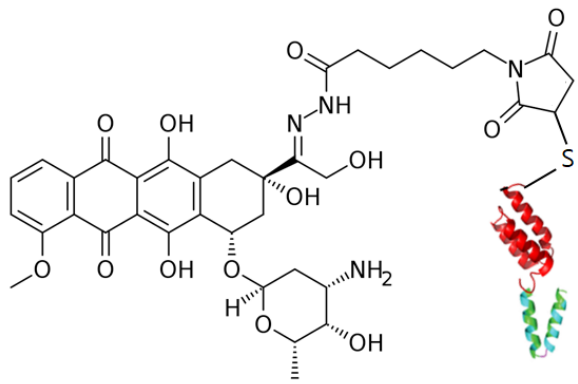

Figure 14. The chemical structure of aldoxorubicin conjugated on the LK-2-Z_{HER2} vehicle via a thioester bond.

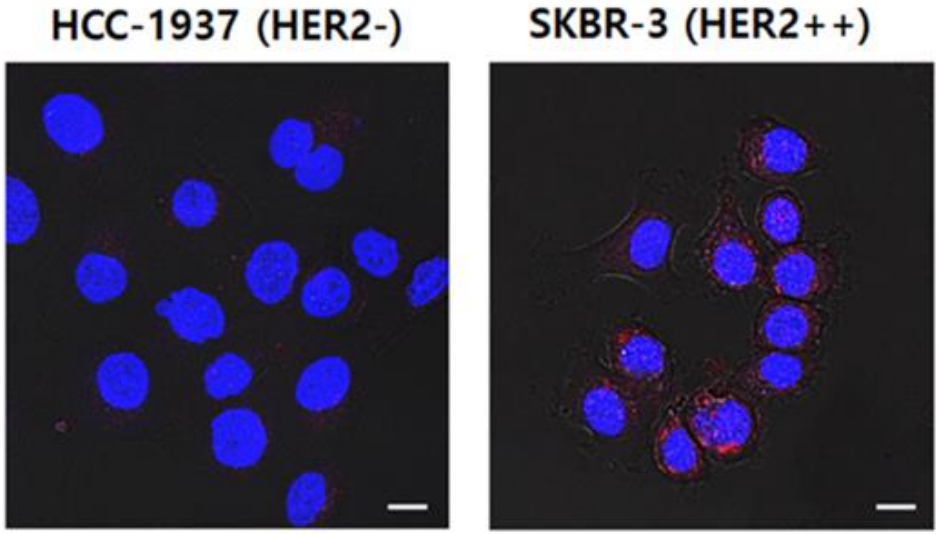

Figure 15. The representative CLSM images of *HCC-1937* and *SKBR-3* cells treated with LK-2-Z_{HER2}-DOX at 200 nM for 24 h. DOX fluorescence is shown as red. Nuclei was stained with Hoechst 33342. Scale bar = 10 μm.

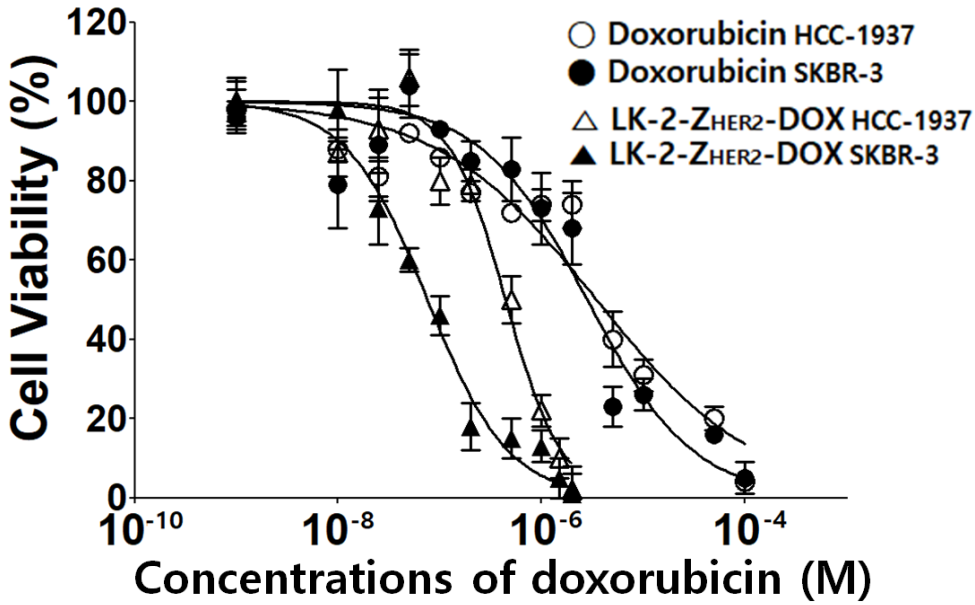

Figure 16. Cytotoxicity of free DOX and LK-2-Z_{HER2}-DOX on *HCC-1937* and *SKBR-3* cells after 24 h-incubation. The data are shown as the average values with ± standard deviations (*n*=3).

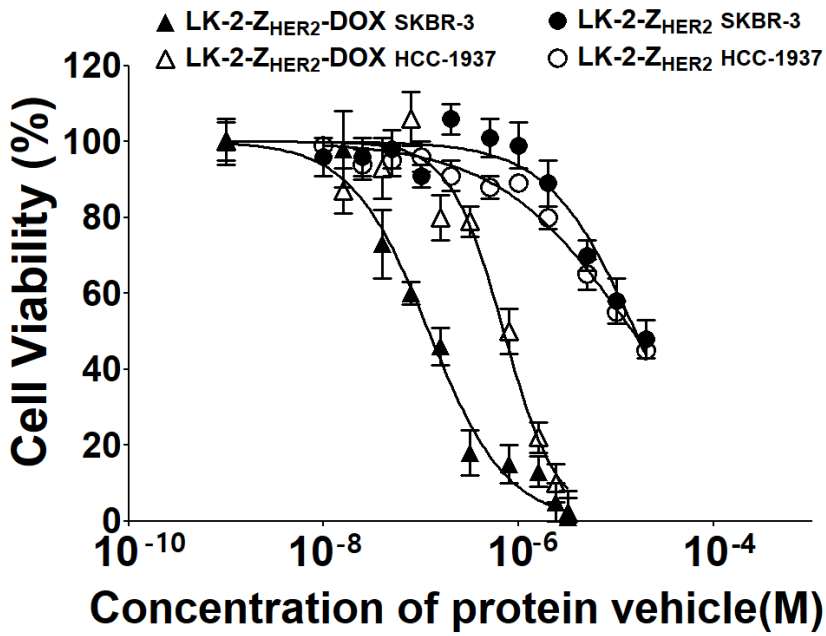

Figure 17. Comparison of toxicity of LK-2-Z$_{HER2}$ and LK-2-Z$_{HER2}$-DOX on *HCC-1937* and *SKBR-3* cells. The cells were treated with the proteins for 24 h and cell viability was measured using the CCK-8 assay kit. The data points are shown as the average values ± standard deviation (n = 3).

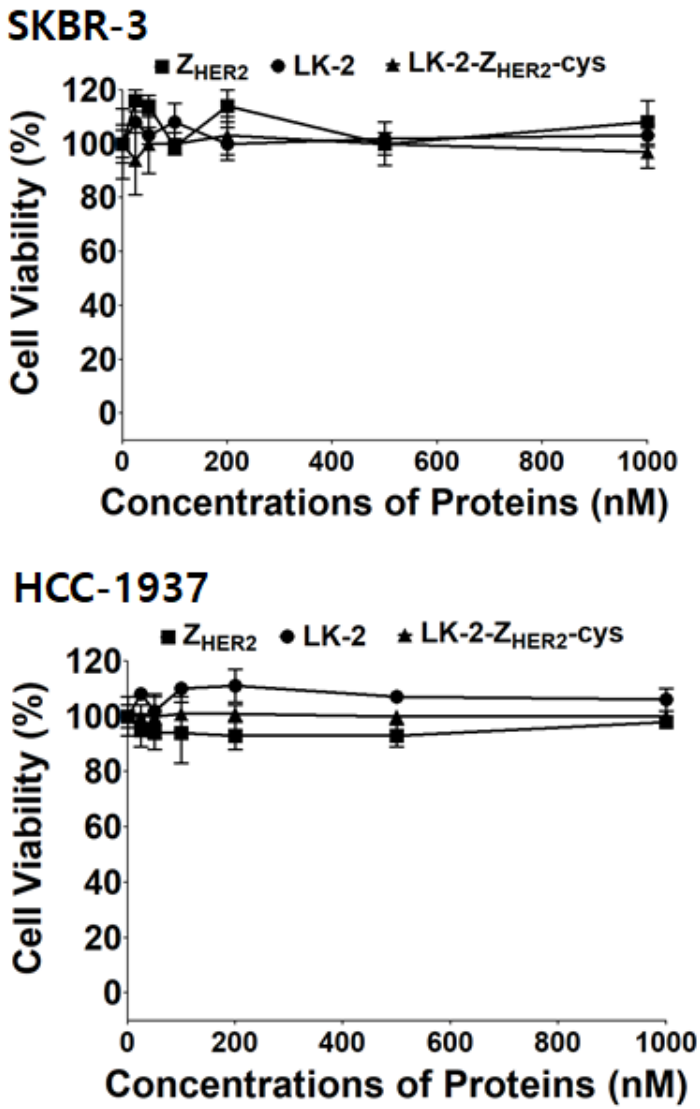

Figure 18. Cytotoxicity of LK-2, Z_{HER2} and LK-2-Z_{HER2}-cys on *SKBR-3* and *HCC-1937* cells after 24h-incubation. The proteins were treated for 24 h and cell viability was measured using the CCK-8 assay kit. The data points are shown as the average values ± standard deviation (n = 3).

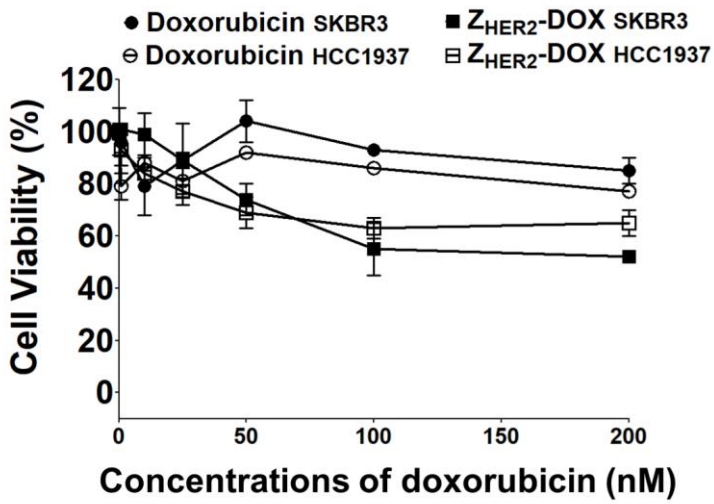

Figure 19. Cytotoxicity of free DOX and Z_{HER2}-DOX conjugates on *SKBR-3* and *HCC-1937* cells. Cells were treated with the samples for 24 h and the toxicity was measured using the CCK-8 assay kit. The data are shown as the average values with ± standard deviations (n = 3).

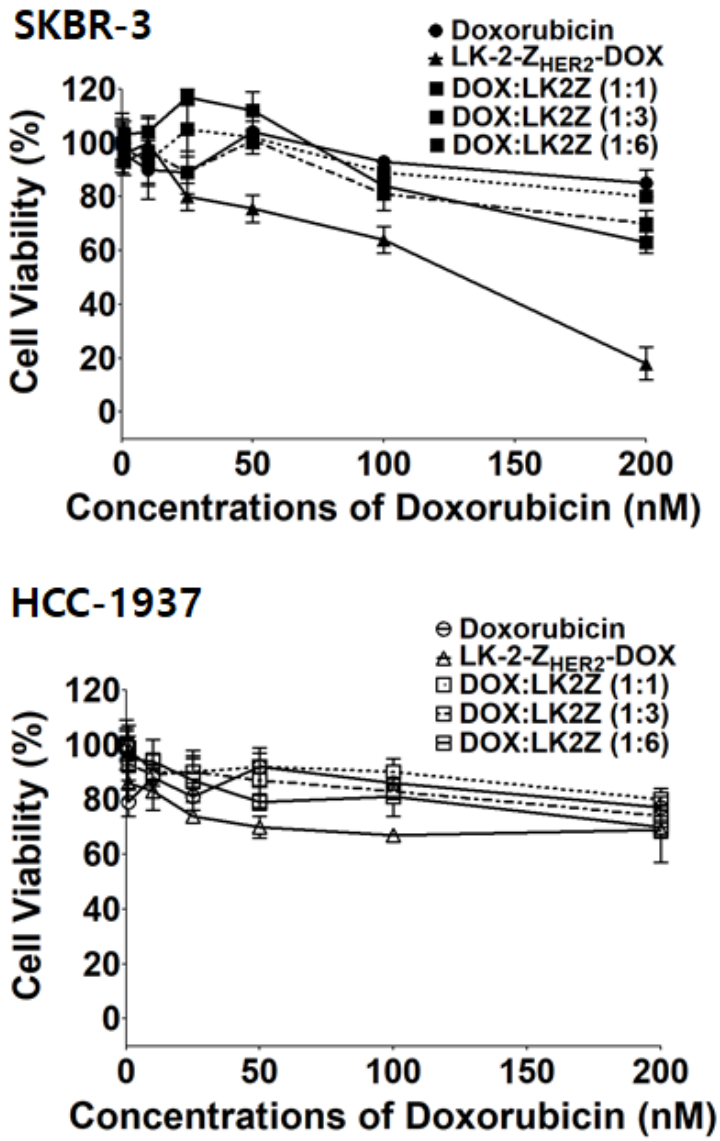

Figure 20. Cytotoxicity of non-covalent mixture of LK-2-Z_{HER2} and free DOX. Comparison of anti-cancer effect of doxorubicin, LK-2-Z_{HER2}-DOX and the simple mixtures of doxorubicin and LK-2-Z_{HER2} with various ratio (1:1, 1:3, 1:6) on *SKBR-3* (top) and *HCC-1937* (bottom). The data are shown as the average values with ± standard deviations (n = 3).

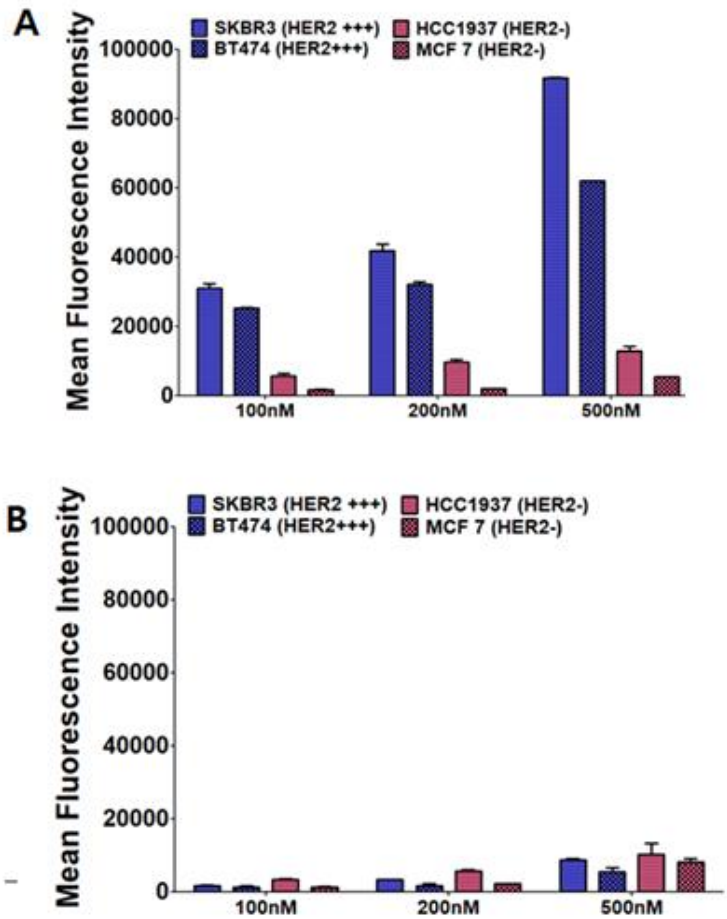

Figure 21. Cellular uptake of FITC-labeled LK-2-Z_{HER2} and LK-2-Z_{wt} on *SKBR-3, HCC-1937, BT474* and *MCF7* cells. (A) FACS results for selective cellular uptake of FITC-labeled LK-2-Z_{HER2} on HER2-overexpressed cells (*SKBR-3* and *BT474*) and HER2-negative cells (*HCC-1937* and MCF7). (B) FACS results for the cellular uptake of FITC-labeled LK-2-Z_{wt} on HER2-overexpressed cells (*SKBR-3* and *BT474*) and HER2-negative cells (*HCC-1937* and MCF7). The proteins were treated on cells for 1 h. The data points are shown as the average values ± standard deviation (n = 3).

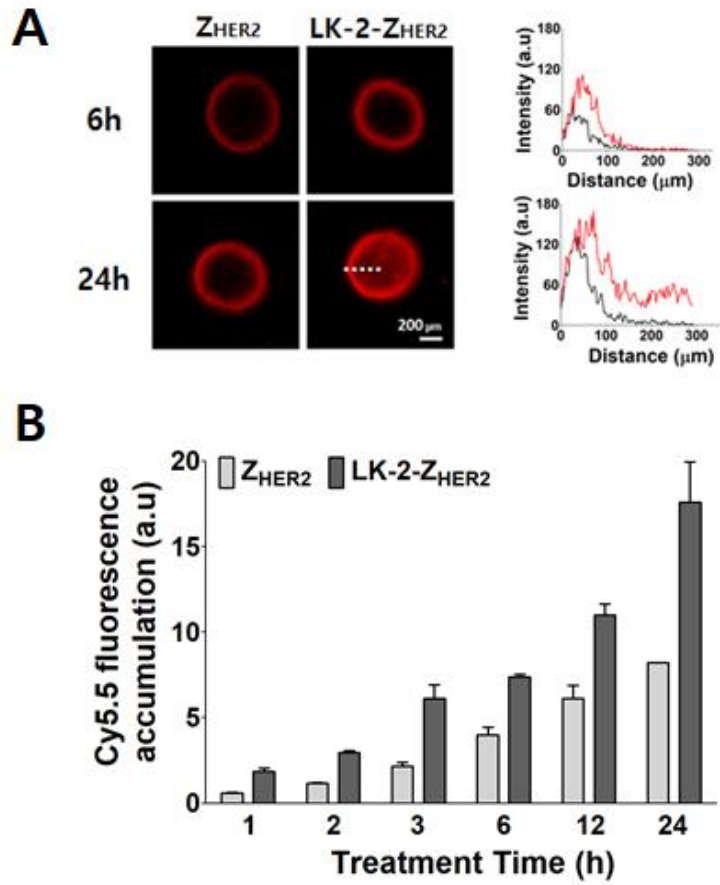

Figure 22. Penetration into *BT474* spheroid. (A) The CLSM images of *BT474* spheroids treated with Cy5.5-labeled Z_{HER2} and LK-2-ZHER$_2$ at 200 nM with varying the incubation time. (B) Accumulation of Cy5.5 fluorescence inside the spheroids treated with Z_{HER2} and LK-2-Z_{HER2}. The data are shown as the average values with ± standard deviations (*n*=3).

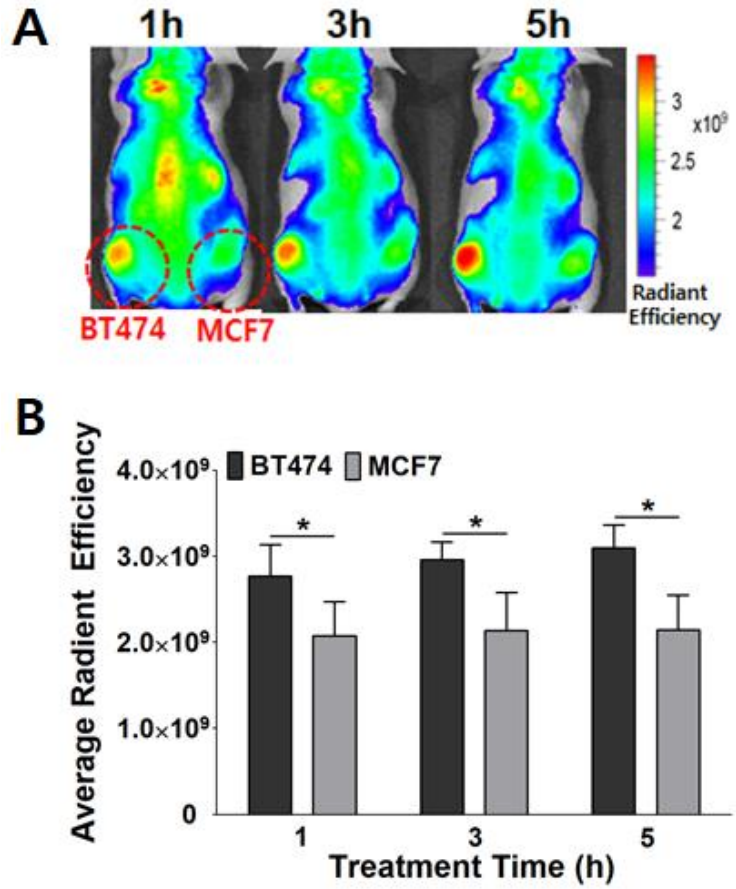

Figure 23. *In vivo* biodistribution of LK-2-Z_{HER2} in tumor-xenografted mice. Cy5.5-labeled LK-2-Z_{HER2} was intravenously injected into the mice and the images were acquired by IVIS. (A) Time-dependent Near-infrared fluorescence whole body images of the mice. The left and right red dotted circles indicate *BT474* (HER2+) tumor and *MCF7* (HER2-) tumors, respectively. (B) Quantitative comparison of the fluorescence accumulation on *BT474* and *MCF7* tumors. The data were analyzed using two-tailed Student's *t*-tests. (*) indicates $p \leq 0.05$.

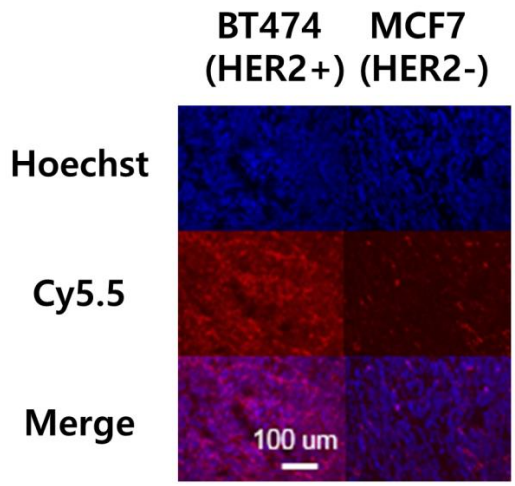

Figure 24. Representative CLSM images of the sliced *BT474* and *MCF7* tumor tissues. The tissues were harvested 5 h after the intravenous injection of Cy5.5-labeled LK-2-Z_{HER2} (red). Nuclei were stained with Hoechst 33342 (blue).

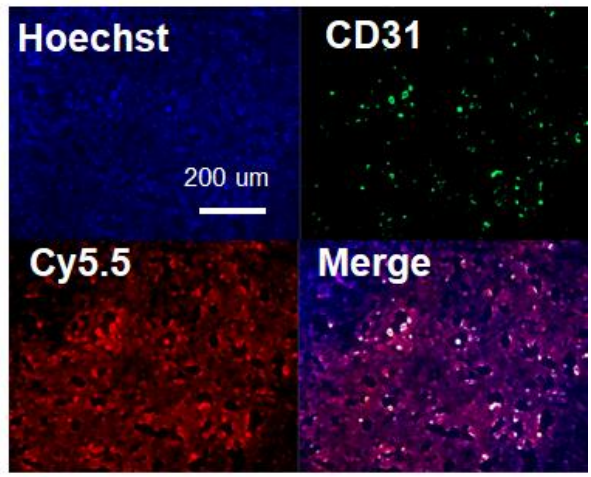

Figure 25. Immunofluorescence images of the sliced *BT*474 tumor tissue stained with FITC-labeled anti-CD31 antibody. Blue: nucleus, red: LK-2-Z_{HER2}

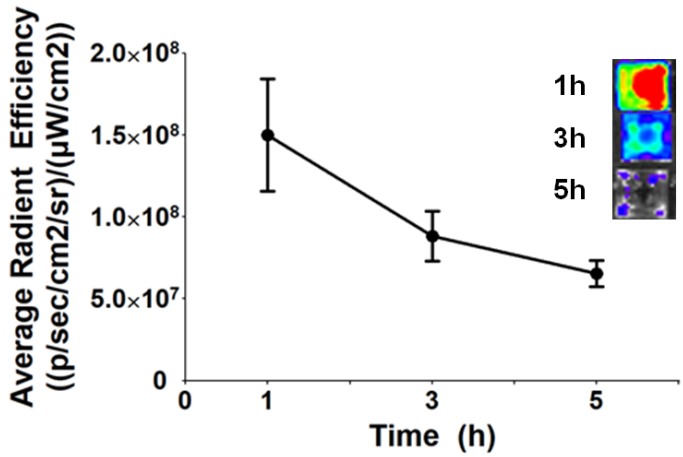

Figure 26. Remaining Cy5.5 fluorescence in blood samples after the intravenous injection. The data are shown as the average values with ± standard deviations (*n*=3).

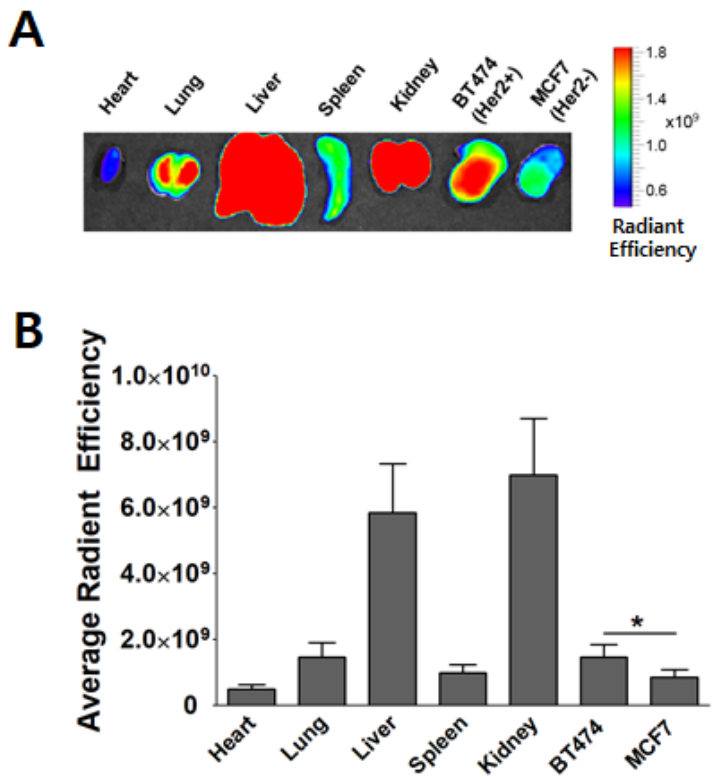

Figure 27. *Ex vivo* biodistribution of LK-2-Z_{HER2} in tumor-xenografted mice. Cy5.5-labeled LK-2-Z_{HER2} was intravenously injected into the mice and the images were acquired by IVIS. (A) *Ex vivo* fluorescent images of various organs and tumors of the mice at 5h post-injection. (B) Quantitative comparison of the fluorescence intensity in various organs and tumors. The data are shown as the average values with ± standard deviations (n=3). The data were analyzed using two-tailed Student's t-tests. (*) indicates $p \leq 0.05$.

	Sequence
LK-2	LKKLLKLLKKLLKLGGLKKLLKLLKKLLKLAG
Domain Z (Z_{wt})	VDNKFNKEQQNAFYEILHLPNLNEEQRNAFIQSLKDDPSQSANLLAE AKKLNDAQAPK
$Z_{HER2:342}$ (Z_{HER2})	VDNKFNKEMRNAYWEIALLPNLNNQQKRAFIRSLYDDPSQSANLLAE AKKLNDAQAPK

Table 1. Amino acid sequences of LK-2, Domain Z (Z_{wt}), and $Z_{HER2:342}$

Gene constructs	Primers (5′ to 3′)	Method
Domain Z (Z_{wt}) amplifications	For: TTCGAGCTCCGTCGAC	Gene synthesis and amplification
	Rev : GTGCTCGAGTTATTTCGGGG	
Z_{HER2} gene amplification	For:CAAGAGCTCCGTCGACGTTGACAACAAATTCAACAA	Gene synthesis and amplification
	Rev. GTGCTCGAGTTATTTCGGGGCCTGCG	
pET28b - LK-2 – Z_{HER2}	for: AGCTCCGTCGACGTTG	Blunt-end ligation
	Rev: CTTGAACTCAGAGCCACCA	
pET28b - LK-2 – Z_{wt}	for: AGCTCCGTCGACGTTG	Blunt-end ligation
	Rev: CTTGAACTCAGAGCCACCA	
pET28b – Z_{HER2}	For: GTCGACGTTGACAACAAATTCAAC	Blunt-end ligation
	Rev : GAATTCCATATGGCTGCCG	

Table 2. Primer sequences for the recombinant DNA constructs

Groups	ALT [a] [U/L]	AST [b] [U/L]	ALP [c] [U/L]	BUN [d] [mg/dL]	CREA [e] [mg/dL]
Saline	33±2.64	81±33.29	375.0±116.2	21.9±1.68	0.10±0.04
LK-2-Z_{HER2}	32±6.93	89±14.73	282.3±47.3	20.8±0.5	0.14±0.03

[a] alanine transaminase; [b] aspartate transaminase; [c] alkaline phosphatase; [d] blood urea nitrogen; [e] creatinine

Table 3. Acute toxicity analysis of mouse plasma

Abstract in Korean (국문 초록)

세포는 인지질 이중층으로 이루어진 세포막으로 둘러쌓여 있다. 이러한 세포막은 세포의 내부와 외부의 물질교환을 선택적이고 효과적으로 조절하며 세포 생존에 매우 중요한 역할을 한다. 이러한 세포막 때문에 사이즈가 크거나 세포막과 상호작용을 못하는 물질은 세포 내부로 전달 되지 못한다. 이러한 세포 비투과 물질 중에는 치료 약물로 사용가능한 항암제나 항체를 포함한 다양한 단백질 등이 포함 된다. 많은 세포 비투과 약물들이 세포에 중요한 역할을 하기 때문에, 과거부터 이러한 약물을 세포 내부로 전달하기 위한 나노입자물질, 하이드로겔, 공중합체를 포함한 많은 전달체들이 개발 되어 왔다.

세포 투과성 펩타이드 (Cell Penetrating Peptide)는 세포 비투과 물질을 효율적으로 세포내부로 전달하는 효율적인 전달체 중 하나이다. 특히 이 물질은 펩타이드로 만들어졌기 때문에 다른물질들에 비해 상대적으로 독성이 낮으며 생체적합성이 높아 널리 이용되고 있다. 과거 HIV-1로 부터 유래된 Tat (Transactivator of transcription) 펩타이드가 처음 발견 된 이후 poly arginine, penetratin 과 같은 다양한 세포투과성 펩타이드들이 개발되었고, 이들은 주로 음성 전하를 가지는 세포막과 잘 상호작용 할 수 있는 양성 전하를 띄는 아미노산들로 이루어져 있다. 이러한 세포투과성 펩타이드들은 보통 비투과물질을 수 마이크로몰랄 농도에서 적은 독성을 보이며 살아있는 세포 내부로 전달하는 것이 가능했다.

서울대학교 생체재료화학연구실에서는 기존에 존재하는 세포투과성 펩타이드 보다 훨씬 높은 효율적인, 수 나노몰랄 농도에서 작동이 가능한 새로운 종류의 양친매성(amphipathic) 성질을 세포투과성 펩타이드를 개발 하는것을 성공하였다. 새로이 발견된 이 펩타이드는 루신과 라이신이 반복되는 LK 펩타이드 이며 이것의 시퀀스는 LKKLLKLLKKLLKLAG 이다. 후속 연구에서 이 펩타이드의 시퀀스가 여러번 반복 될 수록 더 높은 세포투과 효율을 보이는 것을 알 수 있었다. LK가 두번 반복되는 LK-2 와 같은 경우에는 고체상 펩타이드 합성법으로 얻을 수 있지만, 그 이상 반복되는 펩타이드는 너무 길기 때문에 대장균 단백질 발현 방법 (E.coli protein expression)으로 얻을 수 있었고 LK가 네번 반복되는 LK-4에서 세포투과도의 효율이 가장 높았음을 알 수 있었

다. 더 나아가 대장균에서 LK 시퀀스를 발현 가능 하게 함으로써 다양한 단백질 및 펩타이드 시퀀스를 DNA 재조합 기술을 이용하여 LK와 함께 한번에 정제 해 낼 수 있게 되어 LK 세포투과성 펩타이드의 다양한 활용이 가능하게 되었다.

본 박사학위 논문에서는 대장균 발현을 통한 LK 시퀀스를 이용한 두 가지 활용 연구를 진행하였다. 논문의 PART I 에서는 LK 시퀀스에 항체에 선택적으로 결합이 가능하다고 알려진 Domain Z of *Staphylococcus* protein A를 DNA 재조합 방법으로 도입하여, 거대한 세포 비투과성 단백질인 항체를 매우 저농도에서 효율적으로 살아있는 세포 내부로 전달 하는 것을 가능하게 함으로써 새로운 항체 전달 물질 개발에 성공 하였다. 이 연구에서 만들어진 LK-Domain Z 단백질은 domain Z 파트의 영향으로 항체와 일정한 비율로 매우 효율적인 비공유성 결합을 형성한다. 그 이후 LK의 높은 세포투과성 때문에 항체가 살아있는 세포의 세포질 내부로 효과적으로 들어갈 수 있다. 본 연구에서는 이 효율적인 항체 전달물질의 성질과 그에 대한 투과 기전에 대해 밝혔으며 전달된 항체가 실제로 세포 내부에서 정확한 역할이 가능한지에 대한 연구 또한 진행 되었다. LK-Domain Z 를 이용하여 암세포의 신호전달에 관여하는 NF-κB 의 역할을 방해하는 anti-NF-κB 항체를 이용하여 실제로 암세포의 증식에 필요한 유전자의 발현이 억제되면서 세포사멸이 일어나는 것을 관찰 할 수 있었다. 이를 통해 새로이 발견된 LK-Domain Z 단백질이 세포 내부에서 작용하는 다양한 항체를 전달하여 향후 다양한 생물 세포학적 연구 및 약물 연구에 사용 가능 할 것임을 확인 하였다.

논문의 PART II 에서는 LK 시퀀스에 세포 선택성을 부여하여 표적세포에 효율적으로 작용하는 세포투과성 펩타이드 개발에 대해 서술 하였다. 수많은 약물전달체와 마찬가지로 LK 시퀀스 또한 세포 선택성이 없다는 단점을 가진다. 약물전달체가 세포에 대한 선택성을 가지면 다양한 약물의 복용량을 낮출 수 있고 정상세포에 대한 부작용을 줄일 수 있는 장점을 가진다. 본 연구에서는 LK 시퀀스에 세포선택성을 부여하기 위해 20~30% 정도의 유방암 세포에 과발현 되어있는 HER2 리셉터에 특이적으로 결합이 가능하다고 알려진 $Z_{HER2:342}$ (Z_{HER2})단백질을 DNA 재조합 방법을 통해 LK에 도입하였다. 이 연구에서 개발된 LK-Z_{HER2} 단백질은 HER2가 없는 세포에는 아주 느리고 비효율적으로 세포투과도를 보이는 반면, HER2가 과발현 된 세포에서는 매우 빠르고 효율적

인 세포투과성을 보였다. 본 연구에서는 LK-Z_{HER2}의 세포투과성과 HER2 리셉터 발현과의 관계에 대해 밝힐 수 있었으며, LK-Z_{HER2} 단백질에 항암제인 doxorubicin을 결합하여 세포를 선택적으로 죽이는 표적치료제로서의 역할을 *in vitro* 상에서 확인 할 수 있었다. 더 나아가 *in vivo* 에서도 이 LK-Z_{HER2}가 HER2 과발현 세포에 매우 높은 선택성을 보인다는 것을 밝혔다.

본 박사학위 연구에서는 LK 시퀀스에 다양한 성질을 가지는 단백질은 DNA 재조합 방법으로 도입하여 새로운 기능을 가지는 세포투과성펩타이드 개발에 성공하였다. Domain Z, Z_{HER2} 외에도 굉장히 많은 종류의 기능성 단백질들이 존재하기 때문에 위와같은 방법으로 LK에 도입이 된다면, 향후 LK는 더욱 다양한 기능을 가지는 세포투과성 펩타이드로 발전할 수 있을 것이라 기대된다.

Acknowledgement (감사의 글)

2015년 석.박사 통합과정으로 학위를 시작하여 졸업을 하기까지 굉장히 긴 시간 이었지만 지나고 보니 매우 짧게 느껴집니다. 저의 연구에 여러가지 방법으로 도움을 주신 수 많은 분들께 감사하다는 말씀 전하고 싶습니다. 특히 연구에 대한 깊은 토론을 하며 많은 시간을 보낸 저희 CPP팀과 지도교수님이신 이연교수님께 감사드립니다. 또한 오랜시간 저를 믿고 기다려주시며 아낌없이 지지해주신 부모님께 감사드립니다. 앞으로 더욱 발전하는 연구자로서 세상에 도움이 될 수 있는 사람으로 살아갈 수 있도록 하겠습니다. 감사합니다.

2021년

정승은